https://doi.org/10.5194/egusphere-2026-6854
Preprint. Discussion started: 19 November 2026
© Author(s) 2026. CC BY 4.0 License.

Offsetting Impacts of Aromatic Autoxidation on Organic and Inorganic Aerosols Modelled by GEOS-Chem-TOMAS during Winter Haze in Nanjing, China

Benjamin Foreback[1,2,3], Lukas Pichelstorfer[4,1], Rima Baalbaki[5,1], Haitong Zhang[1,2], Ximeng Qi[6], Lauri Franzon[7], Freja F. Østerstrøm[3], Petri Clusius[1,2], Taiwo Ashu[2,8], Matti Rissanen[7,9], Jessica Haskins[10], Carlton Xavier[10], Alexander Mahura[1], Zihao Fu[1,11], Metin Baykara[12,1,2], Xuguang Chi[13], Tom V. Kokkonen[1,6], Zhi-Song Liu[2,8], Aijun Ding[6,13], and Michael Boy[1,2,8]

[1]Institute of Atmospheric and Earth System Research (INAR), University of Helsinki, 00560 Helsinki, Finland
[2]Atmospheric Modelling Centre Lahti, Lahti University Campus, 15140 Lahti, Finland
[3]Department of Environmental Science, Aarhus University, 4000 Roskilde, Denmark
[4]pi-numerics, Neumarkt am Wallersee 5202, Austria
[5]Climate and Atmosphere Research Center (CARE-C), The Cyprus Institute, 2121, Nicosia, Cyprus
[6]Nanjing-Helsinki Institute in Atmospheric and Earth System Sciences, Nanjing University, Suzhou 215163, China
[7]Department of Chemistry, University of Helsinki, 00014 Helsinki, Finland
[8]Computational Engineering, School of Engineering Science, Lappeenranta-Lahti University of Technology (LUT), 53851 Lappeenranta, Finland
[9]Aerosol Physics Laboratory, Tampere University, 33720 Tampere, Finland
[10]Department of Atmospheric Sciences, University of Utah, Salt Lake City, UT 84112, USA
[11]State Key Laboratory of Regional Environment and Sustainability, International Joint Laboratory for Regional Pollution Control, Ministry of Education (IJRC), College of Environmental Sciences and Engineering, Peking University, Beijing 100871, China
[12]Climate and Marine Sciences Department, Eurasia Institute of Earth Sciences, Istanbul Technical University, Maslak, Istanbul, 34469, Türkiye
[13]School of Atmospheric Sciences, Nanjing University, Nanjing 210093, China

Correspondence: Benjamin Foreback (benjamin.foreback@helsinki.fi)

Abstract. Chemical transport models (CTMs) often underestimate secondary organic aerosols, especially during severe haze events. Recent research has shown that autoxidation is a key pathway for rapid organic aerosol (OA) growth, yet few studies to date have attempted to implement this mechanism into large-scale models. This study implemented an aromatic autoxidation mechanism (AAM) produced by the automated mechanism generator, autoAPRAM-fw, into the global CTM, GEOS-Chem, coupled with the TwO-Moment Aerosol Sectional (TOMAS) module, representing one of the first implementations of such a mechanism into a large-scale model. We compared simulations with and without the AAM to measurements in Nanjing, China during winter haze in early 2023. Results demonstrated that the AAM increased modelled OA mass by 3.94 μg/m^3 (12%), reducing the gap between modelled and measured OA. Furthermore, modelled particulate nitrate and ammonium, which were overestimated by GEOS-Chem in China, decreased after introducing the AAM, reducing the bias. These two impacts had an offsetting effect over Nanjing, limiting the AAM's net influence on fine particulate matter ($PM_{2.5}$) mass. The autoxidation chemistry, especially the offsetting effect, was particularly sensitive to NO_x concentration. The AAM produced higher particle number concentrations in the smallest size ranges and improved 3–10 nm particle growth rates when compared

https://doi.org/10.5194/egusphere-2026-6854
Preprint. Discussion started: 19 November 2026
© Author(s) 2026. CC BY 4.0 License.

to the measurements. We additionally ran a sensitivity test with 50% reduced aromatic VOC emissions, which reduced $PM_{2.5}$ but did not significantly affect ultrafine particle number concentration. This demonstrates that under high-haze conditions, lower condensation sink offsets aromatic vapour reductions, favouring ultrafine particle growth.

1 Introduction

Air pollution is one of our society's greatest global health challenges. Over 99% of the world's population breathes unhealthy air, and air pollution is responsible for over 6 million premature deaths annually (WHO, 2025; Lelieveld et al., 2020). Within the Chinese context, more than one million annual deaths are attributed to poor air quality (Tang et al., 2022; Kulmala, 2015; Xie et al., 2019). Air pollution also has substantial economic consequences, such as healthcare costs and loss of working time (Xie et al., 2019; OECD, 2016).

Although China has significantly improved its air quality through comprehensive emission control policies in recent years, severe haze remains a challenge in Chinese megacities (Kang et al., 2025; Jiang et al., 2025). Therefore, characterising and understanding the formation pathways of particulate matter (PM), especially fine particulate matter with particle diameters 2.5 micrometers or smaller ($PM_{2.5}$), including understanding aerosol composition, particle size distribution, and growth, is a critical field of study for protecting human health in China and beyond (Kulmala, 2025; Meng et al., 2026).

Previous studies (e.g., Gao et al., 2022; Sokhi et al., 2022; Zhang et al., 2021; Saide et al., 2020) have examined regional and large-scale air quality models and chemical transport models (CTMs) and compared various air quality parameters, including aerosol optical depth, dust, sea salt, and PM. They found that in general, the models tend to underestimate air quality parameters, especially during haze periods. In particular, CTMs, including GEOS-Chem, are known to underestimate secondary aerosols (Hodzic et al., 2016; Pai et al., 2020; Fu et al., 2023; Chen et al., 2026; Miao et al., 2026), especially in China (Li et al., 2023a). Thus, improving regional and large-scale models for air quality studies, especially in haze-prone regions, is an area of active research.

In megacity environments, when there are high concentrations of atmospheric particles, the growth of small particles during new particle formation (NPF) events is generally thought to be inhibited by pre-existing aerosol loadings, which can reduce the number of clusters, small particles, and vapour molecules available for NPF (Tuovinen et al., 2021; Peräkylä et al., 2020). This can affect air quality, particle size distribution, and lifetime of pollutants. In China, aerosol loadings are often very high, notably during winter haze conditions, which would imply that ultrafine particle growth would be less prominent. However, recent studies (e.g., Kulmala et al., 2017; Du et al., 2022; Deng et al., 2020, 2021) demonstrate that NPF events and small particle growth can still occur even under high pre-existing aerosol conditions, such as those observed in northern and eastern China. In parallel, studies have reported that concentrations of anthropogenic VOCs, particularly benzene and other aromatic species, are substantially higher in China than in many other regions (Mozaffar and Zhang, 2020; Zhang et al., 2017). Considering that aromatic precursors play a significant role in ultrafine particle dynamics and growth (Chen et al., 2024; Foreback, 2025), these findings together highlight the need to represent the chemical and physical processes involving aromatic compounds when investigating and modelling urban air quality.

https://doi.org/10.5194/egusphere-2026-6854
Preprint. Discussion started: 19 November 2026
© Author(s) 2026. CC BY 4.0 License.

Aromatic pollutants, which include benzene, toluene, ethylbenzene, xylenes (collectively BTEX), and trimethylbenzene (TMB), are known for their toxicity and carcinogenic properties, and they cause a significant health and environmental hazard in urban environments (Yu et al., 2022a; Montero-Montoya et al., 2018; Miri et al., 2016; Loomis et al., 2017; Mozaffar and Zhang, 2020). Sources of these aromatic compounds include vehicle emissions, fuel evaporation, coal combustion, petrochemical industries, paints and solvents, incomplete burning of wood, and industrial processes (Yu et al., 2022a; Zhao et al., 2020; Montero-Montoya et al., 2018; Miri et al., 2016). In North and East China, aromatic emissions from vehicles are especially prevalent during winter months when engine cold starts are common (Yu et al., 2022a; Zhong et al., 2026).

In addition to their direct toxicological effects, aromatic volatile organic compounds (VOCs) are precursors to the formation of $PM_{2.5}$ in the atmosphere (Mozaffar and Zhang, 2020). $PM_{2.5}$ is a hazard to human health because it can penetrate deep into the human lungs and enter the bloodstream, leading to cardiovascular diseases, strokes, and respiratory illness (WHO, 2024). Moreover, ultrafine particles, which have diameters less than 100 nm, most easily pass through the lungs and enter the bloodstream (Lelieveld et al., 2026; Kwon et al., 2020). Given the prominent role of aromatics in the ultrafine aerosol budget, quantifying their contribution to particle formation and growth is essential for understanding and mitigating these health risks.

One emerging subject in urban air quality research is complex peroxy radical chemistry and the role of autoxidation of VOC oxidation products—especially those from aromatic VOCs—in particle formation and growth in the atmosphere, thereby enhancing secondary organic aerosol (SOA) formation and growth (Ehn et al., 2014; Rissanen et al., 2014; Bianchi et al., 2019; Iyer et al., 2023; Barua et al., 2026). Atmospheric autoxidation is a sequential reaction chain starting with VOCs oxidising in the atmosphere to form carbon-centred radicals that quickly transform to peroxy radicals (RO_2) by adding ambient O_2. Then, the radicals undergo one or more intramolecular hydrogen shifts or molecular carbon structure rearrangements, after which oxygen can rapidly attach to form a further oxidised peroxy radical. Alternatively, a peroxy radical can react with NO to form an alkoxy radical (RO), which can likewise undergo autoxidation (Wang et al., 2021; Barua et al., 2026). Ultimately, this process can form multi-functionalised species, among which are highly oxygenated organic molecules (HOMs), which often are products of extremely low vapour pressure. HOMs have the potential to rapidly condense on existing particles, and they can also be involved in NPF (Ehn et al., 2014; Bianchi et al., 2019; Peräkylä et al., 2020). Therefore, it is important to consider the process of autoxidation when modelling air quality and PM pollution.

Some recent studies have examined autoxidation of biogenic peroxy radicals in atmospheric models. For example, Roldin et al. (2019) introduced the Peroxy Radical Autoxidation Mechanism (PRAM) for biogenic VOCs and applied the mechanism to the Lagrangian model for Aerosol Dynamics, gas and particle phase CHEMistry and radiative transfer (ADCHEM). Xu et al. (2022) implemented a semi-explicit scheme for monoterpene-derived peroxy radical autoxidation and accretion product formation in GEOS-Chem. Shao et al. (2024, 2026) incorporated autoxidation processes of biogenic VOCs in the Community Earth System Model (CESM). Recently, Shi et al. (2026) developed a semi-explicit mechanism for autoxidation of the β-Caryophyllene sesquiterpene. These studies showed improvement in the chemistry and particle formation in the respective models when accounting for the autoxidation processes. However, these studies primarily focused on processes related to biogenic VOCs rather than autoxidation of aromatic-based compounds.

https://doi.org/10.5194/egusphere-2026-6854
Preprint. Discussion started: 19 November 2026
© Author(s) 2026. CC BY 4.0 License.

While biogenic VOCs play a major role in the global SOA budget, anthropogenically emitted aromatic VOCs are also important in global SOA formation and budgeting (Bates et al., 2021; Mayhew et al., 2025). In urban environments, recent modelling research indicates aromatic autoxidation-to-HOM chemistry may substantially contribute to local and regional aerosol formation and growth, but many of the mechanistic drivers in polluted urban regimes remain unresolved (Fu et al., 2023; Yang et al., 2026; Zhang et al., 2023). These currently unaccounted for chemical pathways are likely causing an underestimation of modelled nucleation and growth rates in urban areas (Wang et al., 2017), which has a consequential impact on modelling both air quality and climate effects of anthropogenic aerosols, and it is an area for improvement in atmospheric modelling (Chen et al., 2026; Yang et al., 2026).

So far, a number of studies have investigated the aromatic autoxidation process from a theoretical and experimental standpoint (e.g., Wang et al., 2017; Molteni et al., 2018; Garmash et al., 2020; Iyer et al., 2023; Barua et al., 2026; Ojala et al., 2026; Le Bayon et al., 2026). However, very few studies to date have attempted to develop these chemical mechanisms in atmospheric models, especially large-scale models, likely in part because such mechanisms can become exponentially large, leading to heavy computational and technical burden (Ervens et al., 2024). An example of recent work on the subject includes Mielczarek et al. (2017), which developed a detailed chemical mechanism for liquid-phase autoxidation of toluene. Tsiligiannis et al. (2019) used a kinetic box model to demonstrate autoxidation reactions related to TMB. Using a recently developed box model, Fu et al. (2026) showed that the aerosol-forming impact of autoxidation of polycyclic aromatic hydrocarbons can offset reductions in primary emissions from solid fuels in China, especially in low-NO environments. In terms of large-scale modelling, Mayhew et al. (2025) recently demonstrated the global significance of peroxy radical reactions on SOA loading in GEOS-Chem, although this study did not explicitly model the autoxidation pathway from aromatic VOC precursors.

In the context of applied, multi-scale atmospheric models, Pichelstorfer et al. (2024) introduced a novel automated reaction mechanism generator called the Automated Alkoxy/Peroxy Radical Autoxidation Mechanism Framework (autoAPRAM-fw). This framework is used to generate Kinetic PreProcessor (KPP)-based autoxidation chemistry mechanisms that can be used in regional and large-scale models. When tested with benzene in ADCHEM over the Copenhagen–Malmö metropolitan area in April 2021, the new chemistry mechanism substantially improved the aerosol dynamics and SOA formation. This mechanism was expanded to include additional aromatics and was used in Foreback et al. (2025), which applied a Lagrangian modelling framework to investigate the formation and transport of pollutants during a severe haze episode in Beijing. This modelling system was evaluated with and without aromatic autoxidation in Foreback (2025), and when the aromatic autoxidation mechanism from autoAPRAM-fw was included in the model, there was a substantial improvement to the modelled representation of NPF events, including an enhancement of sub-30 nm particles and an order-of-magnitude increase in 3–10 nm growth rates. This demonstrates the importance of considering this chemical mechanism in air quality modelling, especially as a pathway to SOA formation during poor air quality conditions when there are high concentrations of aromatic VOCs that are precursors to secondary aerosols.

In this study, we focus on the role of aromatic autoxidation in chemical and aerosol modelling in the global CTM, GEOS-Chem, with an emphasis on air quality in the megacity of Nanjing in the Yangtze River Delta (YRD) of eastern China. We ran GEOS-Chem during the winter in early 2023, when eastern China experienced several haze periods (Chen et al., 2025a). We

https://doi.org/10.5194/egusphere-2026-6854
Preprint. Discussion started: 19 November 2026
© Author(s) 2026. CC BY 4.0 License.

then compared results from the model to observations at a comprehensive measurement site known as the Station for Observing Regional Processes of the Earth System (SORPES) in Nanjing (Ding et al., 2016). By testing the model with and without the aromatic autoxidation mechanism (AAM) produced by autoAPRAM-fw and evaluating the results with station measurements, we can demonstrate the significance of the aromatic autoxidation process.

GEOS-Chem is a three-dimensional, community-developed CTM (Bey et al., 2001), driven by assimilated meteorological fields from NASA's Goddard Earth Observing System (GEOS) framework, such as the Modern-Era Retrospective analysis for Research and Applications, Version 2 (MERRA-2) datasets (NASA GMAO, 2025). The model has been widely applied to investigate air quality, atmospheric oxidation chemistry, aerosol–climate interactions, and atmospheric composition across a range of spatial and temporal scales (Yang et al., 2023; Keller and Evans, 2019; Eastham et al., 2018; Westervelt et al., 2013; Pye and Seinfeld, 2010). Like with other regional and large-scale CTMs, GEOS-Chem generally underestimates organic aerosols, along with total PM. However, overestimation of nitrate and ammonium aerosol, especially over Asia, is a known issue in GEOS-Chem, likely in part because the formation processes are not accurately represented in the model (Norman et al., 2025). In addition to investigating the impacts of aromatic autoxidation on urban SOA, this study evaluates the AAM's effects on these inorganic aerosol compounds.

Although this study focuses on a megacity in the YRD region of China, the modelling framework, chemical mechanism, and insights presented here are broadly applicable to other densely populated urban areas with elevated aromatic emissions. This is particularly relevant for rapidly industrialising regions across South Asia, Southeast Asia, and Africa, where severe public health challenges arise from high anthropogenic emissions and subsequent haze pollution (Khoshakhlagh et al., 2024; Xia et al., 2026). This work serves as a proof-of-concept demonstration, showing that explicit autoxidation pathways can be successfully integrated into a large-scale modelling framework, with results quantifying the impacts of the mechanism. This is one of the first studies to evaluate near-explicit aromatic autoxidation chemistry in GEOS-Chem with application to urban air quality. While future iterations may move toward further-reduced or parameterised versions of this chemistry, this study helps reconcile the previously missing aromatic contribution to SOA, bridging the gap between models and observations. Ultimately, the goal is to help improve the representation of aromatic autoxidation chemistry in models, especially in polluted environments and to provide new insight into the dynamics and processes behind urban secondary aerosol formation.

2 Methods

To investigate the role of the aromatic autoxidation process in SOA growth during Chinese haze events, which may partially answer the persistent underestimation of SOA in large-scale models, we have run the GEOS-Chem model coupled with the TwO-Moment Aerosol Sectional (TOMAS) microphysics module, with and without a recently developed aromatic autoxidation mechanism, and we compared the results to measurements in the megacity of Nanjing. Using this framework, we can evaluate the role of aromatic autoxidation as a component of Chinese haze while identifying the strengths and limitations of the GEOS-Chem-TOMAS framework, as well as large-scale models in general, for simulating Chinese urban haze.

https://doi.org/10.5194/egusphere-2026-6854
Preprint. Discussion started: 19 November 2026
© Author(s) 2026. CC BY 4.0 License.

2.1 Modelling Setup

In this study, we started with an out-of-the-box (without modification) simulation from GEOS-Chem, including full chemistry and the 40-bin TOMAS aerosol module as a control case. To assess the role of aromatic autoxidation processes in particle and haze formation, we then integrated an aromatic autoxidation mechanism (AAM) generated by autoAPRAM-fw (Pichelstorfer et al., 2024) into GEOS-Chem's full chemistry as an experimental case. The experimental setup includes condensation of terminal species produced by the AAM into TOMAS's organic aerosol bins. Additionally, using the AAM in the model, we simulated a hypothetical case where emissions of aromatic precursor VOCs over Asia were reduced by 50% to further investigate the impact of the aromatic species in the model. An overview of the modelling cases is described in Table 1. Details on the computing architecture, setup, and benchmarking are available in Appendix A.

Table 1. Model configurations and experimental cases for the GEOS-Chem simulations.

Case	Chemical configuration	Description
Control	fullchem	Standard out-of-the-box GEOS-Chem v. 14.6.3 with the 40-bin TOMAS module.
AAM	fullchem + AAM	Implementation of the aromatic autoxidation mechanism (AAM) merged with fullchem, and condensation in TOMAS.
AAM, Reduced Aromatic Emissions	fullchem + AAM	Sensitivity test with a 50% reduction in aromatic precursor emissions to evaluate haze response.

2.1.1 GEOS-Chem-TOMAS

In this study, we used GEOS-Chem version 14.6.3 (Bey et al., 2001; The International GEOS-Chem User Community, 2025) with MERRA-2 meteorology. The model setup included full chemistry (fullchem) and the 40-bin TOMAS aerosol microphysics module, which discretizes the aerosol size distribution of organic aerosols (OA), elemental carbon (EC), sulfate, dust, and sea salt into 40 sectional, mass-doubling particle size bins ranging from approximately 1 nm to 10 µm in diameter (Kodros and Pierce, 2017; Trivitayanurak et al., 2008). TOMAS provides detailed aerosol size resolution, offering the ability to compare to PM_1 (particulate matter less than 1 µm in diameter) composition measurements, and particle number size distribution (PNSD) simulations to comprehensive PNSD measurements. To calculate emissions, GEOS-Chem uses the Harmonized Emissions Component (HEMCO) driver (Lin et al., 2021). The nucleation scheme uses the Vehkamäki et al. (2002) binary and Napari et al. (2002) ternary parameterisations.

We ran the model globally with $2^\circ \times 2.5^\circ$ resolution, along with a $0.5^\circ \times 0.625^\circ$ nest over Asia, which was defined using the "Asia" domain option in the CreateRunDir script. Originally implemented and described by Wang et al. (2004), this nested domain ranges from 11° S through 55° N latitude and 60° through 150° east longitude, which covers much of the Asian conti-

https://doi.org/10.5194/egusphere-2026-6854
Preprint. Discussion started: 19 November 2026
© Author(s) 2026. CC BY 4.0 License.

nent, including East, South, and Southeast Asia. We used 47 vertical levels in both the global and nested runs and ran one year of spin-up before the analysis period. The global run used time steps of 10 minutes for transport and 20 minutes for chemistry, while the nest used 5-minute transport and 10-minute chemistry time steps. Hourly averages of mass composition, chemical concentrations, and aerosol properties from TOMAS, including SOA production rate, were saved to the output collections. Additionally, PNSD was saved at 10-minute resolution on selected NPF event days for detailed analysis of growth rates.

GEOS-Chem considers nitrate and ammonium as bulk aerosol throughout the model, and TOMAS does not discretize them into size bins. Because these aerosols generally remain primarily in the accumulation mode size range, and PM_1 is considered to represent 70–75% of the PM_{10} during the wintertime in Nanjing and surrounding areas (Jiang et al., 2019; Chen et al., 2021; Xue et al., 2014), we applied a scaling factor of 70% to the simulated nitrate and ammonium to approximate the PM_1/PM_{10} fraction.

2.1.2 The autoAPRAM framework

AutoAPRAM-fw was developed as an efficient method to generate gas-phase autoxidation reaction mechanisms for VOCs. Designed to bridge the gap between initial oxidation and SOA formation, autoAPRAM-fw utilizes a near-explicit approach to model the complex series of reactions. The framework operates primarily through two core submodules. The first is autoReactions, which calculates the requisite reaction pathways and outputs a Fortran-readable chemistry scheme. To estimate reaction rate coefficients and branching ratios, autoReactions iteratively matches simulated mass spectra with experimental high-resolution data from nitrate chemical ionization mass spectrometry (i.e., nitrate-CIMS), yielding optimized potential solutions for the chemical pathways. The second submodule is autoSMILES, which predicts and tracks the specific molecular structures of the reaction products based on the suggested peroxy radical structures. By automating the generation of these extensive reaction mechanisms, autoAPRAM-fw enables a robust, scalable representation of intermediate species, facilitating their direct integration into atmospheric and chemical transport models.

As input, autoAPRAM-fw takes in the peroxy radical (RO_2) names and chemical compositions from the Master Chemical Mechanism (MCM), which provides a near-explicit, detailed representation of the gas-phase tropospheric oxidation of over 140 VOCs (Jenkin et al., 1997, 2003; Saunders et al., 2003; Bloss et al., 2005). Although MCM includes oxidation of aromatic VOCs, it does not include the autoxidation processes involved with these species (Wang et al., 2020b; Mehra et al., 2020). In addition to species defined in MCM, autoAPRAM-fw can accept user-defined RO_2 names and compositions. For this study, the chemical mechanistic information and species definitions were taken from MCM v3.3.1, via the MCM website, http://mcm.york.ac.uk. The output from autoAPRAM-fw is a KPP definition file representing the AAM, which has been integrated into GEOS-Chem. Details on the scheme generation and quantifications of rate coefficients therein can be found in Pichelstorfer et al. (2024).

In Pichelstorfer et al. (2024), autoAPRAM-fw was used to generate the autoxidation chemistry for benzene, which was tested in the ADCHEM model. An updated scheme, which included additional aromatics VOCs from MCM, was developed using autoAPRAM-fw and evaluated in Foreback et al. (2025) during a late autumn haze episode in Beijing using the Lagrangian FLEXPART-SOSAA modelling system (Clusius et al., 2026).

https://doi.org/10.5194/egusphere-2026-6854
Preprint. Discussion started: 19 November 2026
© Author(s) 2026. CC BY 4.0 License.

The mechanism developed in this study accounts for BTEX and TMB, representing some of the most dominant aromatic compounds in urban atmospheres globally (e.g., Liu et al., 2025; da Rocha et al., 2023; Hu et al., 2015; Słomińska et al., 2014), with particularly high prevalence and relevance in China (Mozaffar and Zhang, 2020; Barletta et al., 2005). After toluene, ethylbenzene, xylene, and trimethylbenzene, undergo initial oxidation reactions, the HOM formation follows a nearly identical autoxidation pathway as the benzene scheme due to structural similarity to the benzene-based peroxy radicals. Highly reactive but lower-abundance species, such as styrene, were not included in this pilot study.

Merging this chemistry scheme into GEOS-Chem allows us to understand in detail how autoxidation of aromatics impacts SOA formation and air quality. The schematic in Fig. 1 summarises the most relevant chemical pathways in the AAM, starting with initial BTEX and TMB oxidation and ultimately ending in HOM formation, which is then passed into TOMAS (see Sect. 2.1.5) and condensed into SOA. After initial formation of RO_2/RO radicals, the radicals can undergo multiple H-shifts during the process. The mechanism also consists of HO_x recycling reactions, such as unimolecular decomposition of the RO_2/RO, which eliminates a radical (typically OH). These radicals can be recycled back into the mechanism and therefore introduce competing reactions to autoxidation by driving subsequent oxidation cycles. In addition to unimolecular decomposition, reactions with NO_x is a potential termination pathway for RO_2/RO radicals, which is especially relevant in high NO_x conditions (Zhang et al., 2023; Wu et al., 2026).

2.1.3 Chemical mechanism reduction

Before merging the AAM into GEOS-Chem's fullchem scheme, a mechanism reduction was performed on the AAM for computational feasibility. First, the reduction entailed lumping intermediate closed-shell isomers into representative species. By lumping these structural isomers, we significantly reduced the number of transported tracers and differential equations in GEOS-Chem without compromising the total organic mass tracked by the model. This step of lumping the closed-shell isomers reduced the mechanism size by approximately 40%. This simplification is justified by the fact that structural isomers within a single chemical class often exhibit similar atmospheric fates and volatility profiles. To preserve the radical chemistry, this lumping does not include peroxy and alkoxy radicals, which ensures that the chemical kinetics of the autoxidation process, such as unimolecular hydrogen shifts versus bimolecular reactions with NO_x or HO_2, are accurately represented. Maintaining this distinction also ensures that alkoxy radicals are not inadvertently lumped as peroxy radicals and vice-versa, which is important considering that RO and RO_2 are different classes of species with different reactivities.

Next, MCM species names (used by autoAPRAM-fw) were mapped to GEOS-Chem names. This step included lumping multiple isomers of xylene and TMB into a single tracer for each. To reconcile the isomeric differences in reaction rates for xylene oxidation in the lumped XYLE tracer, we applied a weighted-average rate constant. We assumed an isomer ratio of 2:1 for m-xylene to o-xylene and 2:1 for p-xylene to o-xylene, a value consistent with extensive urban measurements across China (Barletta et al., 2005). For TMB, we assumed a relative abundance of 60% (1,2,4-TMB), 30% (1,3,5-TMB), and 10% (1,2,3-TMB), based on urban concentration ratios (Barletta et al., 2005) and global emission inventories (Harley and Cass, 1995; Chen et al., 2014). The mapping of MCM species names to GEOS-Chem names in this work is similar to and has been

https://doi.org/10.5194/egusphere-2026-6854
Preprint. Discussion started: 19 November 2026
© Author(s) 2026. CC BY 4.0 License.

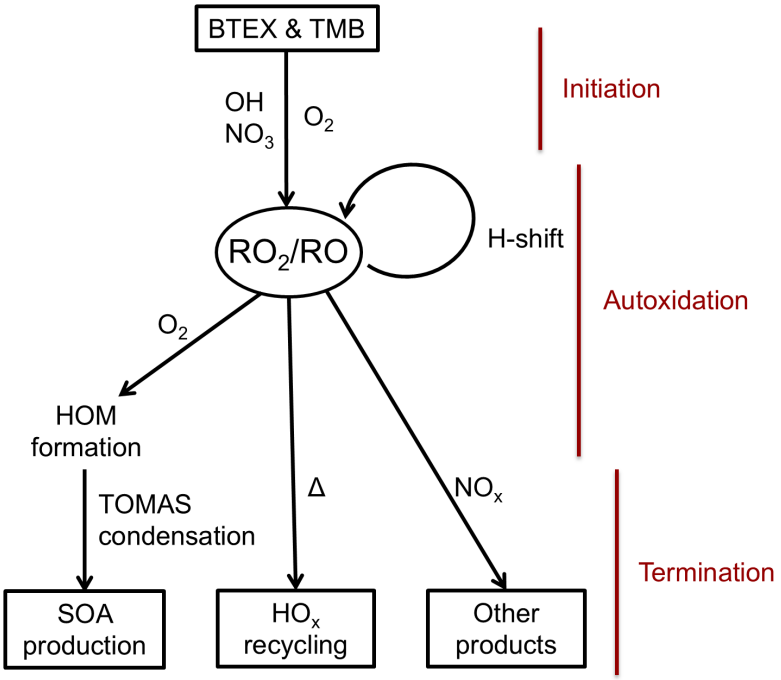


Figure 1. Schematic of the novel aromatic autoxidation mechanism (AAM) generated by autoAPRAM-fw for BTEX+TMB, integrated into GEOS-Chem and coupled with TOMAS. This includes the initial oxidation, one or more hydrogen shifts on the radical, followed by potential termination pathways: 1.) the formation of HOM species through addition of oxygen, which are then condensed in TOMAS to form SOA; 2.) unimolecular decomposition involving the separation of a HO_x radical, which can be recycled in the atmospheric chemical processes; and 3.) reaction with NO_x, forming non-HOM products. Note that this figure shows three of the most significant chemical pathways in the context of this study, but these are not the only possible chemical pathways for the RO_2/RO species.

cross-referenced with Mayhew et al. (2025), ensuring consistency with current literature while extending GEOS-Chem's full chemistry scheme to include autoxidation of peroxy radicals from BTEX+TMB.

Lastly, we lumped the AAM's terminal species into two volatility classes (Donahue et al., 2012). One class is low-volatility organic compounds (LVOC), and for purposes of this study, extremely low volatility organic compounds (ELVOC) are included in the LVOC category. The second class is semi-volatile organic compounds (SVOC). The volatility class was determined by vapour pressure, using the thresholds and methodology described in Stolzenburg et al. (2022). Mass balance was preserved by mapping individual species to their respective bins using the molecular weight ratio $MW_{species}$ / $MW_{volatility_class}$ as a stoichiometric multiplier, ensuring that the total mass of condensable vapour remains constant despite the reduction in chemical complexity. For simplicity in coupling tracers between GEOS-Chem and TOMAS, the lumped LVOC values concentrations were passed into TOMAS as a single tracer (with variable name AUTOAPRAM_LVOC), and the same was done for SVOCs (with variable name AUTOAPRAM_SVOC). In GEOS-Chem's species database, which includes information passed through the coupler to TOMAS, we used a representative molecular weight of $MW_{volatility_class} = 350$ g/mol for AUTOAPRAM_LVOC

https://doi.org/10.5194/egusphere-2026-6854
Preprint. Discussion started: 19 November 2026
© Author(s) 2026. CC BY 4.0 License.

and AUTOAPRAM_SVOC and ensured this value was used consistently throughout the chemical mechanism and aerosol module.

To ensure the chemical accuracy of the lumping methodology, the chemical mechanism reduction was validated using ARCA-box (Clusius et al., 2022) under different temperatures and NO_x conditions. This validation is explained in further detail in Appendix B.

2.1.4 Integration into GEOS-Chem as custom chemistry

For the AAM case, we merged GEOS-Chem's fullchem scheme with the AAM using the "Create Chemistry Scheme" tool provided in ARCA-box, which generates a combined KPP-based chemistry scheme usable in GEOS-Chem. In cases where duplicate reactions existed between GEOS-Chem's full chemistry mechanism and the AAM, the rates from the AAM were chosen to maintain consistency in the mechanism used in this study.

The aromatic oxidation pathways that previously existed in GEOS-Chem's fullchem for BTEX & TMB were replaced by the AAM. This avoids the concern that condensing gases could be double counted in the gas-to-particle processes in TOMAS. Because the AAM does not include styrene, the oxidation pathway of styrene from the fullchem was left intact.

In order to reduce computational demands, radical species and short-lived intermediates with significantly shorter lifetimes compared to the model transport time step were excluded from the list of advected species. Because many of the radical species have atmospheric lifetimes ranging from a fraction of a second to less than a minute (Bianchi et al., 2019; Zhang et al., 2024a; Harb et al., 2025), we assume that they are not transported outside of the grid box in which they are formed. This simplification is necessary because the computational and memory overhead of this framework is primarily limited by the number of advected tracers rather than the number of chemical reactions.

2.1.5 Condensation in TOMAS

In this implementation, the LVOC and SVOC variables (named AUTOAPRAM_LVOC and AUTOAPRAM_SVOC, respectively) are passed through the coupler between GEOS-Chem and TOMAS. The coupler automatically converts the concentrations into units of mass per grid box, and the mass is then condensed in the TOMAS module using the EZCOND subroutine, which is a wrapper to TMCOND that assumes the species fully condenses under typical atmospheric conditions. Because the given mass is assumed to condense onto existing aerosol surfaces in TOMAS, this step is done immediately after the sulfate nucleation and condensation subroutine (named COND_NUC) is called within each time step. This means that the mass is condensing onto freshly nucleated particles, along with the updated surface area following condensation in COND_NUC. The SVOC and LVOC condensation is allocated to the organic aerosol bins. Since this study is focused on condensational growth, we did not implement additional nucleation, nor did we modify the existing nucleation scheme. This methodology follows the existing framework of TOMAS, described in D'Andrea et al. (2013) and Pierce and Adams (2009).

For this case study, we assume that the LVOC (including ELVOC) species have low enough volatility that 100% of the mass condenses each time step. In the species database, we assigned a Henry's law volatility constant (H_{CR}) of $12,000$ K and a Henry's Law solubility constant (H_0) of 1.0×10^{14} M atm^{-1}. Given the high degree of oxygenation in these species, these

https://doi.org/10.5194/egusphere-2026-6854
Preprint. Discussion started: 19 November 2026
© Author(s) 2026. CC BY 4.0 License.

values are consistent with the upper-end estimates of HOM species, and in this case, they are assumed to be effectively non-volatile and nearly infinitely soluble in the aqueous phase (Sander, 2023; Poulain et al., 2022; Knote et al., 2015; Hodzic et al., 2014).

For the SVOC species, we assumed a gas-to-aerosol partitioning of 70%, based on previous literature in GEOS-Chem (Pye and Seinfeld, 2010) and literature specific to China (Chen et al., 2025b; Huang et al., 2024a). Using this fixed value, rather than adding and compiling additional information to the coupler between GEOS-Chem and TOMAS, ensures the model remains computationally manageable and simplifies the model configuration to avoid unnecessary overhead. For SVOCs, we chose somewhat more conservative representative properties, setting H_{CR} to $6,000$ K and H_0 to 1.0×10^5 M atm^{-1}. These properties align with typical parameterisations used for semi-volatile gas-phase SOA precursors in regional and global models (Hodzic et al., 2014; Knote et al., 2015; Pye and Seinfeld, 2010).

We assume dry deposition to be true for both the SVOC and LVOC species, although due to the short-lived nature of these species, this is likely insignificant. To maintain computational efficiency, we did not include wet deposition for these species. As with dry deposition, we believe this is not significant, notably in Nanjing, due to the short-lived nature of the species and the fact that very little precipitation was measured during the study period. The representative SVOC species was added to the list of transported species, but because the LVOC species condenses completely at each time step and is therefore not transported, it was not added to the advected species list.

2.1.6 Reduced aromatic VOC emission scenario

To evaluate the sensitivity of the updated model to aromatic precursors and to further demonstrate the impact of the newly implemented chemistry on particle formation and growth, we conducted an emission sensitivity test. In this experiment, emissions of BTEX & TMB were reduced by 50% over the Asia domain. This reduction was defined directly in the HEMCO configuration file.

2.2 SORPES measurement site

This study evaluates the AAM using ambient observations from SORPES, an urban background station located in northeastern Nanjing, situated along the lower Yangtze River in eastern China, approximately 250 km west of Shanghai (Ding et al., 2016). Nanjing is a city of over 9 million residents in the heart of the YRD region, which frequently experiences the impact of urban and regional air pollution and haze (Sun et al., 2020). In collaboration between the University of Helsinki and Nanjing University, the station was constructed in 2011 at the Xianlin Campus of Nanjing University (32°07'14"N, 118°57'10"E) and has since collected continuous measurements to study air quality, Earth-atmosphere interactions, and air pollution–climate interactions (Niu et al., 2026; Ding et al., 2016). Nanjing University is a core member of the Pan-Eurasian Experiment (PEEX), and GEOS-Chem is part of the PEEX Modelling Platform (Lappalainen et al., 2022; Mahura et al., 2024). With comprehensive measurements of aerosol size distribution and composition, this station is ideal for providing a rigorous dataset to evaluate the AAM in GEOS-Chem-TOMAS.

https://doi.org/10.5194/egusphere-2026-6854
Preprint. Discussion started: 19 November 2026
© Author(s) 2026. CC BY 4.0 License.

Ambient aerosol mass, chemical composition, and PNSD were characterised using a suite of high-temporal-resolution instruments stationed at the SORPES site. Measurements of $PM_{2.5}$ mass concentration were obtained using a Synchronized Hybrid Ambient Real-time Particulate (SHARP; Thermo Scientific Model 5030) monitor, which combines beta-ray attenuation with light-scattering methods to continuously determine particulate mass loadings (Shen et al., 2018). Chemical composition, including organic aerosol (OA), sulfate, nitrate, ammonium, and chloride was measured using a Long-Time-of-Flight Aerosol Mass Spectrometer (LTOF-AMS; Aerodyne Research Inc.) with a PM_1 lens (Liu et al., 2026; Dou et al., 2025). To characterise particle size distributions and capture early-stage NPF events, a Differential Mobility Particle Sizer (DMPS) and a Neutral Cluster and Air Ion Spectrometer (NAIS) were included in the analysis. The DMPS monitored PNSD across a diameter range of 6–820 nm (Zhang et al., 2025; Chen et al., 2023; Shen et al., 2018), and the NAIS provided size distributions from 0.8 to 40 nm for naturally charged particles and from ~2 to 40 nm for total (naturally charged and neutral) particles (Zhang et al., 2024b, 2025).

Meteorological measurements, including temperature, relative humidity (RH), precipitation, and wind speed, were obtained from a Campbell Scientific GRWS1000 weather station at SORPES (Niu et al., 2023; Ge et al., 2022). Boundary layer height (BLH) was measured with a Vaisala CL51 ceilometer situated alongside the weather station (Ge et al., 2022).

2.3 Study period and haze episodes

For this study, we performed the model runs from January 1 through February 15, 2023. Several widespread severe haze episodes occurred in eastern China during this study period, and the region experienced near-continuous elevated PM concentrations (Chen et al., 2025a; An et al., 2023). The following five specific haze episodes were identified and selected for analysis of their origins and chemical composition (dates are inclusive):

I. **January 3–9:** This episode included the highest measured $PM_{2.5}$ during the study period, which was over 150 μg/m^3, on January 9.

II. **January 10–13:** This episode, which began immediately after the termination of the previous episode, was shorter lived without as distinctive of a peak near the end. It was likely terminated by precipitation in the late night on January 13.

III. **January 15–24:** This period includes the Chinese New Year (CNY), which was on January 22. An increase in $PM_{2.5}$ was observed on January 22, but it was likely mitigated by precipitation.

IV. **January 25–February 1:** Compared to the other episodes, measurements showed that this episode had a higher relative fraction of organic aerosols. This episode followed the pattern of gradual buildup followed by rapid termination, described in Zheng et al. (2016), Shen et al. (2020) and Foreback et al. (2025).

V. **February 2–8:** This episode included higher concentrations of inorganic compounds in the PM_1 sizes measured by the LTOF-AMS. The episode also followed the gradual buildup, rapid termination pattern, ending abruptly late on February 8.

https://doi.org/10.5194/egusphere-2026-6854
Preprint. Discussion started: 19 November 2026
© Author(s) 2026. CC BY 4.0 License.

Although there is no universally standard definition of haze, literature generally classifies haze based on reduced visibility (typically less than 10 km) and RH below a certain threshold (e.g., 80% or 90%; Cai et al., 2022; Yang et al., 2016). Alternatively, haze can be defined solely based on PM concentration (Wei et al., 2020). For purposes of this study, we define a haze episode as a period when the 24-hour average $PM_{2.5}$ concentration is greater than 35 μg/m^3, based on the Chinese Ambient Air Quality Standards (Ministry of Ecology and Environment of the People's Republic of China, 2016; Wang et al., 2023b), for three or more consecutive days. For simplicity, we will assume a haze day to be a full day (midnight to midnight local time). Because pollution on January 1-2 is residual from a previous haze episode rather than a full episode within the analysis, it is not mentioned in the list above.

The measurement period includes the Chinese New Year (CNY) on January 22, which is known to cause a sudden increase in PM concentrations due to firework/firecracker emissions (Huang et al., 2024b; Foreback et al., 2022; Kong et al., 2015). Because emission inventories used in the models do not account for sporadic events such as firework celebrations (Seidel and Birnbaum, 2015; Yang et al., 2025), we expect that the models will underestimate pollutant concentrations during the CNY period.

2.4 Calculation of growth rates and condensation sink

Apparent particle growth rates (GR_{app}) were determined over the mobility-diameter range of approximately 3–20 nm using the 50% appearance-time method (Lehtipalo et al., 2014; Stolzenburg et al., 2018). The calculation was based on PNSD measured with the NAIS in positive-particle mode. For each size channel, the increase in particle concentration during the selected growth period was fitted by least squares with a sigmoid function:

$$N(t) = \frac{a}{1 + e^{-b(t - t_{\mathrm{app}})}} \tag{1}$$

where a is the plateau concentration, b describes the steepness of the concentration increase, and t_{app} is the appearance time at which the fitted concentration reaches 50% of its plateau value. The growth period was selected manually to capture the onset and development of the event and to distinguish individual events when multiple growth periods occurred on the same day. The mobility diameter of each size channel was then plotted as a function of t_{app}, and GR_{app} was obtained as the slope of an orthogonal linear regression. The standard error of GR_{app} was estimated from the 95% confidence interval of the fitted slope.

The derived rate is termed "apparent" because the appearance-time method attributes changes in the particle size distribution entirely to condensational growth or shrinkage. Consequently, the estimate may be biased by other aerosol-dynamic processes, particularly coagulation. Additional biases may arise in diameter ranges with strong concentration gradients, especially below 10 nm, where stochastic growth becomes important.

The condensation sink (CS; s^{-1}) was calculated from the DMPS and the modelled PNSD using the following equation:

$$\mathrm{CS} = 2\pi D_{\mathrm{AB}} \sum_i \beta_{m,i} d_{p,i} N_i \tag{2}$$

https://doi.org/10.5194/egusphere-2026-6854
Preprint. Discussion started: 19 November 2026
© Author(s) 2026. CC BY 4.0 License.

where D_{AB} is the temperature- and pressure-dependent binary diffusion coefficient of the condensable vapours in air, $d_{p,i}$ is the midpoint diameter of size bin i, N_i is the number concentration in that bin, and $\beta_{m,i}$ is the transitional correction factor for mass transfer to a sphere (Tuovinen et al., 2021; Westervelt et al., 2013; Dal Maso et al., 2005; Kerminen and Kulmala, 2002).

3 Results and discussion

Results showed an offsetting effect between organic and inorganic aerosol when introducing the AAM. Particle size distribution and growth rates (GR) were also impacted by the AAM. High condensation sink (CS) was observed during the heavy haze conditions, and the additional OA mass resulting from the introduction of the AAM further increased the CS. This led to most of the additional SOA mass from the AAM being added directly to accumulation mode size bins. We found that >99.9% of the SOA mass from the AAM condensed in TOMAS was from LVOC species as opposed to SVOCs. Gas-phase SVOC concentrations remained extremely low, and advective transport out of the domain outpaced their local production. The SVOC/LVOC ratio is discussed in further detail along with the box model validation of the AAM in Appendix B.

To fully understand the effects of introducing the new chemical mechanism, we start with evaluating thes mechanism's impacts in the larger-scale context, looking at the impacts on OA, nitrate, ammonium, and net change in $PM_{2.5}$ over the Asia domain. Then we investigate how the meteorological conditions impacted the haze conditions during the study period. After evaluating the regional and meteorological context of the observed haze, we compare the modelled organic and inorganic aerosols and $PM_{2.5}$ with measurements, followed by analysing the particle size distribution, growth rates, SOA production rate, and condensation sink. Lastly, we examine the effects of the reduced emission sensitivity test.

3.1 Impact of the AAM in the Asia domain

Based on the GEOS-Chem-TOMAS control runs, the highest mean concentrations of OA in the $PM_{2.5}$ size range throughout the study period in the Asia domain are the eastern Indo-Gangetic Plain, the Middle Yangtze River Basin centred around Wuhan, and the North China Plain (NCP) region south of Beijing and northwest of Nanjing (Fig. 2a). When introducing the AAM, the greatest increase is in the Sichuan Basin, centred around the city of Chengdu (Fig. 2b), where the change of OA was almost 7 μg/m^3. The AAM also introduced a significant increase in OA over the Indo-Gangetic Plain, especially over Bangladesh, and throughout eastern China, including the YRD, NCP, Middle Yangtze Basin, and the Pearl River Delta. The increased OA over the Indian Ocean is likely transported from the Indo-Gangetic Plain.

Counteracting the OA increase, the AAM introduced a substantial decrease of nitrate and ammonium aerosols over the southern NCP and over the YRD (Fig. 2c), with a reduction of more than 4 μg/m^3. A slight decrease (~2 μg/m^3) also occurred over the Indo-Gangetic Plain.

Adding these two impacts together shows that net $PM_{2.5}$ increased over much of eastern China and South Asia, but the decrease in inorganic aerosol mass significantly offset the OA mass increase over Nanjing and the greater YRD and NCP regions (Fig. 2d).

https://doi.org/10.5194/egusphere-2026-6854
Preprint. Discussion started: 19 November 2026
© Author(s) 2026. CC BY 4.0 License.

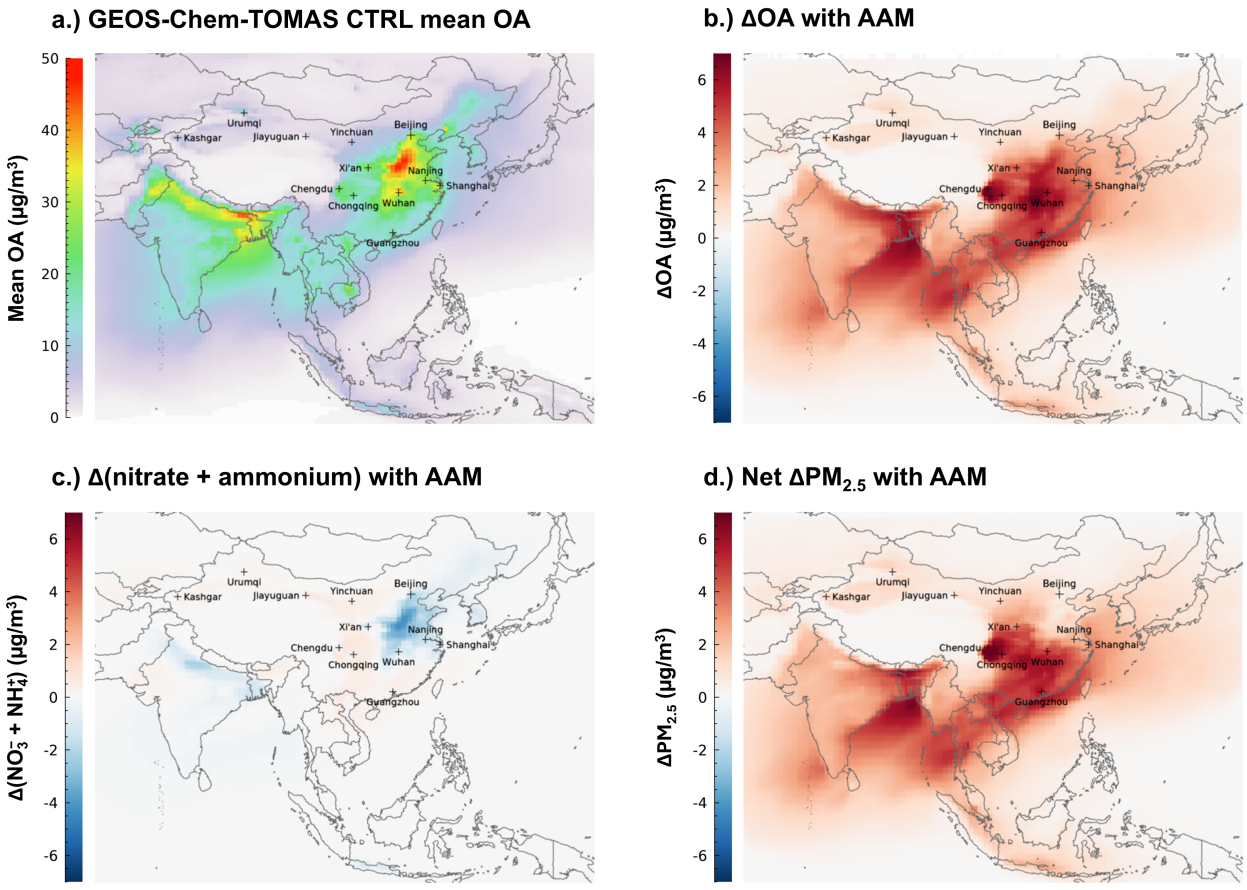


Figure 2. (a) Mean organic aerosol (OA) mass in the $PM_{2.5}$ size range simulated by GEOS-Chem-TOMAS over the Asia domain during the simulation period (January 1–February 15, 2023); (b) change in mean OA mass introduced by the aromatic autoxidation mechanism (AAM); (c) change in mean nitrate and ammonium introduced by the AAM; and (d) net change in mean $PM_{2.5}$ introduced by the AAM.

This offsetting effect is likely explained by the impact that the added autoxidation and HO_x recycling reactions have on the average fate of RO_2 in the simulation. In polluted environments, the major fate of RO_2 is the bimolecular reaction with NO, which either forms an organic nitrate species (R1a) or an alkoxy radical and NO_2 (R1b). The NO_2 may then be involved in the formation of nitric acid (HNO_3) through its reactions with HO_x radicals, which then contributes to nitrate aerosol. The addition of unimolecular RO_2 reactions, i.e. autoxidation (R2), or HO_x recycling (R3 & R4) adds competing pathways, decreasing the formation of NO_2 and thus HNO_3. The recycling reactions of HO_x produced from RO_2 decomposition play an especially important part in this decrease because unlike autoxidation reactions, they do not form RO_2 products, and thus results in a net decrease of RO_2 concentrations. This decrease in modelled RO_2 concentrations due to the addition of unimolecular RO_2 reactions was also observed in a recent work featuring explicit RO_2 autoxidation in 0D box models (Franzon et al., 2026).

https://doi.org/10.5194/egusphere-2026-6854
Preprint. Discussion started: 19 November 2026
© Author(s) 2026. CC BY 4.0 License.



$$\mathrm{RO_2 + NO} \xrightarrow{\alpha} \mathrm{RONO_2} \tag{R1a}$$

$$\xrightarrow{1-\alpha} \mathrm{RO + NO_2} \tag{R1b}$$

$$\mathrm{RO_2} \rightarrow \mathrm{R(O_2)O_2} \tag{R2}$$

$$\mathrm{RO_2} \rightarrow \mathrm{R{=}O + OH} \tag{R3}$$

$$\mathrm{RO_2} \rightarrow \mathrm{R{=}O + HO_2} \tag{R4}$$

In reaction (R1), α is the branching ratio of $RONO_2$, which depends on both the thermodynamic conditions and on the exact chemical composition of the RO_2 (Jenkin et al., 2019). Parametrisations estimating α are present in both GEOS-Chem (e.g., Bates et al., 2021; Fisher et al., 2016) and autoAPRAM-fw (Pichelstorfer et al., 2024). Reactions (R3) and (R4) are examples of HO_x radical recycling reactions. The HO_x radicals produced in these reactions can be recycled into the mechanism's oxidation reactions, or they can react with NO_x in the atmosphere. This combination of newly introduced RO_2 sinks and depletion of NO_x results in both a limitation on OA-forming HOMs—due to the fate of RO_2 through non-HOM-forming pathways, especially in the presence of high NO_x (Zhang et al., 2023)—and lowered nitrate production. At the same time, autoxidation via the alkoxy radical path is activated. Thus, the AAM tends to favour SOA production over nitrate and ammonium production.

Although Norman et al. (2025) suggests that in most atmospheric environments, the formation of organic nitrates should generally have a minor impact on ammonium particle formation in GEOS-Chem, this case study in Nanjing appears to be an exception. As shown in Fig. C1 in Appendix C, the areas with reduced nitrate and ammonium after introducing the AAM correspond precisely with the areas of high NO_x in the YRD and southern NCP regions. In Nanjing, the mean NO concentration during the study period was 6.7 ppb and the mean NO_2 concentration was 20.1 ppb, which is well into the high-NO_x regime.

In ammonia-rich and high-NO_x regimes such as eastern China, ammonium formation can be limited by the availability of nitric acid (Wang et al., 2020a; Shen et al., 2011). Within the AAM, the formation of organic nitrates via $RO_2 + NO \rightarrow RONO_2$ reactions acts as a sink for reactive NO_x, thus limiting HNO_3 production via the $OH + NO_2$ pathway. This lower HNO_3 availability consequently suppresses the formation of NH_4^+. Thus, in the region around Nanjing, more NH_3 stays in the gas phase rather than forming ammonium aerosols in the AAM case compared to the control case (Fig. C2 in Appendix C). This demonstrates that the aerosol processes in the AAM are especially sensitive to NO_x, and these counteracting effects are enhanced in the YRD and NCP regions. This contrasts with the Sichuan Basin, which has high aromatic emissions but lower NO_x (Figures C1 and C3), where the offsetting does not happen when introducing the AAM. Furthermore, the higher NO_x concentrations in the YRD and NCP may reduce the concentration of LVOC and SVOC produced from autoxidation and subsequently condensed in TOMAS compared to lower NO_x areas in China (Yang et al., 2026), aligning with Pichelstorfer et al. (2024), who reported an underestimation of SOA production by this scheme under high-NO_x conditions.

https://doi.org/10.5194/egusphere-2026-6854
Preprint. Discussion started: 19 November 2026
© Author(s) 2026. CC BY 4.0 License.

3.2 Meteorological conditions in Nanjing

Before comparing the modelled and observed results in Nanjing, it is important to understand the local meteorological conditions that occurred at the time. The meteorological conditions measured at SORPES are shown in Fig. 3. Overall, the haze episodes in this study (described in Sect. 2.3) were dry with measurable precipitation mostly between episodes or near the ends of episodes. Relative humidity was below 80% during the buildup phase of the five haze episodes, with higher relative humidity near the ends of II, III, and V. Stagnant conditions, which are defined as periods when wind speed is less than 3.2 m/s (Huang et al., 2017, 2018; Gao et al., 2020), persisted during almost the entirety of the study period; the maximum hourly average wind speed at SORPES was 3.17 m/s. The Chinese New Year experienced roughly 2 mm of precipitation at midnight, which likely mitigated the celebration impacts on air quality.

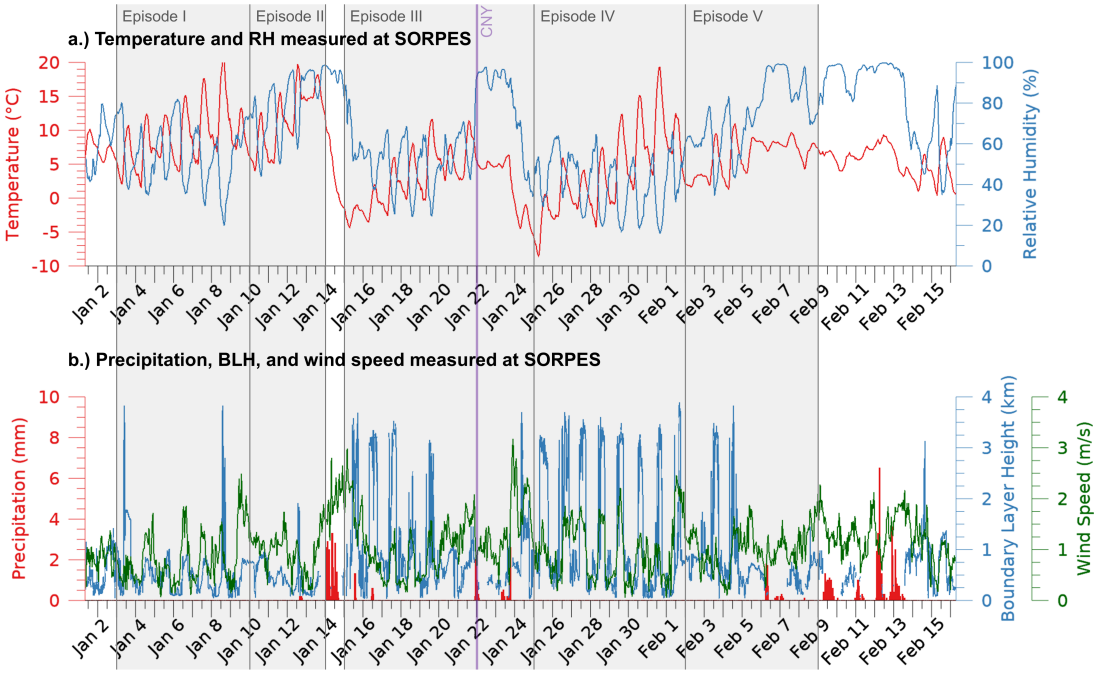


Figure 3. Meteorological conditions observed at SORPES during the study period, including (a) measurements of temperature and relative humidity (RH); and (b) precipitation, boundary layer height (BLH), and wind speed.

Temperatures during the study varied from a few degrees below freezing to warm, which is not unusual for the season (Yin et al., 2019; Wang et al., 2019). Temperatures peaked at over 20°C on January 8 and remained warm with daytime high temperatures over 10°C during Episodes I and II. Episode III was characterised by cooler temperatures compared to the previous two episodes, with low temperatures below freezing and high temperatures peaking between 6–10°C the last three days of the episode. Episode IV started with cold temperatures below freezing, with −8°C as the lowest temperature during

https://doi.org/10.5194/egusphere-2026-6854
Preprint. Discussion started: 19 November 2026
© Author(s) 2026. CC BY 4.0 License.

the study period on January 25, followed by gradual warming to over 18° on January 31. Finally, Episode V was characterized by temperatures mostly below 10° that did not significantly change during the episode.

We speculate that the periods of warmer temperatures may have partially reduced emissions during the study period because of lower heating usage and less cold-start vehicle emissions. Nonetheless, these conditions set the stage for the observed episodes, aligning with the recipe for haze described in Zheng et al. (2015, 2016) and Yin et al. (2019), and observations at SORPES show the five significant haze episodes in detail.

3.3 Aerosol composition in Nanjing

Figure 4(a–c) presents a time series of the composition simulated by GEOS-Chem-TOMAS at Nanjing in the control run and with the AAM, along with the LTOF-AMS measurements from SORPES. When comparing the results of the control run to the observations, it is evident that OA mass is significantly underestimated by the model while nitrate and ammonium aerosol mass is overestimated. Including the AAM in the chemistry noticeably reduced the modelled nitrate and ammonium mass concentrations, bringing the values closer to the observations and reducing the model bias (shown in Table 2). The AAM slightly increased OA mass, also reducing the bias, but the results remain underestimated compared to the measured OA. While the highest peaks in $PM_{2.5}$ during the haze episodes were reduced after the introduction of the AAM, which is due to the reduction in nitrate and ammonium, the mean $PM_{2.5}$ during the study period increased due to the increased OA in the AAM case. This demonstrates that the model is particularly sensitive to the chemical processes during extreme events.

The decreased nitrate and ammonium offset the increased OA, as seen in Fig. 4(d), which shows $PM_{2.5}$ with and without the AAM compared to the measurements from the SHARP instrument. Through much of the study period, the difference in the net $PM_{2.5}$ between the AAM and control runs appears to fluctuate between positive and negative. The mean OA modelled by GEOS-Chem-TOMAS during the study period increased by 3.94 μg/m^3 (12%) with the introduction of the AAM, while the mean nitrate and ammonium decreased by 1.66 μg/m^3 (7%). Adding these two together, we found that the net mean $PM_{2.5}$ in Nanjing increased by only 2.28 μg/m^3, which is slightly over 4%.

These results show that the counteracting impacts described in Sect. 3.1 are evident in this modelling study in Nanjing. The result of nominal impact on total $PM_{2.5}$ in Nanjing is similar to Figure 5(c–d) in Mayhew et al. (2025), which showed that when RO_2 accretion reactions were added to GEOS-Chem, there was little to no change in total $PM_{2.5}$ over eastern China in the winter. As described in Sect. 3.1, we interpret that this is due to RO_2 + NO reactions (R1) overwhelming both autoxidation and RO_2 + RO_2 reactions in these conditions. Nonetheless, there was a noticeable impact on OA mass in Nanjing, and in other regions of China and areas of South and Southeast Asia, OA and $PM_{2.5}$ mass substantially increased with the introduction of the AAM, as seen in Fig. 2, demonstrating the importance and relevance of the autoxidation processes in urban and regional air quality.

Measurements from the SHARP instrument showed a sudden, short-lived increase in $PM_{2.5}$ immediately following the CNY on January 22. This spike does not appear in the modelled $PM_{2.5}$. There is a small but noticeable increase in sulfate measured by the LTOF-AMS at this time, but otherwise, the LTOF-AMS, which shows PM_1 sizes, does not indicate a significant increase in small aerosols. This aligns with previous literature showing that CNY events result primarily in sulfur and coarse particle

https://doi.org/10.5194/egusphere-2026-6854
Preprint. Discussion started: 19 November 2026
© Author(s) 2026. CC BY 4.0 License.

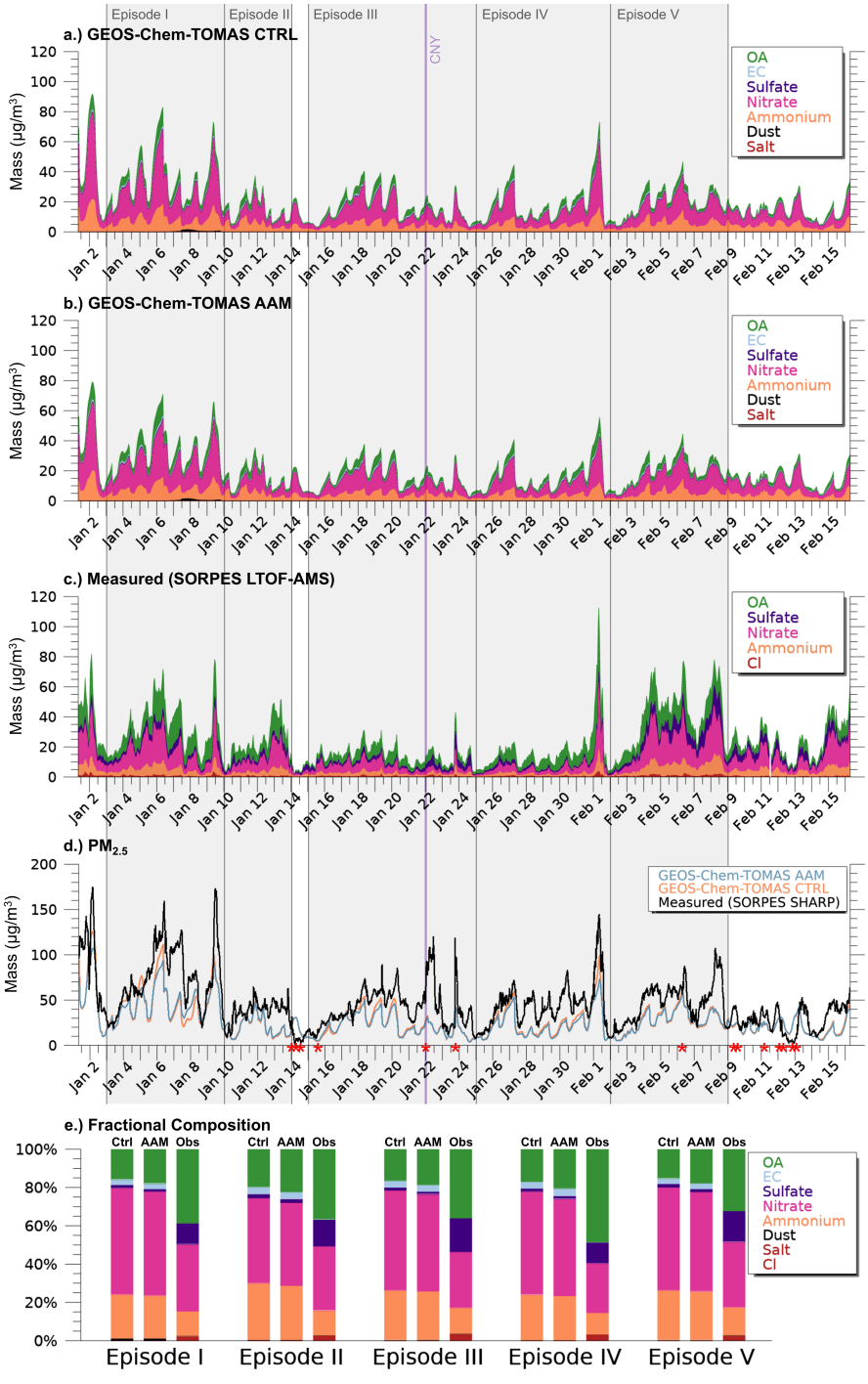


Figure 4. (a–b) PM_1 aerosol mass composition modelled by GEOS-Chem-TOMAS without and with the aromatic autoxidation mechanism (AAM); (c) composition of PM_1 measured by the LTOF-AMS; (d) $PM_{2.5}$ from the model with and without the AAM and measured by the SHARP instrument, where asterisks indicate periods with measured precipitation > 1 mm; and (e) relative fractions of modelled and observed composition during each of the five haze episodes.

https://doi.org/10.5194/egusphere-2026-6854
Preprint. Discussion started: 19 November 2026
© Author(s) 2026. CC BY 4.0 License.

emissions (Huang et al., 2024b; Foreback et al., 2022). The precipitation observed at exactly midnight of the CNY likely mitigated the impact of the holiday celebrations through wet deposition.

Panel (e) in Fig. 4 compares the mean fractional composition of each of the episodes. Here, we see from the measurements that Episode IV had the highest average fraction of OA and lowest fraction of nitrate and ammonium. The other four episodes showed quite similar measured and modelled fractional composition, and the effects of the AAM are consistent between the episodes. In all episodes, the model overestimates nitrate and ammonium while underestimating OA, and the results reiterate the findings that the AAM reduces both of these biases. Additionally, this figure demonstrates that the model consistently underestimates sulfate in Nanjing throughout the study period, especially during the peaks of the episodes. This is a known issue, partiularly during haze conditions, due to the lack of aqueous-phase and multiphase oxidation of SO_2 in GEOS-Chem (See Sect. 3.8, Limitations).

Despite the AAM not significantly improving GEOS-Chem's underestimation of $PM_{2.5}$ due to the offsetting impacts, the AAM reduced the model's bias of the individual aerosol components of OA, nitrate, and ammonium. Figure 5 shows a time series of the model bias and the improvement from the AAM in each of these components, along with scatterplots comparing the modelled OA, nitrate, and ammonium to the SORPES measurements during haze and non-haze periods. As seen in the scatterplots, the haze periods have higher correlation compared to the non-haze periods (e.g., $R^2 = 0.32$ for OA during haze, compared to 0.06 during the non-haze periods in the AAM case), and the haze periods are also closer to the 1:1 line compared to non-haze (e.g., slope for OA $= 0.25$ for the haze periods compared to 0.15 during non-haze for the AAM case. For OA (Fig. 5c–d), the AAM increased the R^2 and brouhgt the results closer to the 1:1 line. However, for nitrate and ammonium, this was only the case during the non-haze periods (Fig. 5f). During the haze periods (Fig. 5e), the AAM increased the R^2 value for nitrate + ammonium marginally from 0.21 in the control case to 0.23 in the AAM case, but the slope decreased from 0.58 to 0.51, moving it farther from the 1:1 line. The discrepancy with the nitrate + ammonium haze case is likely due to the most extreme points in the modelled concentrations during the peak of the haze episodes disproportionately influencing the overall statistics, and the AAM reduced those most disproportionately biased values.

Figure 5 also shows a general trend of greater bias as the episodes progress, with the highest bias near the ends of the episodes. This is especially noticeable in Episodes I and IV. Timing of the terminations of the episodes may also play a role in the bias. These episodes, especially Episode IV, follow the typical wintertime haze pattern of slow buildup and rapid cessation (Zheng et al., 2016; Shen et al., 2020; Foreback et al., 2025). During the rapid cessation of an episode, the $PM_{2.5}$ concentrations can drop from over 100 to less than 10 μg/m^3 within one or two hours. These sudden terminations of haze episodes are often caused by synoptic-scale weather systems and changes in airmasses, frequently associated with frontal passages (Zheng et al., 2016). A small miscalculation in the timing of the airmass shift—sourced in the model's meteorological input—can lead to a significant mistiming of the haze episode's termination in the model, consequently resulting in the appearance of an extreme bias for a short period of time (Foreback et al., 2024). This may explain some of the sudden, sharp peaks in model bias seen in Fig. 5(a).

The effect of CNY shows an especially pronounced signature in Fig. 5(a). On January 22, there was suddenly a negative model bias, most likely because of CNY-related emissions. The AAM did not change this bias (Fig. 5b), indicating that the root

https://doi.org/10.5194/egusphere-2026-6854
Preprint. Discussion started: 19 November 2026
© Author(s) 2026. CC BY 4.0 License.

of this bias lies in the fact that this one-off event is not included in the emission inventories used by GEOS-Chem, as opposed to inaccuracies in the model's chemical mechanisms.

Mean bias, mean fractional bias (MFB), and coefficient of determination (R^2) between the model and measurements are reported in Table 2, which shows that not only are the biases in these three components reduced when the AAM was included, but the correlation with the measurements was also improved. Thus, the introduction of AAM successfully helps to mitigate two long-standing model biases of underpredicted OA and overpredicted inorganic nitrate and ammonium, as well as pointing out that accurately accounting for VOC chemistry offers noticeable model improvements.

Table 2. Mean bias, mean fracitonal bias (MFB), and R^2 values of aerosols simulated by GEOS-Chem-TOMAS with and without the AAM compared to the measurements.

Variable	Mean bias (μg/m^3)		MFB (%)		R^2	
	Control	AAM	Control	AAM	Control	AAM
OA	-5.2	-4.8	-81.5	-72.1	0.38	0.41
Ammonium	1.8	1.5	43.3	39.0	0.26	0.28
Nitrate	2.7	1.8	33.5	28.2	0.32	0.34
$PM_{2.5}$	-18.6	-19.7	-48.8	-51.2	0.54	0.57

3.4 Particle Number Size Distribution (PNSD)

In addition to simulating mass and composition, TOMAS includes PNSD, which can be directly compared to the NAIS and DMPS measurements at SORPES using normalised concentrations with respect to particle diameter and bin size ($dN/d\log_{10}dP$). This is shown in Fig. 6(a–c). The first thing to notice in the TOMAS output (Fig. 6a for the control case and 6b for the AAM case) is that primary particle emissions are not included in size ranges below 10 nm (Croft et al., 2024). Thus, only newly formed and grown particles are included in these bins, and once all particles in these bins grow larger than 10 nm, these bins remain empty until the next NPF occurs. This contrasts with the NAIS measurements, which show concentrations of sub-10 nm particles even when NPF events are not actively occurring. Generally, the NPF events are more noticeable in the AAM case, and this will be further analysed in Sect. 3.5, which investigates the impact of the AAM on the TOMAS growth rates.

The solid line over the PNSD in Fig. 6(a–c) indicates the median particle diameter. The GEOS-Chem-TOMAS results (both the control and AAM) showed significantly lower median particle diameter compared to the DMPS, meaning that it is underestimating the size of particles. This underestimation of particle size could be partially related to—but is not necessarily the cause of—the model's underestimation of mass, especially since the mass is most sensitive to the largest diameter size ranges.

As an example, we looked at three snapshots in time: 20:00 local time on January 14, which is in between Episodes II and III and thus representative of background concentrations; 12:00 on January 15th, when an NPF event occurred, and 14:00 on January 18th, which is in the middle of Haze Episode III. For these three snapshots, we looked at the instantaneous PNSD, and

https://doi.org/10.5194/egusphere-2026-6854
Preprint. Discussion started: 19 November 2026
© Author(s) 2026. CC BY 4.0 License.

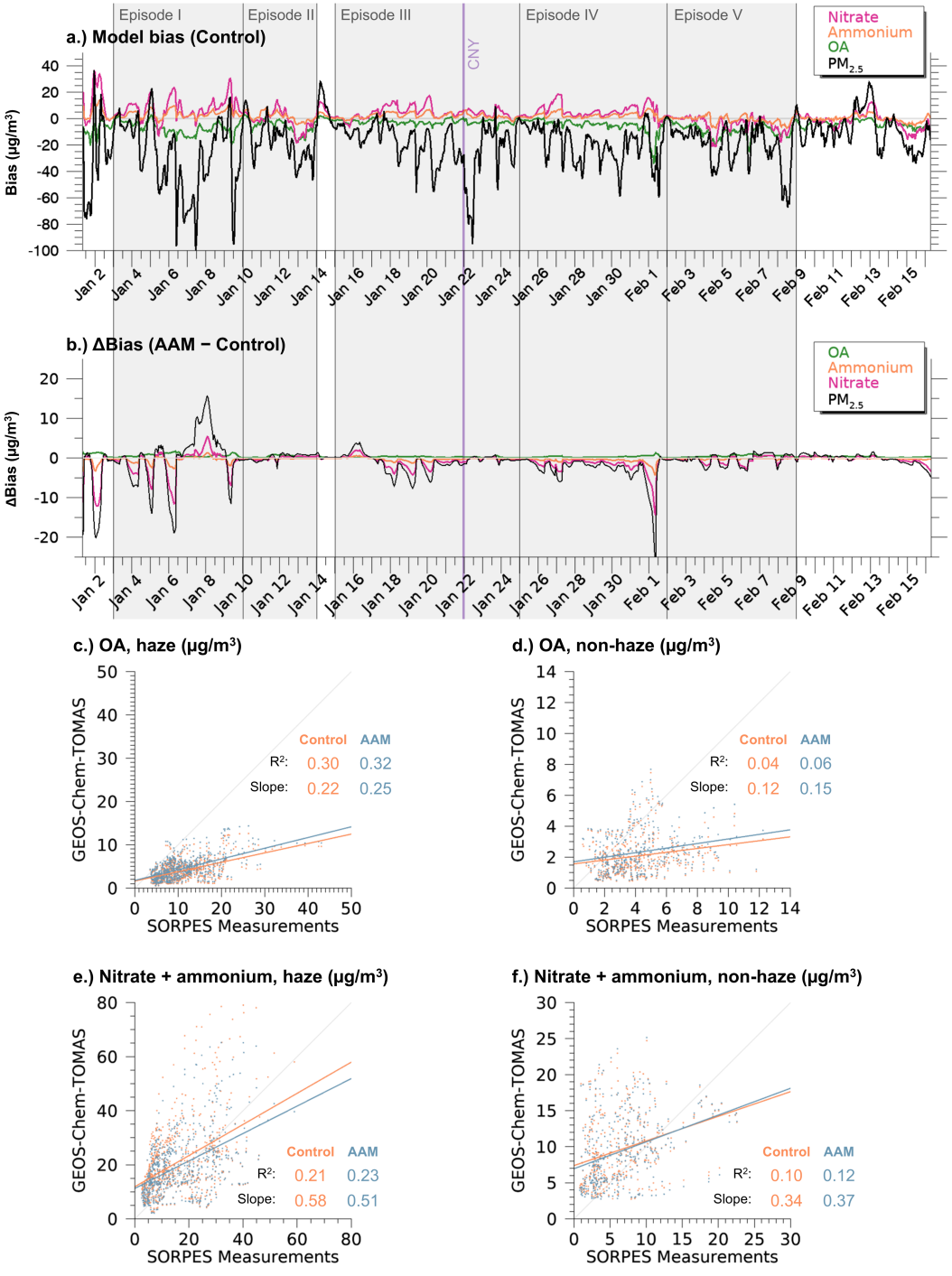


Figure 5. (a) Model bias of OA, nitrate, ammonium, and $PM_{2.5}$ in the control run compared to measurements in Nanjing; (b) change in bias compared to measurements introduced by the AAM; (c) scatterplot showing the model bias of OA with and without the AAM during the haze periods and (d) during non-haze; and (e) scatterplot of (nitrate + ammonium) bias with and without the AAM during the haze periods and (f) during non-haze.

https://doi.org/10.5194/egusphere-2026-6854
Preprint. Discussion started: 19 November 2026
© Author(s) 2026. CC BY 4.0 License.

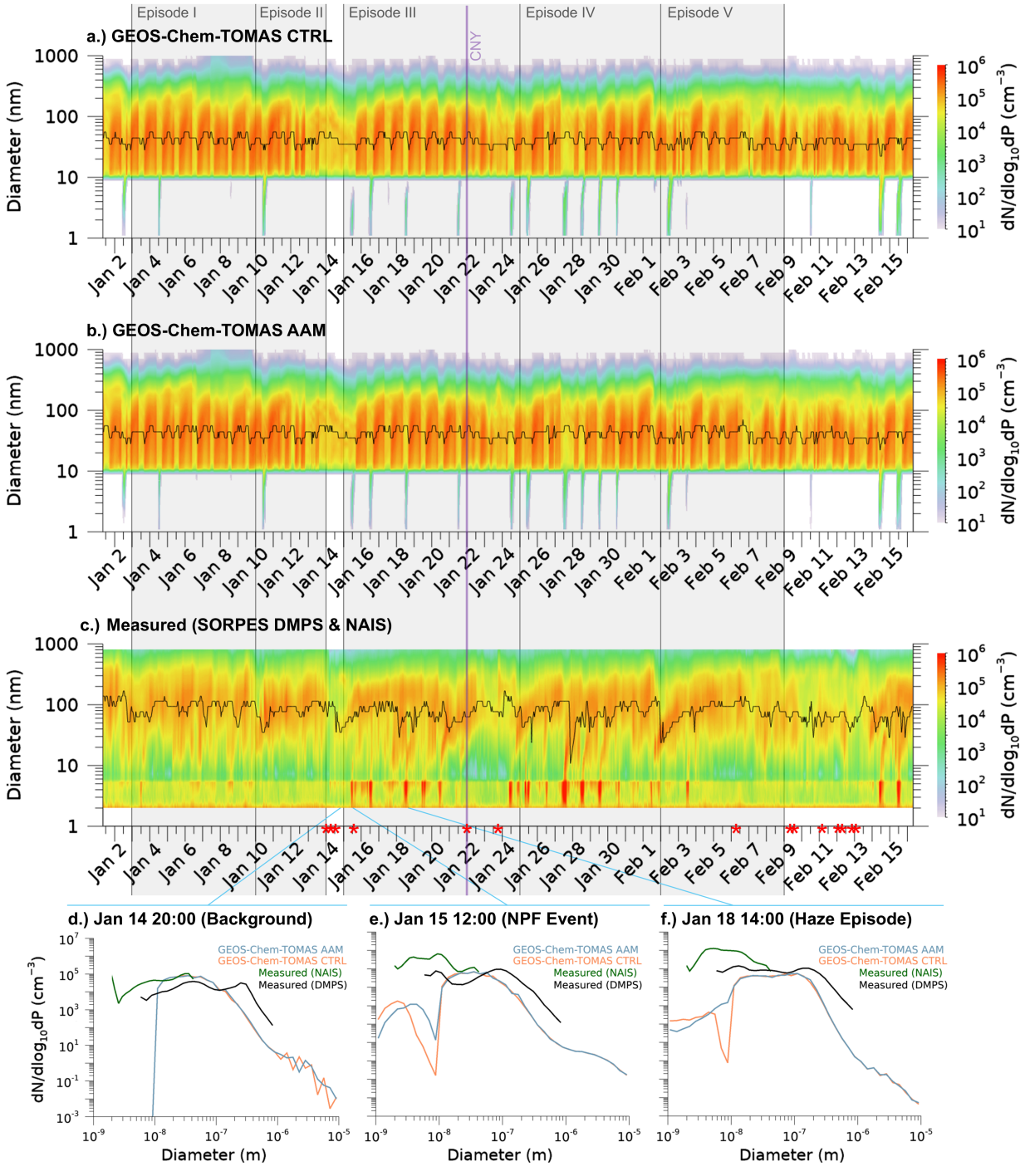


Figure 6. (a-b) Particle number size distribution (PNSD) modelled by GEOS-Chem-TOMAS without and with the aromatic autoxidation mechanism (AAM); (c) PNSD measured by the DMPS (6–820 nm) and NAIS (2–6 nm), where asterisks indicate periods with measured precipitation $>$ 1 mm; and snapshots of PNSD showing (d) background concentrations between haze episodes, (e) during an NPF event on January 15, and (f) during a haze episode.

https://doi.org/10.5194/egusphere-2026-6854
Preprint. Discussion started: 19 November 2026
© Author(s) 2026. CC BY 4.0 License.

we see that during the non-haze background time (Fig. 6d), neither the control nor the AAM case included particles less than 10 nm, likely because there were no nucleated particles simulated by the model, meaning that even the AAM case did not have any surface area in this size range on which to condense. Overall, this background case showed very little difference between the control and AAM cases. In contrast, during the NPF event (Fig. 6e), the AAM showed higher number concentrations of particles between 3 and 10 nm compared to the control case, whereas the control case showed higher number concentrations below 3 nm. This is most likely due to the condensable vapours in the AAM finding the surface area of the >3 nm more readily available for condensation. As previously mentioned, this study only added condensation of the AAM's SVOC and LOVC species and does not include additional nucleation in TOMAS. Even during the NPF event, number concentrations modelled by GEOS-Chem-TOMAS were considerably lower than the DMPS measurements in sizes larger than 100 nm, which helps explain the model's known underestimation of PM mass. The snapshot during the haze episode (Fig. 6f) showed similar results to the NPF case. Notably, the control case had a significant gap in number concentration between 5 and 10 nm, which was filled in the AAM case, although the AAM case still underestimates particle number concentrations during the haze episode. During the episode, the model underestimates particle number concentrations in all sizes, indicating that in addition to underestimating mass, it is also underestimating total particle number concentration.

Wang et al. (2023a) showed comparable results in Beijing using particle number and mass concentrations from GEOS-Chem coupled with the Advanced Particle Microphysics (APM) module. In addition to uncertainties in the model's chemistry, aerosol physics, and subgrid processes, Wang et al. (2023a) cited uncertainties in emission inventories as a possible cause for the model's underestimation of particle number and mass in China.

3.5 Growth rates

In addition to evaluating the modelled particle number size distributions, we examined the effects of the AAM on particle growth rates. For this analysis, we identified NPF events on ten days during the study period (January 10, 15, 16, 18, 24, 25, 27, 28, and 29; and February 14). Figure 7(a–i) compares three representative events simulated by GEOS-Chem-TOMAS under the control (a–c) and AAM (d–f) configurations against NAIS observations (g–i). In panels (a–i), the overlaid markers and linear regression lines indicate the 50% appearance times and their orthogonal fits, from which apparent growth rates between approximately 3 and 20 nm were derived. Finally, Fig. 7(j) summarizes and compares the modelled and NAIS-derived growth rates for all ten events in a model-vs.-observed scatterplot.

The mean NAIS-derived growth rate was 5.59 nm hr^{-1}, compared with 2.85 nm hr^{-1} in the control simulation and 3.98 nm hr^{-1} in the AAM simulation. Thus, relative to the mean observed GR, the control and AAM simulations underestimated particle growth by 49% and 29%, respectively. Including the AAM increased the mean modelled GR by approximately 40%. On an event-by-event basis, the mean absolute percentage error between the GRs calculated from the model output and measurements decreased from 45% in the control case to 27% in the AAM case, corresponding to a 39% reduction. The mean absolute error decreased from 2.8 to 1.7 nm hr^{-1}, while the root-mean-square error decreased from 3.2 to 2.2 nm hr^{-1}. The AAM simulation produced growth rates closer to the observations for 8 of the 10 events, and Fig. 7(j) shows that the AAM growth rates are closer to the one-to-one line with a χ^2 linear fit slope of 0.407 and R^2 of 0.33 in the AAM case compared to a slope of 0.182

https://doi.org/10.5194/egusphere-2026-6854
Preprint. Discussion started: 19 November 2026
© Author(s) 2026. CC BY 4.0 License.

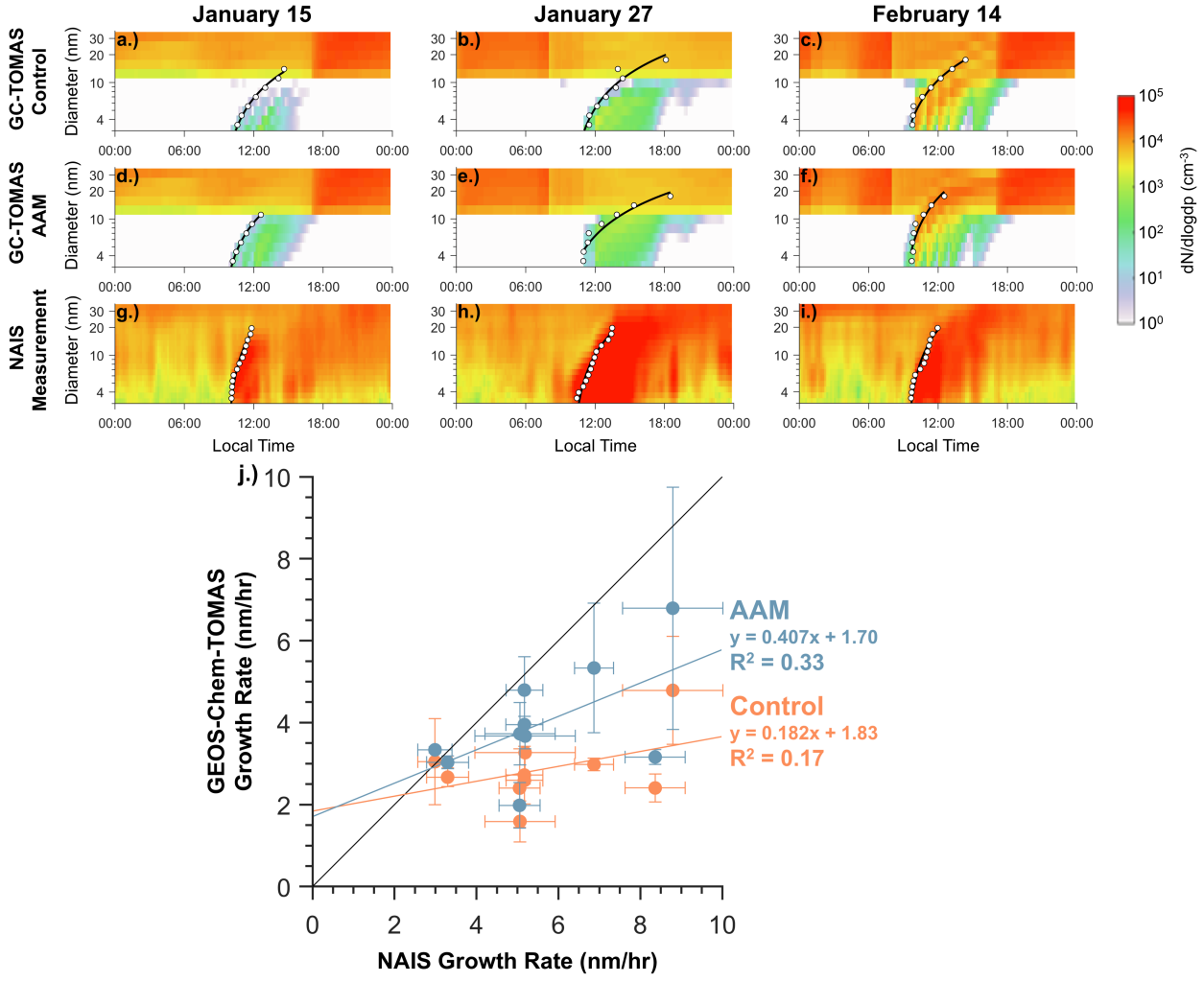


Figure 7. Comparison of particle size distributions and growth rates between model simulations and observations: (a–i) three representative NPF events from GEOS-Chem-TOMAS in the (a–c) control and (d–f) AAM configurations, alongside (g–i) NAIS observations. Overlaid circle markers and solid lines denote the 50% appearance times and their orthogonal linear fits, respectively, used to calculate apparent growth rates (~3–20 nm). (j) Comparison of modelled (control and AAM) and NAIS-derived growth rates across all ten identified NPF events. The error bars represent ±1 standard error, estimated from the 95% confidence intervals of the fitted growth rates. The solid black line represents the 1:1 line.

https://doi.org/10.5194/egusphere-2026-6854
Preprint. Discussion started: 19 November 2026
© Author(s) 2026. CC BY 4.0 License.

and R^2 of 0.17 in the control run. Overall, these results indicate that aromatic-derived condensable vapours account for an important fraction of particle growth.

The improved agreement obtained with the AAM highlights the importance of representing the formation and condensation of low-volatility aromatic oxidation products when simulating nanoparticle growth in polluted urban environments such as Nanjing. This interpretation is consistent with Li et al. (2023b), who estimated that aromatic oxidation products accounted for 32.6–46.1% of particle growth across multiple size intervals (e.g., 4–7 nm, 7–15 nm, 15–25 nm, and 25–40 nm) during NPF events in Nanjing. By accelerating growth through the size range in which coagulation losses are high, these vapours may increase the probability that newly formed particles survive to larger sizes, which are relevant to air quality and climate.

Nevertheless, discrepancies remained between the AAM and NAIS-derived growth rates. These differences may reflect uncertainties in the model representation of condensable vapours, their volatilities, and aerosol dynamics, as well as uncertainties and potential biases in the NAIS-derived apparent growth rates.

3.6 SOA production rate and condensation sink (CS)

We evaluated the SOA production rate from the TOMAS output collection and found that throughout the study period, most of the SOA mass is condensed into accumulation mode bins, around 100 nm in diameter and larger. This is true for both the control run (Fig. 8a) and the AAM run. The difference between the AAM and control are shown in Fig. 8(b), which indicates slightly higher values for the AAM case during the times of peak SOA production. The total SOA production rate (μg m^{-3} hr^{-1}) is shown as a timeseries in Fig. 8(c), revealing that the late morning peaks almost every day are significantly stronger with the AAM. Figure 8(d) presents the size distribution of the mean production rate through the study period, showing that the difference in SOA mass production between the control and AAM runs is almost entirely in the accumulation mode, peaking at slightly over 100 nm diameter. In this context, negative values for SOA production rate usually arises when very rapid particle growth occurs, and many particles move from one size bin to a larger size bin, resulting in net removal of mass form the smaller bin.

Condensation sink, shown in Fig. 9(a), is underestimated by the model during most of the study period. This is expected, considering that the model underestimates PM mass. Figure 9(b) shows the change in CS from the introduction of the AAM, indicating that the AAM increases the CS at every time point in the study period. The highest increase was during the end of Episode II and the second-to-last day of Episode III. The increased CS with the AAM agrees with the finding that SOA production increased with the AAM mostly in accumulation mode size ranges, which is the size range that primarily dominates CS. Counterintuitively, the increased CS did not suppress NPF or small particle growth, as characteristic "banana" features in the PNSD remained evident across both control and AAM cases (Sect. 3.4, Fig. 6), with AAM systematically enhancing growth rates on NPF days (Sect. 3.5, Fig. 7).

3.7 50% BTEX+TMB emission reduction scenario

As expected, reducing the VOC precursors, which are the initial precursor inputs to the autoxidation process, reduced modelled $PM_{2.5}$ mass throughout the study period (Fig. 10a), especially in the regions where these emissions were highest in the control

https://doi.org/10.5194/egusphere-2026-6854
Preprint. Discussion started: 19 November 2026
© Author(s) 2026. CC BY 4.0 License.

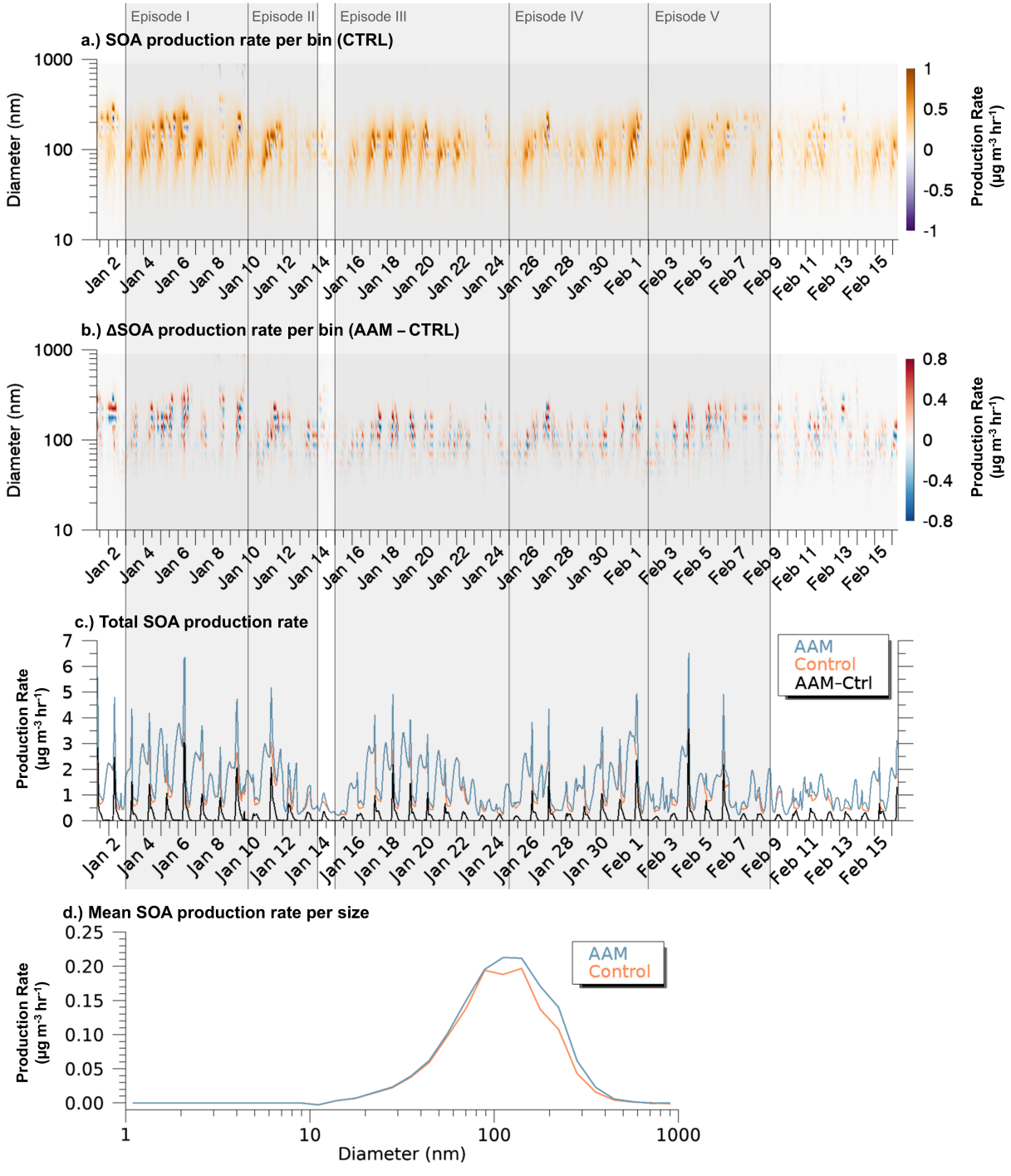


Figure 8. (a) SOA production rate simulated by GEOS-Chem-TOMAS without the AAM; (b) change in SOA production rate with the introduction of the AAM; (c) total SOA production rate through the study period; and (d) mean SOA production rate during the study period as a function of particle size.

https://doi.org/10.5194/egusphere-2026-6854
Preprint. Discussion started: 19 November 2026
© Author(s) 2026. CC BY 4.0 License.

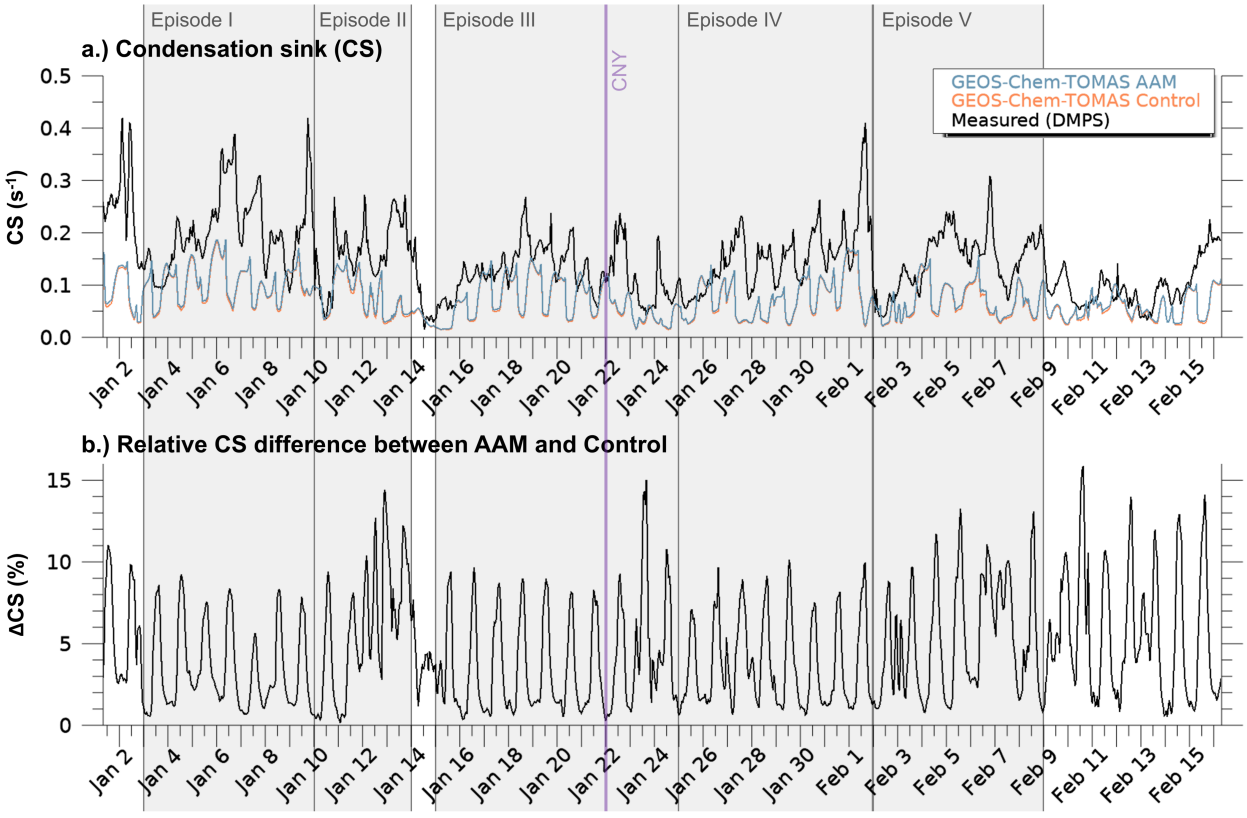


Figure 9. (a) condensation sink (CS) with and without the AAM compared to DMPS measurements, and (b) relative change in CS in GEOS-Chem-TOMAS with the AAM.

case (Fig. C3 in Appendix C). The largest reduction occurs in the Sichuan Basin, along with the Middle Yangtze River Basin (centred over Wuhan), where the mean $PM_{2.5}$ reduction was as much as 3 μg/m^3, which is nearly a 10% reduction in mean $PM_{2.5}$ mass. In Nanjing, the mean reduction during the study period was 1.5 μg/m^3, or slightly under 5%. Reduced organic aerosol mass (OA) accounts for nearly all of this decrease (Fig. 10b). The change in nitrate and ammonium mass is virtually negligible (Fig. 10c), and their concentrations did not return to values comparable to the control case despite the reduction of OA. This demonstrates the AAM's chemical mechanics and ability to simulate such a scenario, and these mechanics continued to function when the input emissions were changed.

Figure 10(d) shows the CS change in Nanjing for the reduced emission scenario. As expected, throughout almost the entire study period, the reduced emissions resulted in less condensation sink. Figure 10(e–f) shows that in Nanjing, the modelled $PM_{2.5}$ mass reduction occurred mostly in the accumulation mode size range, with particle diameter over 100 nm and that ultrafine concentrations were almost completely unchanged.

A comparison of the GRs calculated from the reduced emission scenario to the AAM GRs (Fig. 11) shows that in the reduced emissions case, GRs are generally slightly lower, but they are still higher than the control case. Thus, with the AAM enabled,

https://doi.org/10.5194/egusphere-2026-6854
Preprint. Discussion started: 19 November 2026
© Author(s) 2026. CC BY 4.0 License.

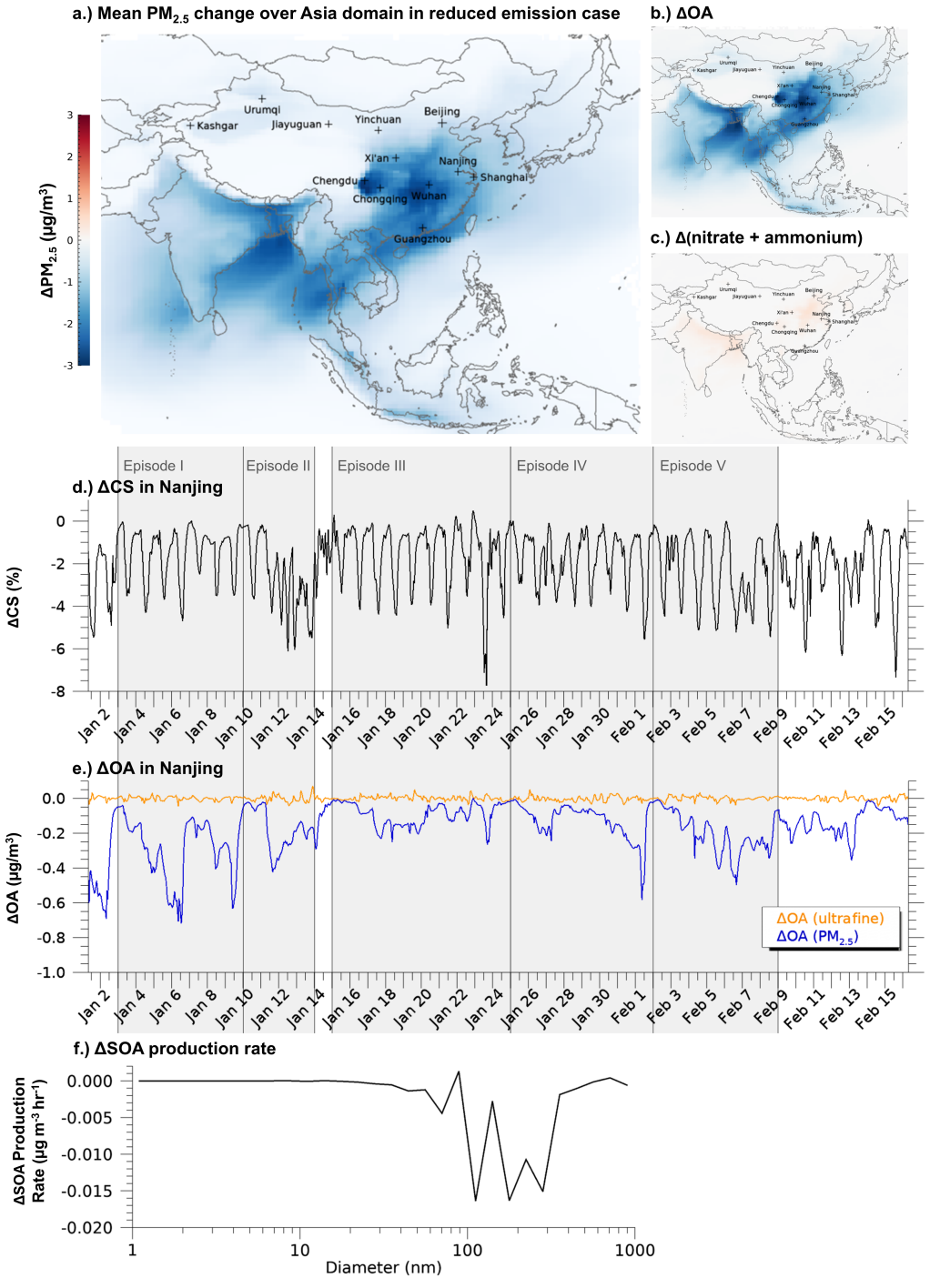


Figure 10. (a) Simulated reduction of $PM_{2.5}$ over the Asia domain using the AAM in a scenario where BTEX+TMB emissions were reduced by 50%. This shows the difference between the reduced emissions case and the AAM case. (b) OA component of the $PM_{2.5}$ change. (c) Nitrate and ammonium component of the $PM_{2.5}$ change. (d) Change in condensation sink in the reduced emission scenario. (e) Change in OA in Nanjing in the reduced emission scenario in ultrafine (sub-100 nm) and $PM_{2.5}$ size ranges. (f) Change in SOA production rate in Nanjing in the reduced emission scenario.

https://doi.org/10.5194/egusphere-2026-6854
Preprint. Discussion started: 19 November 2026
© Author(s) 2026. CC BY 4.0 License.

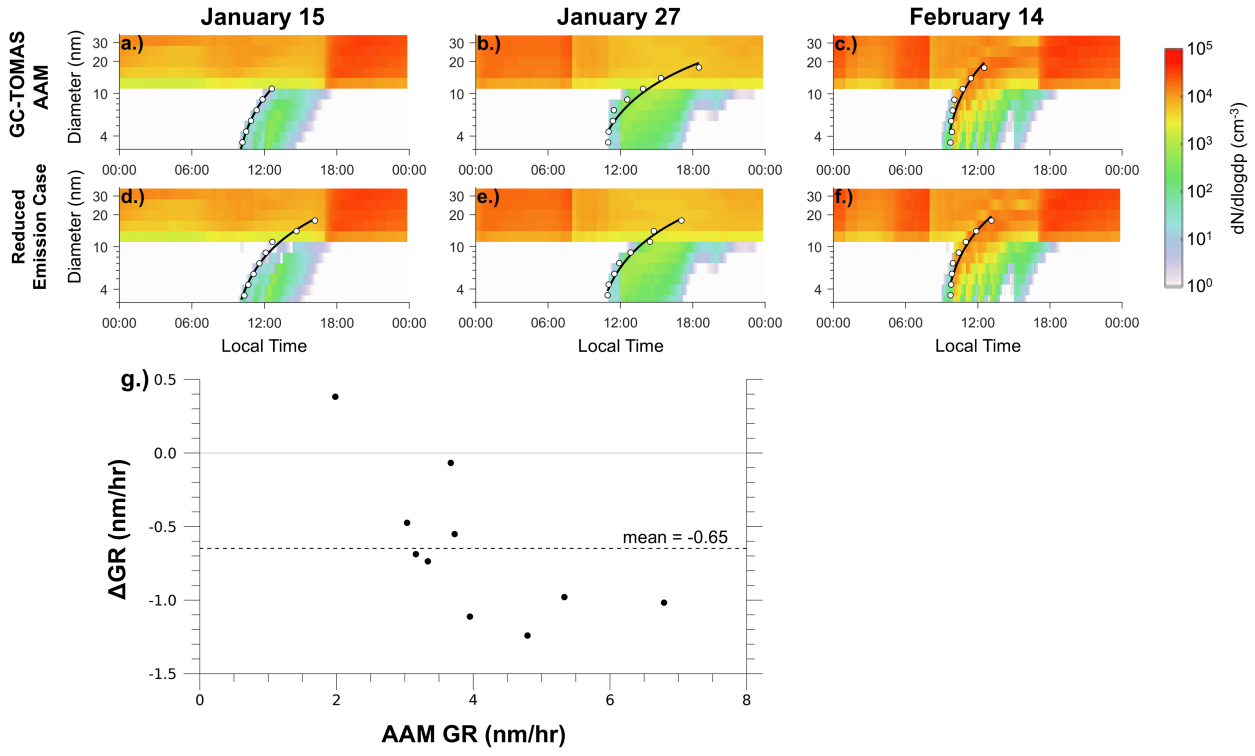


Figure 11. Size distribution with calculated growth rates from GEOS-Chem-TOMAS for the three example NPF event days in the AAM case (a–c) and the 50% BTEX & TMB reduction case (d–f). Panel (g) shows a difference-vs.-reference plot of calculated growth rates for the ten NPF event days in the reduced emissions case compared to the AAM case.

particles are grown in small sizes both during the existing high emission case as well as in a hypothetical reduced aromatic VOC emission case. This implies that even when the aromatic emissions are reduced, the autoxidation process introduced by the AAM remains important, and it is a significant driver of small particle growth.

The results shown in Figs. 10 and 11 have implications for potential air pollution abatement strategies. On one hand, we demonstrate that aromatic autoxidation is an important driver of SOA in eastern China. Thus, according to this result, reducing emissions of five significant aromatic VOCs mitigated $PM_{2.5}$ pollution by up to 10% in some regions. On the other hand, ultrafine particles (<100 nm in diameter) were virtually unaffected by these emission cuts. Thus, while a 10% reduction in $PM_{2.5}$ mass appears significant, $PM_{2.5}$ mass alone does not fully reflect the potential human exposure to the most harmful particles. From a health perspective, the most hazardous ultrafine particles remained despite the lower emissions, indicating that reducing CS results in more favourable conditions for growth of these smallest particles. In other words, reducing $PM_{2.5}$ does not necessarily make the air healthier.

These results illustrate the complex nature of haze-forming chemical processes in China, the non-linear relationship between total aerosol mass and size distribution in the smallest size ranges, and the inverse correlation between CS and small particle

https://doi.org/10.5194/egusphere-2026-6854
Preprint. Discussion started: 19 November 2026
© Author(s) 2026. CC BY 4.0 License.



growth. Furthermore, the results demonstrate that comprehensive emission control across multiple sectors and sources may be more effective than reducing emissions in only individual sectors, a finding previously identified in Foreback et al. (2025).

3.8 Limitations

The AUTOAPRAM_LVOC and AUTOAPRAM_SVOC variables represent many individual species, and when lumped together, these species are assumed to share the same condensation parameters. In this proof-of-concept implementation, the EZCOND subroutine relies on this assumption when condensing this mass. However, future iterations may want to consider developing a dedicated HOM-specific condensation routine that explicitly accounts for species-specific microphysical properties. A further limitation with this methodology is that only the terminal species from the AAM are included in AUTOAPRAM_LVOC and AUTOAPRAM_SVOC and subsequently condensed in TOMAS. In reality, some of the intermediate oxygenated organic molecules in the mechanism with low enough volatility may condense partway through the process. However, to prevent the model from becoming overly complicated and computationally unfeasible, the assumption that only terminal species condense needed to be made. Therefore, the potential condensation path of intermediate products is currently omitted from the AAM. Although the formation of HOM and condensable species is known to occur rapidly, the intermediate species are, by definition, formed earlier in the process, and including their condensation would improve model predictions in a dynamic simulation. Yet, because the current work acknowledges the limitation of not considering such dynamic effects while the AAM represents the likely final oxygenated product distribution (that is, the AAM contains the most condensable species), the improvement that condensation of intermediates could potentially offer to the AAM would likely be nominal. However, this common perspective, which assumes that intermediate radicals undergo condensation more readily than closed-shell end products, may potentially also be flawed. This remains an open question, given current limitations in knowledge in the field.

In its current implementation, autoAPRAM-fw does not account for further oxidation of closed-shell species, and therefore, the radical chemistry leading to HOM formation may be under-represented (Pichelstorfer et al., 2024). In addition to the chemical processes, determining the exact vapour pressures of HOMs remains a challenge in modelled and experimental aerosol physics (Peräkylä et al., 2020), which may lead to uncertainties in the microphysics and partitioning between gas and particle phases. Furthermore, as described in Sect. 3.1, the current chemical schemes produced by autoAPRAM-fw are known to underestimate SOA production in high-NO_x environments.

Missing aqueous-phase and multiphase sulfate chemistry, resulting in an underestimation of sulfate aerosol, especially in East Asia, is a known limitation in GEOS-Chem (Travis et al., 2025). Notably, multiphase oxidation of SO_2 is a chemical pathway absent from many current CTMs (Ma et al., 2023). Under high aerosol loadings, such as during haze events, sulfate can form from SO_2 through multiphase reactions even in cloud-free conditions (Liu et al., 2020, 2021). The results in Nanjing indeed show that GEOS-Chem-TOMAS underestimates sulfate compared to the measurements (Fig. 4). Because the current AAM implementation relies on condensation onto existing aerosol, including sulfate, the condensed organics in this study may contain slight uncertainties in modelled particle size distribution due to the underestimation of sulfate. This issue is addressed in GEOS-Chem version 14.8.0, which was released after completing this study (The International GEOS-Chem Community, 2026; Travis et al., 2025).

https://doi.org/10.5194/egusphere-2026-6854
Preprint. Discussion started: 19 November 2026
© Author(s) 2026. CC BY 4.0 License.

Finally, we are aware of the potential bias in GR derived with the appearance time method in diameter-ranges with strong concentration gradients. These are typically found at in size-range below 10 nm where stochastic growth is of importance. Further, in situations when aerosol dynamics (coagulation or losses) considerably affect the evolution of the particle size distribution, GR_{app} is biased as it interprets the aerosol dynamics as condensational growth/shrinkage (Olenius et al., 2018; Cai et al., 2021).

3.9 Future work

Future work should be done to further reduce the AAM to be more computationally manageable. For example, machine learning tools could be implemented to develop a reduced surrogate mechanism, which may help to balance chemical accuracy with computational efficiency (e.g., Yang et al., 2024). Improving the accuracy of reaction rates, for instance, with the autoCONSTRAINT tool, which is a new development in autoAPRAM-fw (Pichelstorfer et al., 2025), could be done in the future. Furthermore, future work may include adding additional aromatics to the mechanism, such as styrene, which has the potential to efficiently form SOA, especially during low RH conditions (Yu et al., 2022b).

While this study used a fixed partitioning of LVOC and SVOC species into particle phase via condensation in the TOMAS module (100% and 70%, respectively), future work could utilise the exact volatility ranges and physical calculations to more accurately partition the autoxidation products in the model.

4 Conclusions

Existing research has shown that CTMs typically underestimate $PM_{2.5}$, especially SOA. This study integrated a novel aromatic autoxidation mechanism (AAM) into the full chemistry scheme of GEOS-Chem-TOMAS, which included the oxidation of BTEX and TMB, followed by autoxidation to form HOMs, which were condensed into SOA in the TOMAS module. This introduced additional organic aerosol mass, addressing the model's underestimation. When applying the AAM in GEOS-Chem to winter haze in Nanjing, the mechanism also reduced the model's previously overestimated nitrate and ammonium mass concentrations in Nanjing.

Although the AAM did not significantly improve total $PM_{2.5}$ because the increase in OA and the decrease in nitrate and ammonium offset each other in Nanjing, an evaluation of each of these individual modelled components showed that they were improved by the introduction of the AAM. Therefore, we conclude that evaluating CTMs solely on total $PM_{2.5}$ masks the underlying chemical processes and components. The mechanism introduced in this study fixed two opposing biases simultaneously, improving the quality of the model, even though the net mass appears unchanged specifically in the YRD and NCP regions.

Addition of the AAM to GEOS-Chem's fullchem scheme also improved the modelled growth rates in the 3–20 nm size range, calculated from the particle number size distribution produced by TOMAS, compared to the growth rates calculated from the size distribution measured by the NAIS. While particles in this size range have nearly negligible mass with respect to $PM_{2.5}$, this improvement is significant because accurate representation of particle growth and size distribution is important

https://doi.org/10.5194/egusphere-2026-6854
Preprint. Discussion started: 19 November 2026
© Author(s) 2026. CC BY 4.0 License.

for health, policy, and climate studies. Therefore, this study has demonstrated that accounting for the autoxidation pathways of aromatic VOCs in a haze-prone environment, including Nanjing, is indispensable for scientific understanding of the underlying chemical and physical processes behind aerosol growth.

This study demonstrated that reducing emissions of five significant aromatic VOCs by 50% can reduce total $PM_{2.5}$ mass by as much as 10% in some regions. While this may have policy significance, $PM_{2.5}$ only tells a high-level story. Results from the reduced emission scenario showed that this lowered mass was almost entirely in the particle size range of 100 nm and larger. Considering that ultrafine particles have the most serious health impact, this scenario alone may offer only marginal health improvement. This demonstrates the complex nature and interactions between atmospheric chemistry and aerosol processes, and successful air quality management strategies must account for these chemical and small-scale aerosol processes that lead to ultrafine particles. Furthermore, this highlights the importance of comprehensive emission control across multiple sectors, targeting all PM precursors, as a more effective strategy than only reducing individual precursors.

Although incorporating such a complex chemical scheme into a large-scale CTM such as GEOS-Chem can be computationally challenging, this study proves that a detailed chemical mechanism, including the AAM generated from autoAPRAM-fw, can be successfully integrated into a large-scale/global CTM and that near-explicit gas-phase autoxidation kinetics can be represented in such models and run on modern high-performance supercomputers. Because this exact implementation is computationally heavy, it is not intended to be included in a future public release of GEOS-Chem. Nonetheless, the AAM merged with the fullchem scheme can be used for research purposes for evaluating aerosols and haze, including the Nanjing haze case study. Considering that our findings have demonstrated the importance of aromatic autoxidation in a region with high aromatic emissions, including this mechanism—or more realistically, a further reduced version that represents the important aromatic autoxidation processes—should be considered when modelling urban aerosols and air quality.

Code and data availability. The aromatic autoxidation mechanism merged with the fullchem mechanism in GEOS-Chem v.14.6.3 (saved as custom.eqn), modified TOMAS code, and modified species database files used in this study are available at https://doi.org/10.5281/zenodo.23363431. The measurement data from SORPES are available upon request.

Appendix A: Computing architecture and benchmarking

We ran GEOS-Chem Classic with fullchem and TOMAS on the Mahti supercomputer at CSC – IT Center for Science, Finland (CSC – IT Center for Science, 2025) using 64 CPU cores. Although Mahti's partitioning allows up to 128 CPU cores on a single node, we found that using more than 64 cores did not offer any performance benefit, likely due to the overhead in OpenMP's array parallelisation onto too many cores outweighing the benefit of the distributed array calculations. Computational time with the AAM was approximately 2.25 times that of the control run.

Because the AAM is a chemically near-explicit mechanism, even the reduced version is very computationally heavy for use in GEOS-Chem. Therefore, this is intended only as a proof-of-concept study for demonstration of the effects of aromatic

https://doi.org/10.5194/egusphere-2026-6854
Preprint. Discussion started: 19 November 2026
© Author(s) 2026. CC BY 4.0 License.

autoxidation in a hazy environment. This implementation could be used by researchers for specific aromatic SOA related studies, but it is not intended to be added to a future release of GEOS-Chem.

Appendix B: Evaluation of the reduced AAM with ARCA-box

To verify the numerical consistency and chemical accuracy of the lumping methodology that was used when reducing the AAM for use in GEOS-Chem, we validated the reduced AAM against the full AAM using the ARCA-box model (Clusius et al., 2022). Starting with typical atmospheric conditions representative of Nanjing in wintertime (Huang et al., 2026; Shen et al., 2018), we tested four combinations of low/high temperature and low/high NO_x. Details of these test cases are outlined in Table B1. These tests evaluate the gas-phase chemistry to ensure that the total mass of the lumped SVOC plus LVOC categories, which are the values passed through the coupler between GEOS-Chem and TOMAS, is equivalent to the combined mass of the individual HOM species produced in the full, unlumped mechanism. This verification isolates the gas-phase mechanism and does not validate the subsequent condensation or aerosol microphysics handled by TOMAS.

Table B1. Test cases for the ARCA-box validation of the reduced aromatic autoxidation mechanism used in this study.

	Temperature	**NO_x**
Low Case	0 °C	0.1 ppb NO 2 ppb NO_2
High Case	15 °C	5 ppb NO 30 ppb NO_2

We ran ARCA-box for these four setups with 10-second time steps for 12 hours starting at 8:00 am local time (00:00 UTC), using clear-sky solar input for January 1 and the latitude and longitude coordinates of SORPES. Then we compared the sum of the gas-phase terminal HOM mass concentrations in the full mechanism to the mass concentrations of the reduced mechanism's final lumped SVOC + LVOC (including ELVOC) values (i.e., AUTOAPRAM_SVOC + AUTOAPRAM_LVOC).

As illustrated in Fig. B1, the total simulated mass concentration of highly oxygenated organic molecules (HOMs) shows exceptional agreement between the full and reduced mechanisms ($R^2 = 0.99998$), aligning nearly exactly on the 1:1 reference line across all four simulated environments.

The simulated values varied less than 2% across the multiple cases, which is a direct reflection of the mass conservation within idealised, precursor-limited box model conditions. Because these zero-dimensional simulations isolate chemical kinetic branching pathways in a closed system over the 12-hour period, the initial volatile organic precursors undergo near-complete chemical consumption. As a result, the total mass of the HOMs remains constrained by the initial VOC inputs. This lack of variance under contrasting environmental inputs demonstrates that the mechanism reduction methodology introduces negligible error and preserves the underlying chemical behaviour of the full system.

The most significant difference between test cases was observed in the high- and low-NO_x scenarios. This aligns with our expectations and previous literature (e.g., Yang et al., 2026; Zhang et al., 2023) that autoxidation is suppressed under high-NO_x

https://doi.org/10.5194/egusphere-2026-6854
Preprint. Discussion started: 19 November 2026
© Author(s) 2026. CC BY 4.0 License.

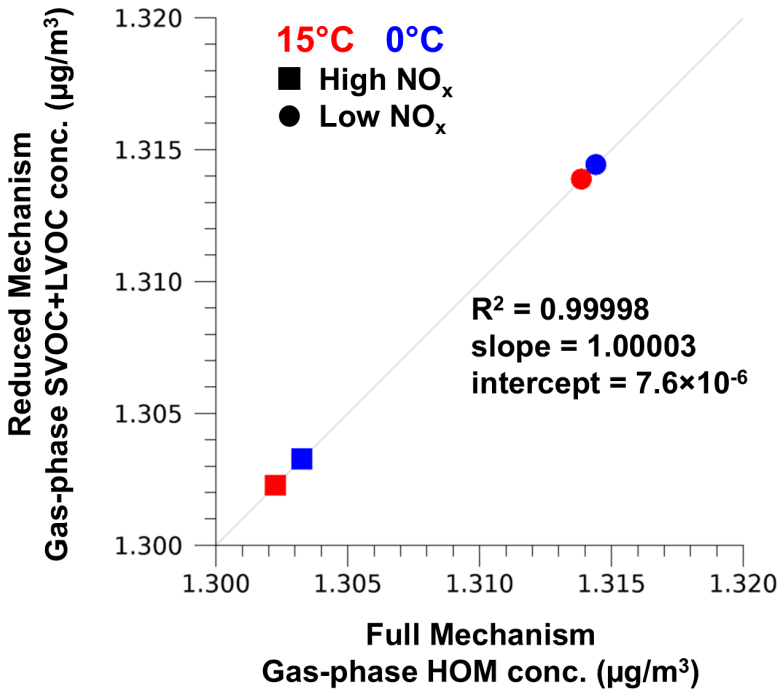


Figure B1. Validation of the reduced AAM compared to the non-reduced AAM using ARCA-box.

conditions. The extremely small difference in mass between the full and reduced AAM is likely caused by an accumulation of very small double precision computational rounding errors in the reduced mechanism's stoichiometric multiplier and when summing the mass concentrations of the individual HOMs versus summing the lumped SVOC and LVOC species.

In the box model tests, over 99.9% of the gas-phase LVOC + SVOC mass simulated with the reduced AAM was in the LVOC species. This heavy partitioning toward the LVOC category is expected, in part due to the fact that less than 2% of the lumped species were categorised in the SVOC category. Moreover, as the simulation progresses, semivolatile intermediates are continuously oxidised to form highly oxygenated species, rapidly lowering their volatility until they ultimately accumulate as low and extremely low volatility terminal products. The result of LVOC/(LVOC+SVOC) $>$ 99.9% is consistent with the results when running the reduced AAM in GEOS-Chem-TOMAS (Sect. 3).

Appendix C: Supplementary Figures

https://doi.org/10.5194/egusphere-2026-6854
Preprint. Discussion started: 19 November 2026
© Author(s) 2026. CC BY 4.0 License.

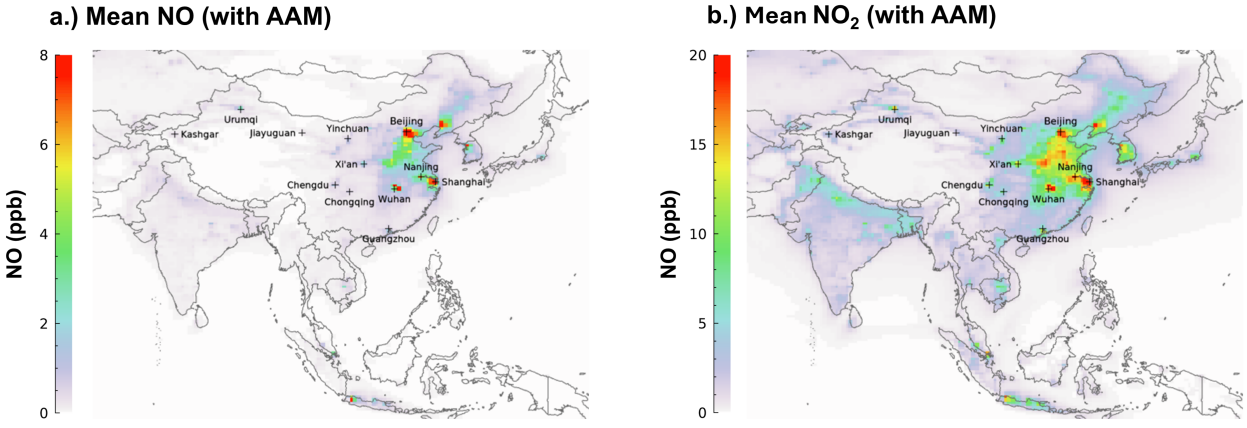


Figure C1. Modelled NO_x in the Asia domain during the study period: (a) mean NO concentration in the AAM run; (b) mean NO_2 concentration in the AAM run.

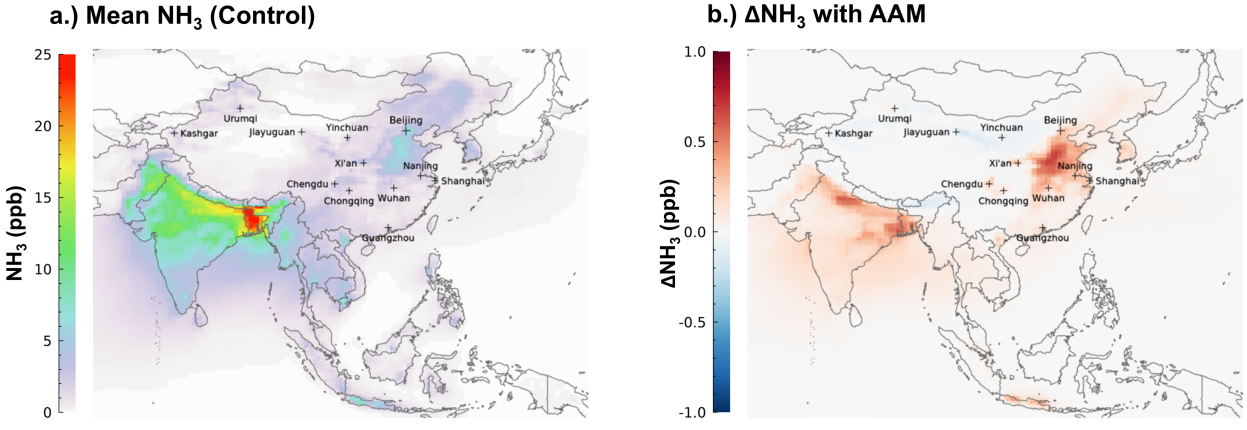


Figure C2. (a) Gas-phase NH_3 concentrations over the Asia domain in the control run and (b) difference in gas-phase NH_3 concentrations between the AAM and the control case.

https://doi.org/10.5194/egusphere-2026-6854
Preprint. Discussion started: 19 November 2026
© Author(s) 2026. CC BY 4.0 License.

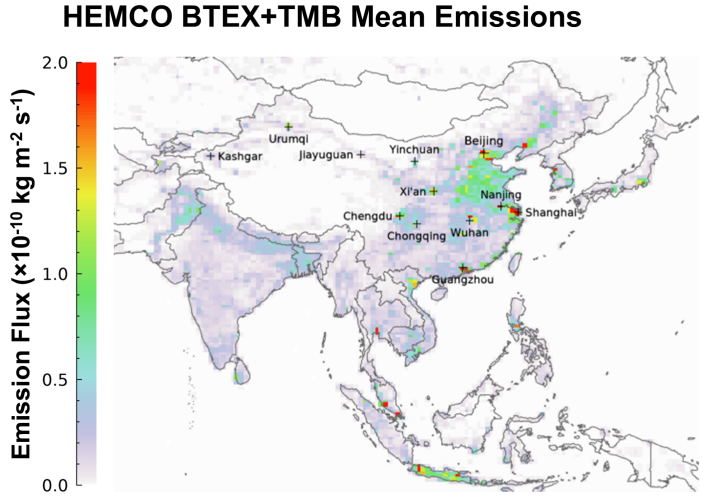


Figure C3. Emission of BTEX & TMB calculated by HEMCO over the Asia domain

https://doi.org/10.5194/egusphere-2026-6854
Preprint. Discussion started: 19 November 2026
© Author(s) 2026. CC BY 4.0 License.

Author contributions. BF ran the GEOS-Chem model simulations and drafted and edited the manuscript. LP provided the aromatic autoxidation mechanism from autoAPRAM-fw and contributed to the development of the lumped mechanism. RB performed the growth rate calculations and contributed to figures, analysis, and text. HZ, TA, FFØ, and MBa provided support with modelling architecture and analysis. FFØ assisted with visualisations. XC managed the instrument data. LF, PC, MR, JH, CX, and ZF provided support with the chemical mechanism and analysis. AD, XQ, and TVK provided measurement data and support. AM, Z-SL, FFØ, and MBo provided supervision and senior leadership for the study. All co-authors contributed to the conceptualisation, theory, discussions, and editing stages that led to the success of this study.

Competing interests. The authors declare that there are no known competing financial interests or personal relationships that would have influenced the work presented in this paper.

Acknowledgements. The authors wish to acknowledge the Institute of Atmospheric and Earth System Research (INAR) for the opportunity to work on and develop this study, as well as the Atmosphere and Climate Competence Center (ACCC) flagship organisation for its support in atmospheric science research in Finland, which made this study possible. The authors also wish to acknowledge CSC – IT Center for Science, Finland, for generous computational resources for this study. The authors acknowledge the Lahti University Consortium (Ministry of Education), Finland, and Novo Nordisk Foundation, Denmark for funding for this study. Furthermore, the authors wish to acknowledge colleagues at INAR and Lahti University Campus for the discussions and coffee room chats which offered motivation to keep the study going.

https://doi.org/10.5194/egusphere-2026-6854
Preprint. Discussion started: 19 November 2026
© Author(s) 2026. CC BY 4.0 License.

References

An, X., Chen, W., Li, C., Sheng, L., Zhang, W., Hai, S., and Hu, P.: Influence of rainfall-induced diabatic heating on southern rainfall-northern haze over eastern China in early February 2023, Science China Earth Sciences, 66, 2579–2593, https://doi.org/10.1007/s11430-023-1181-3, 2023.

Barletta, B., Meinardi, S., Sherwood Rowland, F., Chan, C.-Y., Wang, X., Zou, S., Yin Chan, L., and Blake, D. R.: Volatile organic compounds in 43 Chinese cities, Atmospheric Environment, 39, 5979–5990, https://doi.org/https://doi.org/10.1016/j.atmosenv.2005.06.029, 2005.

Barua, S., Kumar, A., Seal, P., Bezaatpour, M., Jha, S., Myllys, N., Iyer, S., and Rissanen, M.: Nitric oxide can enhance secondary aerosol precursor formation from aromatic carbonyls, Nature Communications, 17, 5454, https://doi.org/10.1038/s41467-026-72628-w, 2026.

Bates, K. H., Jacob, D. J., Li, K., Ivatt, P. D., Evans, M. J., Yan, Y., and Lin, J.: Development and evaluation of a new compact mechanism for aromatic oxidation in atmospheric models, Atmospheric Chemistry and Physics, 21, 18 351–18 374, https://doi.org/10.5194/acp-21-18351-2021, 2021.

Bey, I., Jacob, D. J., Yantosca, R. M., Logan, J. A., Field, B. D., Fiore, A. M., Li, Q., Liu, H. Y., Mickley, L. J., and Schultz, M. G.: Global modeling of tropospheric chemistry with assimilated meteorology: Model description and evaluation, Journal of Geophysical Research: Atmospheres, 106, 23 073–23 095, https://doi.org/https://doi.org/10.1029/2001JD000807, 2001.

Bianchi, F., Kurtén, T., Riva, M., Mohr, C., Rissanen, M. P., Roldin, P., Berndt, T., Crounse, J. D., Wennberg, P. O., Mentel, T. F., Wildt, J., Junninen, H., Jokinen, T., Kulmala, M., Worsnop, D. R., Thornton, J. A., Donahue, N., Kjaergaard, H. G., and Ehn, M.: Highly Oxygenated Organic Molecules (HOM) from Gas-Phase Autoxidation Involving Peroxy Radicals: A Key Contributor to Atmospheric Aerosol, Chemical Reviews, 119, 3472–3509, https://doi.org/10.1021/acs.chemrev.8b00395, 2019.

Bloss, C., Wagner, V., Jenkin, M. E., Volkamer, R., Bloss, W. J., Lee, J. D., Heard, D. E., Wirtz, K., Martin-Reviejo, M., Rea, G., Wenger, J. C., and Pilling, M. J.: Development of a detailed chemical mechanism (MCMv3.1) for the atmospheric oxidation of aromatic hydrocarbons, Atmospheric Chemistry and Physics, 5, 641–664, https://doi.org/10.5194/acp-5-641-2005, 2005.

Cai, J., Wu, C., Wang, J., Du, W., Zheng, F., Hakala, S., Fan, X., Chu, B., Yao, L., Feng, Z., Liu, Y., Sun, Y., Zheng, J., Yan, C., Bianchi, F., Kulmala, M., Mohr, C., and Daellenbach, K. R.: Influence of organic aerosol molecular composition on particle absorptive properties in autumn Beijing, Atmospheric Chemistry and Physics, 22, 1251–1269, https://doi.org/10.5194/acp-22-1251-2022, 2022.

Cai, R., Li, C., He, X.-C., Deng, C., Lu, Y., Yin, R., Yan, C., Wang, L., Jiang, J., Kulmala, M., and Kangasluoma, J.: Impacts of coagulation on the appearance time method for new particle growth rate evaluation and their corrections, Atmospheric Chemistry and Physics, 21, 2287–2304, https://doi.org/10.5194/acp-21-2287-2021, 2021.

Chen, L., Qi, X., Nie, W., Wang, J., Xu, Z., Wang, T., Liu, Y., Shen, Y., Xu, Z., Kokkonen, T. V., Chi, X., Aalto, P. P., Paasonen, P., Kerminen, V.-M., Petäjä, T., Kulmala, M., and Ding, A.: Cluster Analysis of Submicron Particle Number Size Distributions at the SORPES Station in the Yangtze River Delta of East China, Journal of Geophysical Research: Atmospheres, 126, e2020JD034 004, https://doi.org/https://doi.org/10.1029/2020JD034004, e2020JD034004 2020JD034004, 2021.

Chen, L., Qi, X., Niu, G., Li, Y., Liu, C., Lai, S., Liu, Y., Nie, W., Yan, C., Wang, J., Chi, X., Paasonen, P., Hussein, T., Lehtipalo, K., Kerminen, V.-M., Petäjä, T., Kulmala, M., and Ding, A.: High Concentration of Atmospheric Sub-3 nm Particles in Polluted Environment of Eastern China: New Particle Formation and Traffic Emission, Journal of Geophysical Research: Atmospheres, 128, e2023JD039 669, https://doi.org/https://doi.org/10.1029/2023JD039669, e2023JD039669 2023JD039669, 2023.

https://doi.org/10.5194/egusphere-2026-6854
Preprint. Discussion started: 19 November 2026
© Author(s) 2026. CC BY 4.0 License.

Chen, N., Du, Y., Wang, Y., Yi, Y., Wilasang, C., Feng, J., Zhang, K., Manomaiphiboon, K., Huang, L., Yang, X., and Li, L.: Source Identification of PM2.5 and Organic Carbon During Various Haze Episodes in a Typical Industrial City by Integrating with High-Temporal-Resolution Online Measurements of Organic Molecular Tracers, Sustainability, 17, https://doi.org/10.3390/su172310587, 2025a.

Chen, S.-P., Liu, W.-T., Ou-Yang, C.-F., Chang, J. S., and Wang, J.-L.: Optimizing the emission inventory of volatile organic compounds (VOCs) based on network observations, Atmospheric Environment, 84, 1–8, https://doi.org/https://doi.org/10.1016/j.atmosenv.2013.10.059, 2014.

Chen, T., Liu, J., Chu, B., Ge, Y., Zhang, P., Ma, Q., and He, H.: Insufficient oxidation capacity in the photooxidation of aromatic VOCs results in underestimation of SOA yield, Science Bulletin, https://doi.org/https://doi.org/10.1016/j.scib.2026.01.016, 2026.

Chen, T.-L., Hsiao, T.-C., Chen, A. Y., Chang, K.-E., Lin, T.-C., Griffith, S. M., and Chou, C. C.-K.: A traffic-induced shift of ultrafine particle sources under COVID-19 soft lockdown in a subtropical urban area, Environment International, 187, 108 658, https://doi.org/https://doi.org/10.1016/j.envint.2024.108658, 2024.

Chen, Y., Xia, M., Zheng, P., Li, Y., Zou, Z., Tong, S., Li, K., Feng, X., Hui, L., Yuan, Q., Li, J., Yu, J. Z., Lee, S., Wang, T., and Wang, Z.: Complex gas-particle partitioning of nitro-phenolic compounds: field-based insights and determination of apparent activity coefficient, npj Climate and Atmospheric Science, 8, 266, https://doi.org/10.1038/s41612-025-01156-z, 2025b.

Clusius, P., Xavier, C., Pichelstorfer, L., Zhou, P., Olenius, T., Roldin, P., and Boy, M.: Atmospherically Relevant Chemistry and Aerosol box model – ARCA box (version 1.2), Geoscientific Model Development, 15, 7257–7286, https://doi.org/10.5194/gmd-15-7257-2022, 2022.

Clusius, P., Baykara, M., Xavier, C., Zhou, P., Tyree, J., Foreback, B., Äijälä, M., Graeffe, F., Petäjä, T., Kulmala, M., Paasonen, P., Palmer, P. I., and Boy, M.: Modelling the impact of anthropogenic aerosols on CCN concentrations over a rural boreal forest environment, Atmospheric Chemistry and Physics, 26, 1967–1992, https://doi.org/10.5194/acp-26-1967-2026, 2026.

Croft, B., Martin, R. V., Chang, R. Y.-W., Bindle, L., Eastham, S. D., Estrada, L. A., Ford, B., Li, C., Long, M. S., Lundgren, E. W., Sinha, S., Sulprizio, M. P., Tang, Y., van Donkelaar, A., Yantosca, R. M., Zhang, D., Zhu, H., and Pierce, J. R.: Toward Fine Horizontal Resolution Global Simulations of Aerosol Sectional Microphysics: Advances Enabled by GCHP-TOMAS, Journal of Advances in Modeling Earth Systems, 16, e2023MS004 094, https://doi.org/https://doi.org/10.1029/2023MS004094, e2023MS004094 2023MS004094, 2024.

CSC – IT Center for Science: Mahti – Technical details about the Mahti supercomputer, https://docs.csc.fi/computing/systems-mahti/, accessed: 2025-11-28, 2025.

da Rocha, F. O. C., Campos, V. P., da Rocha, G. O., Brito, A. V. S., and dos Santos Sampaio, I.: Characterization of airborne gaseous BTEX and aldehydes from populated Brazilian cities as representative atmospheres of typical urban areas from the Southern Hemisphere, Air Quality, Atmosphere & Health, 16, 1271–1289, https://doi.org/10.1007/s11869-023-01341-0, 2023.

Dal Maso, M., Kulmala, M., Riipinen, I., Wagner, R., Hussein, T., Aalto, P. P., and Lehtinen, K. E. J.: Formation and growth of fresh atmospheric aerosols: eight years of aerosol size distribution data from SMEAR II, Hyytiälä, Finland, Boreal Environment Research, 10, 323–336, 2005.

D'Andrea, S. D., Häkkinen, S. A. K., Westervelt, D. M., Kuang, C., Levin, E. J. T., Kanawade, V. P., Leaitch, W. R., Spracklen, D. V., Riipinen, I., and Pierce, J. R.: Understanding global secondary organic aerosol amount and size-resolved condensational behavior, Atmospheric Chemistry and Physics, 13, 11 519–11 534, https://doi.org/10.5194/acp-13-11519-2013, 2013.

Deng, C., Fu, Y., Dada, L., Yan, C., Cai, R., Yang, D., Zhou, Y., Yin, R., Lu, Y., Li, X., Qiao, X., Fan, X., Nie, W., Kontkanen, J., Kangasluoma, J., Chu, B., Ding, A., Kerminen, V.-M., Paasonen, P., Worsnop, D. R., Bianchi, F., Liu, Y., Zheng, J., Wang, L., Kulmala, M., and Jiang, J.: Seasonal Characteristics of New Particle Formation and Growth in Urban Beijing, Environmental Science & Technology, 54, 8547–8557, https://doi.org/10.1021/acs.est.0c00808, 2020.

https://doi.org/10.5194/egusphere-2026-6854
Preprint. Discussion started: 19 November 2026
© Author(s) 2026. CC BY 4.0 License.

Deng, C., Cai, R., Yan, C., Zheng, J., and Jiang, J.: Formation and growth of sub-3 nm particles in megacities: impact of background aerosols, Faraday Discuss., 226, 348–363, https://doi.org/10.1039/D0FD00083C, 2021.

Ding, A., Nie, W., Huang, X., Chi, X., Sun, J., Kerminen, V.-M., Xu, Z., Guo, W., Petäjä, T., Yang, X., Kulmala, M., and Fu, C.: Long-term observation of air pollution-weather/climate interactions at the SORPES station: a review and outlook, Frontiers of Environmental Science & Engineering, 10, 15, https://doi.org/10.1007/s11783-016-0877-3, 2016.

Donahue, N. M., Kroll, J. H., Pandis, S. N., and Robinson, A. L.: A two-dimensional volatility basis set – Part 2: Diagnostics of organic-aerosol evolution, Atmospheric Chemistry and Physics, 12, 615–634, https://doi.org/10.5194/acp-12-615-2012, 2012.

Dou, J., Liu, T., Ge, D., Zhang, Y., Yin, J., Wang, L., Liu, H., Li, D., Niu, G., Chen, L., Wang, J., Qi, X., Nie, W., Chi, X., Huang, X., and Ding, A.: In-situ secondary organic aerosol formation from ambient air in suburban Eastern China: Substantially distinct characteristics between summer and winter, Atmospheric Environment, 356, 121 295, https://doi.org/https://doi.org/10.1016/j.atmosenv.2025.121295, 2025.

Du, W., Cai, J., Zheng, F., Yan, C., Zhou, Y., Guo, Y., Chu, B., Yao, L., Heikkinen, L. M., Fan, X., Wang, Y., Cai, R., Hakala, S., Chan, T., Kontkanen, J., Tuovinen, S., Petäjä, T., Kangasluoma, J., Bianchi, F., Paasonen, P., Sun, Y., Kerminen, V.-M., Liu, Y., Daellenbach, K. R., Dada, L., and Kulmala, M.: Influence of Aerosol Chemical Composition on Condensation Sink Efficiency and New Particle Formation in Beijing, Environmental Science & Technology Letters, 9, 375–382, https://doi.org/10.1021/acs.estlett.2c00159, 2022.

Eastham, S. D., Long, M. S., Keller, C. A., Lundgren, E., Yantosca, R. M., Zhuang, J., Li, C., Lee, C. J., Yannetti, M., Auer, B. M., Clune, T. L., Kouatchou, J., Putman, W. M., Thompson, M. A., Trayanov, A. L., Molod, A. M., Martin, R. V., and Jacob, D. J.: GEOS-Chem High Performance (GCHP v11-02c): a next-generation implementation of the GEOS-Chem chemical transport model for massively parallel applications, Geoscientific Model Development, 11, 2941–2953, https://doi.org/10.5194/gmd-11-2941-2018, 2018.

Ehn, M., Thornton, J. A., Kleist, E., Sipilä, M., Junninen, H., Pullinen, I., Springer, M., Rubach, F., Tillmann, R., Lee, B., Lopez-Hilfiker, F., Andres, S., Acir, I.-H., Rissanen, M., Jokinen, T., Schobesberger, S., Kangasluoma, J., Kontkanen, J., Nieminen, T., Kurtén, T., Nielsen, L. B., Jørgensen, S., Kjaergaard, H. G., Canagaratna, M., Maso, M. D., Berndt, T., Petäjä, T., Wahner, A., Kerminen, V.-M., Kulmala, M., Worsnop, D. R., Wildt, J., and Mentel, T. F.: A large source of low-volatility secondary organic aerosol, Nature, 506, 476–479, https://doi.org/10.1038/nature13032, 2014.

Ervens, B., Rickard, A., Aumont, B., Carter, W. P. L., McGillen, M., Mellouki, A., Orlando, J., Picquet-Varrault, B., Seakins, P., Stockwell, W. R., Vereecken, L., and Wallington, T. J.: Opinion: Challenges and needs of tropospheric chemical mechanism development, Atmospheric Chemistry and Physics, 24, 13 317–13 339, https://doi.org/10.5194/acp-24-13317-2024, 2024.

Fisher, J. A., Jacob, D. J., Travis, K. R., Kim, P. S., Marais, E. A., Chan Miller, C., Yu, K., Zhu, L., Yantosca, R. M., Sulprizio, M. P., Mao, J., Wennberg, P. O., Crounse, J. D., Teng, A. P., Nguyen, T. B., St. Clair, J. M., Cohen, R. C., Romer, P., Nault, B. A., Wooldridge, P. J., Jimenez, J. L., Campuzano-Jost, P., Day, D. A., Hu, W., Shepson, P. B., Xiong, F., Blake, D. R., Goldstein, A. H., Misztal, P. K., Hanisco, T. F., Wolfe, G. M., Ryerson, T. B., Wisthaler, A., and Mikoviny, T.: Organic nitrate chemistry and its implications for nitrogen budgets in an isoprene- and monoterpene-rich atmosphere: constraints from aircraft (SEAC^{4}RS) and ground-based (SOAS) observations in the Southeast US, Atmospheric Chemistry and Physics, 16, 5969–5991, https://doi.org/10.5194/acp-16-5969-2016, 2016.

Foreback, B.: Extreme air pollution events in Beijing: Examining their origins and dynamics, Report Series in Aerosol Science, http://hdl.handle.net/10138/596273, 2025.

Foreback, B., Dada, L., Daellenbach, K. R., Yan, C., Wang, L., Chu, B., Zhou, Y., Kokkonen, T. V., Kurppa, M., Pileci, R. E., Wang, Y., Chan, T., Kangasluoma, J., Zhuohui, L., Guo, Y., Li, C., Baalbaki, R., Kujansuu, J., Fan, X., Feng, Z., Rantala, P., Gani, S., Bianchi, F., Kerminen, V.-M., Petäjä, T., Kulmala, M., Liu, Y., and Paasonen, P.: Measurement report: A multi-year study on the impacts of Chinese New Year

https://doi.org/10.5194/egusphere-2026-6854
Preprint. Discussion started: 19 November 2026
© Author(s) 2026. CC BY 4.0 License.

celebrations on air quality in Beijing, China, Atmospheric Chemistry and Physics, 22, 11 089–11 104, https://doi.org/10.5194/acp-22-11089-2022, 2022.

Foreback, B., Mahura, A., Clusius, P., Xavier, C., Baykara, M., Zhou, P., Nieminen, T., Sinclair, V., Kerminen, V.-M., Kokkonen, T. V., Hakala, S., Aliaga, D., Makkonen, R., Baklanov, A., Nuterman, R., Xia, M., Hua, C., Liu, Y., Kulmala, M., Paasonen, P., and Boy, M.: A new implementation of FLEXPART with Enviro-HIRLAM meteorological input, and a case study during a heavy air pollution event, Big Earth Data, 8, 397–434, https://doi.org/10.1080/20964471.2024.2316320, 2024.

Foreback, B., Clusius, P., Baykara, M., Mahura, A., Pichelstorfer, L., Xavier, C., Zhou, P., Kokkonen, T. V., Kerminen, V.-M., Liu, Y., Xia, M., Chen, X., Hua, C., Wang, Z., Palmer, P. I., Nuterman, R., Baklanov, A., Ciarelli, G., Sinclair, V. A., Liu, Z.-S., Ashu, T., Ashu, V., Kulmala, M., Paasonen, P., and Boy, M.: A Lagrangian view on severe haze in Beijing: local and long-range sources of trace gases and primary and secondary aerosols, Atmospheric Environment, 363, 121 602, https://doi.org/https://doi.org/10.1016/j.atmosenv.2025.121602, 2025.

Franzon, L., Vereecken, L., Valorso, R., Camredon, M., Lee-Taylor, J., Orlando, J., Kurtén, T., and Aumont, B.: Peroxy radical autoxidation in the GECKO-A automated mechanism generator: Box modelling, in preparation, 2026.

Fu, Z., Ma, F., Liu, Y., Yan, C., Huang, D., Chen, J., Elm, J., Li, Y., Ding, A., Pichelstorfer, L., Xie, H.-B., Nie, W., Francisco, J. S., and Zhou, P.: An overlooked oxidation mechanism of toluene: computational predictions and experimental validations, Chem. Sci., 14, 13 050–13 059, https://doi.org/10.1039/D3SC03638C, 2023.

Fu, Z., Zhou, P., Cui, Z., Tan, R., Cheng, X., Iyer, S., Zeng, L., Yao, M., Xie, H.-B., Boy, M. H., Hu, M., and Guo, S.: Atmospheric Autoxidation of Polycyclic Aromatic Hydrocarbons Offset Air Quality and Health Gains from Solid Fuel Restriction, Environmental Science & Technology, https://doi.org/10.1021/acs.est.5c18481, 2026.

Gao, C., Xiu, A., Zhang, X., Tong, Q., Zhao, H., Zhang, S., Yang, G., and Zhang, M.: Two-way coupled meteorology and air quality models in Asia: a systematic review and meta-analysis of impacts of aerosol feedbacks on meteorology and air quality, Atmospheric Chemistry and Physics, 22, 5265–5329, https://doi.org/10.5194/acp-22-5265-2022, 2022.

Gao, Y., Zhang, L., Zhang, G., Yan, F., Zhang, S., Sheng, L., Li, J., Wang, M., Wu, S., Fu, J. S., Yao, X., and Gao, H.: The climate impact on atmospheric stagnation and capability of stagnation indices in elucidating the haze events over North China Plain and Northeast China, Chemosphere, 258, 127 335, https://doi.org/https://doi.org/10.1016/j.chemosphere.2020.127335, 2020.

Garmash, O., Rissanen, M. P., Pullinen, I., Schmitt, S., Kausiala, O., Tillmann, R., Zhao, D., Percival, C., Bannan, T. J., Priestley, M., Hallquist, Å. M., Kleist, E., Kiendler-Scharr, A., Hallquist, M., Berndt, T., McFiggans, G., Wildt, J., Mentel, T. F., and Ehn, M.: Multi-generation OH oxidation as a source for highly oxygenated organic molecules from aromatics, Atmospheric Chemistry and Physics, 20, 515–537, https://doi.org/10.5194/acp-20-515-2020, 2020.

Ge, D., Nie, W., Sun, P., Liu, Y., Wang, T., Wang, J., Wang, J., Wang, L., Zhu, C., Wang, R., Liu, T., Chi, X., and Ding, A.: Characterization of particulate organic nitrates in the Yangtze River Delta, East China, using the time-of-flight aerosol chemical speciation monitor, Atmospheric Environment, 272, 118 927, https://doi.org/https://doi.org/10.1016/j.atmosenv.2021.118927, 2022.

Harb, S., Cirtog, M., Alage, S., Cantrell, C., Cazaunau, M., Michoud, V., Pangui, E., Bergé, A., Giorio, C., Battaglia, F., and Picquet-Varrault, B.: Highly oxygenated molecules (HOMs) and secondary organic aerosol (SOA) formation from the oxidation of α- and β-phellandrenes by NO_3 radicals, Atmospheric Chemistry and Physics, 25, 11 003–11 024, https://doi.org/10.5194/acp-25-11003-2025, 2025.

Harley, R. A. and Cass, G. R.: Modeling the atmospheric concentrations of individual volatile organic compounds, Atmospheric Environment, 29, 905–922, https://doi.org/https://doi.org/10.1016/1352-2310(94)00287-U, 1995.

https://doi.org/10.5194/egusphere-2026-6854
Preprint. Discussion started: 19 November 2026
© Author(s) 2026. CC BY 4.0 License.

Hodzic, A., Aumont, B., Knote, C., Lee-Taylor, J., Madronich, S., and Tyndall, G.: Volatility dependence of Henry's law constants of condensable organics: Application to estimate depositional loss of secondary organic aerosols, Geophysical Research Letters, 41, 4795–4804, https://doi.org/https://doi.org/10.1002/2014GL060649, 2014.

Hodzic, A., Kasibhatla, P. S., Jo, D. S., Cappa, C. D., Jimenez, J. L., Madronich, S., and Park, R. J.: Rethinking the global secondary organic aerosol (SOA) budget: stronger production, faster removal, shorter lifetime, Atmospheric Chemistry and Physics, 16, 7917–7941, https://doi.org/10.5194/acp-16-7917-2016, 2016.

Hu, L., Millet, D. B., Baasandorj, M., Griffis, T. J., Travis, K. R., Tessum, C. W., Marshall, J. D., Reinhart, W. F., Mikoviny, T., Müller, M., Wisthaler, A., Graus, M., Warneke, C., and de Gouw, J.: Emissions of C6–C8 aromatic compounds in the United States: Constraints from tall tower and aircraft measurements, Journal of Geophysical Research: Atmospheres, 120, 826–842, https://doi.org/https://doi.org/10.1002/2014JD022627, 2015.

Huang, L., Wu, Z., Liu, H., Yarwood, G., Huang, D., Wilson, G., Chen, H., Ji, D., Tao, J., Han, Z., Wang, Y., Wang, H., Huang, C., and Li, L.: An improved framework for efficiently modeling organic aerosol (OA) considering primary OA evaporation and secondary OA formation from VOCs, IVOCs, and SVOCs, Environmental Science: Atmospheres, 4, 1064–1078, https://doi.org/10.1039/D4EA00060A, 2024a.

Huang, L., Chen, B., Wu, Z., Tuite, K., Vennam, P., Yarwood, G., and Li, L.: Comparing secondary organic aerosols schemes implemented in current chemical transport models and the policy implications of uncertainties, Atmospheric Chemistry and Physics, 26, 7895–7915, https://doi.org/10.5194/acp-26-7895-2026, 2026.

Huang, Q., Cai, X., Song, Y., and Zhu, T.: Air stagnation in China (1985–2014): climatological mean features and trends, Atmospheric Chemistry and Physics, 17, 7793–7805, https://doi.org/10.5194/acp-17-7793-2017, 2017.

Huang, Q., Cai, X., Wang, J., Song, Y., and Zhu, T.: Climatological study of the Boundary-layer air Stagnation Index for China and its relationship with air pollution, Atmospheric Chemistry and Physics, 18, 7573–7593, https://doi.org/10.5194/acp-18-7573-2018, 2018.

Huang, X., Ge, Y., Yang, T., Song, Z., Yu, S., Li, Q., Wang, X., Wang, Y., Wang, X., Su, J., Xue, L., Mellouki, A., and Chen, J.: Relaxation of Spring Festival Firework Regulations Leads to a Deterioration in Air Quality, Environmental Science & Technology, 58, 10 185–10 194, https://doi.org/10.1021/acs.est.4c00920, 2024b.

Iyer, S., Kumar, A., Savolainen, A., Barua, S., Daub, C., Pichelstorfer, L., Roldin, P., Garmash, O., Seal, P., Kurtén, T., and Rissanen, M.: Molecular rearrangement of bicyclic peroxy radicals is a key route to aerosol from aromatics, Nature Communications, 14, 4984, https://doi.org/10.1038/s41467-023-40675-2, 2023.

Jenkin, M. E., Saunders, S. M., and Pilling, M. J.: The tropospheric degradation of volatile organic compounds: a protocol for mechanism development, Atmospheric Environment, 31, 81–104, https://doi.org/https://doi.org/10.1016/S1352-2310(96)00105-7, 1997.

Jenkin, M. E., Saunders, S. M., Wagner, V., and Pilling, M. J.: Protocol for the development of the Master Chemical Mechanism, MCM v3 (Part B): tropospheric degradation of aromatic volatile organic compounds, Atmospheric Chemistry and Physics, 3, 181–193, https://doi.org/10.5194/acp-3-181-2003, 2003.

Jenkin, M. E., Valorso, R., Aumont, B., and Rickard, A. R.: Estimation of rate coefficients and branching ratios for reactions of organic peroxy radicals for use in automated mechanism construction, Atmospheric Chemistry and Physics, 19, 7691–7717, https://doi.org/10.5194/acp-19-7691-2019, 2019.

Jiang, M., Feng, X., Feng, Y., Lu, Y., Li, L., Chen, Y., and Chen, T.: Field observations of intermediate volatile organic compounds during haze events in three cities of northern China: Characteristics, sources and contributions to SOA formation, Atmospheric Environment, 353, 121 232, https://doi.org/https://doi.org/10.1016/j.atmosenv.2025.121232, 2025.

https://doi.org/10.5194/egusphere-2026-6854
Preprint. Discussion started: 19 November 2026
© Author(s) 2026. CC BY 4.0 License.

Jiang, Q., Wang, F., and Sun, Y.: Analysis of Chemical Composition, Source and Processing Characteristics of Submicron Aerosol during the Summer in Beijing, China, Aerosol and Air Quality Research, 19, 1450–1462, https://doi.org/10.4209/aaqr.2018.12.0480, 2019.

Kang, M., Bao, M., Song, W., Abulimiti, A., Wu, C., Cao, F., Szidat, S., and Zhang, Y.: Significant role of biomass burning in heavy haze formation in Nanjing, a megacity in China: molecular-level insights from intensive $PM_{2.5}$ sampling on winter hazy days, Atmospheric Chemistry and Physics, 25, 73–91, https://doi.org/10.5194/acp-25-73-2025, 2025.

Keller, C. A. and Evans, M. J.: Application of random forest regression to the calculation of gas-phase chemistry within the GEOS-Chem chemistry model v10, Geoscientific Model Development, 12, 1209–1225, https://doi.org/10.5194/gmd-12-1209-2019, 2019.

Kerminen, V.-M. and Kulmala, M.: Analytical formulae connecting the "real" and the "apparent" nucleation rate and the nuclei number concentration for atmospheric nucleation events, Journal of Aerosol Science, 33, 609–622, https://doi.org/https://doi.org/10.1016/S0021-8502(01)00194-X, 2002.

Khoshakhlagh, A. H., Yazdanirad, S., and Ducatman, A.: Climatic conditions and concentrations of BTEX compounds in atmospheric media, Environmental Research, 251, 118 553, https://doi.org/https://doi.org/10.1016/j.envres.2024.118553, 2024.

Knote, C., Hodzic, A., and Jimenez, J. L.: The effect of dry and wet deposition of condensable vapors on secondary organic aerosols concentrations over the continental US, Atmospheric Chemistry and Physics, 15, 1–18, https://doi.org/10.5194/acp-15-1-2015, 2015.

Kodros, J. K. and Pierce, J. R.: Important global and regional differences in aerosol cloud-albedo effect estimates between simulations with and without prognostic aerosol microphysics, Journal of Geophysical Research: Atmospheres, 122, 4003–4018, https://doi.org/https://doi.org/10.1002/2016JD025886, 2017.

Kong, S. F., Li, L., Li, X. X., Yin, Y., Chen, K., Liu, D. T., Yuan, L., Zhang, Y. J., Shan, Y. P., and Ji, Y. Q.: The impacts of firework burning at the Chinese Spring Festival on air quality: insights of tracers, source evolution and aging processes, Atmospheric Chemistry and Physics, 15, 2167–2184, https://doi.org/10.5194/acp-15-2167-2015, 2015.

Kulmala, M.: Atmospheric chemistry: China's choking cocktail, Nature, 526, 497–499, https://doi.org/10.1038/526497a, 2015.

Kulmala, M.: Importance of New Particle Formation for Climate and Air Quality, ACS ES&T Air, 2, 710–712, https://doi.org/10.1021/acsestair.5c00095, 2025.

Kulmala, M., Kerminen, V.-M., Petäjä, T., Ding, A. J., and Wang, L.: Atmospheric gas-to-particle conversion: why NPF events are observed in megacities?, Faraday Discuss., 200, 271–288, https://doi.org/10.1039/C6FD00257A, 2017.

Kwon, H.-S., Ryu, M. H., and Carlsten, C.: Ultrafine particles: unique physicochemical properties relevant to health and disease, Experimental & Molecular Medicine, 52, 318–328, https://doi.org/10.1038/s12276-020-0405-1, 2020.

Lappalainen, H. K., Petäjä, T., Vihma, T., Räisänen, J., Baklanov, A., Chalov, S., Esau, I., Ezhova, E., Leppäranta, M., Pozdnyakov, D., Pumpanen, J., Andreae, M. O., Arshinov, M., Asmi, E., Bai, J., Bashmachnikov, I., Belan, B., Bianchi, F., Biskaborn, B., Boy, M., Bäck, J., Cheng, B., Chubarova, N., Duplissy, J., Dyukarev, E., Eleftheriadis, K., Forsius, M., Heimann, M., Juhola, S., Konovalov, V., Konovalov, I., Konstantinov, P., Köster, K., Lapshina, E., Lintunen, A., Mahura, A., Makkonen, R., Malkhazova, S., Mammarella, I., Mammola, S., Buenrostro Mazon, S., Meinander, O., Mikhailov, E., Miles, V., Myslenkov, S., Orlov, D., Paris, J.-D., Pirazzini, R., Popovicheva, O., Pulliainen, J., Rautiainen, K., Sachs, T., Shevchenko, V., Skorokhod, A., Stohl, A., Suhonen, E., Thomson, E. S., Tsidilina, M., Tynkkynen, V.-P., Uotila, P., Virkkula, A., Voropay, N., Wolf, T., Yasunaka, S., Zhang, J., Qiu, Y., Ding, A., Guo, H., Bondur, V., Kasimov, N., Zilitinkevich, S., Kerminen, V.-M., and Kulmala, M.: Overview: Recent advances in the understanding of the northern Eurasian environments and of the urban air quality in China – a Pan-Eurasian Experiment (PEEX) programme perspective, Atmospheric Chemistry and Physics, 22, 4413–4469, https://doi.org/10.5194/acp-22-4413-2022, 2022.

https://doi.org/10.5194/egusphere-2026-6854
Preprint. Discussion started: 19 November 2026
© Author(s) 2026. CC BY 4.0 License.

Le Bayon, A., Ojala, A., Iyer, S., Wang, Z., Lannuque, V., Couvidat, F., Ciuraru, R., and Sartelet, K.: Molecular representation of benzene and phenol secondary organic aerosols, Atmospheric Chemistry and Physics, 26, 14 749–14 768, https://doi.org/10.5194/acp-26-14749-2026, 2026.

Lehtipalo, K., Leppä, J., Kontkanen, J., Kangasluoma, J., Franchin, A., Wimmer, D., Schobesberger, S., Junninen, H., Petäjä, T., Sipilä, M., Mikkilä, J., Vanhanen, J., Worsnop, D. R., and Kulmala, M.: Methods for determining particle size distribution and growth rates between 1 and 3 nm using the Particle Size Magnifier, Boreal Environment Research, 19, 215–236, http://hdl.handle.net/10138/165200, 2014.

Lelieveld, J., Pozzer, A., Pöschl, U., Fnais, M., Haines, A., and Münzel, T.: Loss of life expectancy from air pollution compared to other risk factors: a worldwide perspective, Cardiovascular Research, 116, 1910–1917, https://doi.org/10.1093/cvr/cvaa025, 2020.

Lelieveld, J., Georgiades, P., Kohl, M., Cheng, Y., Christoudias, T., Sciare, J., Nicolaou, M., Dovrolis, C., Fnais, M., Kulmala, M., Daiber, A., Hahad, O., Kuntic, M., Münzel, T., and Pozzer, A.: Air quality and health implications of exposure to ultrafine particle pollution, Cardiovascular Research, 122, 1660–1671, https://doi.org/10.1093/cvr/cvag136, 2026.

Li, J., Zhang, H., Li, L., Ye, F., Wang, H., Guo, S., Zhang, N., Qin, M., and Hu, J.: Modeling Secondary Organic Aerosols in China: State of the Art and Perspectives, Current Pollution Reports, 9, 22–45, https://doi.org/10.1007/s40726-022-00246-3, 2023a.

Li, Z., Zhao, B., Yin, D., Wang, S., Qiao, X., Jiang, J., Li, Y., Shen, J., He, Y., Chang, X., Li, X., Liu, Y., Li, Y., Liu, C., Qi, X., Chen, L., Chi, X., Jiang, Y., Li, Y., Wu, J., Nie, W., and Ding, A.: Modeling the Formation of Organic Compounds across Full Volatility Ranges and Their Contribution to Nanoparticle Growth in a Polluted Atmosphere, Environmental Science & Technology, 58, 1223–1235, https://doi.org/10.1021/acs.est.3c06708, 2023b.

Lin, H., Jacob, D. J., Lundgren, E. W., Sulprizio, M. P., Keller, C. A., Fritz, T. M., Eastham, S. D., Emmons, L. K., Campbell, P. C., Baker, B., Saylor, R. D., and Montuoro, R.: Harmonized Emissions Component (HEMCO) 3.0 as a versatile emissions component for atmospheric models: application in the GEOS-Chem, NASA GEOS, WRF-GC, CESM2, NOAA GEFS-Aerosol, and NOAA UFS models, Geoscientific Model Development, 14, 5487–5506, https://doi.org/10.5194/gmd-14-5487-2021, 2021.

Liu, H., Liu, T., Yu, C., Xie, Y., Wang, Q., Zha, Q., Chi, X., Song, W., Wang, X., Lou, S., Huang, X., and Ding, A.: Kinetics and Mechanisms of Reactive Uptake of Methylglyoxal on Deliquesced Ammonium Salts: Acid Catalysis and Sulfate Inhibition, Environmental Science & Technology, 60, 5619–5627, https://doi.org/10.1021/acs.est.5c13815, 2026.

Liu, P., Ye, C., Xue, C., Zhang, C., Mu, Y., and Sun, X.: Formation mechanisms of atmospheric nitrate and sulfate during the winter haze pollution periods in Beijing: gas-phase, heterogeneous and aqueous-phase chemistry, Atmospheric Chemistry and Physics, 20, 4153–4165, https://doi.org/10.5194/acp-20-4153-2020, 2020.

Liu, T., Chan, A. W. H., and Abbatt, J. P. D.: Multiphase Oxidation of Sulfur Dioxide in Aerosol Particles: Implications for Sulfate Formation in Polluted Environments, Environmental Science & Technology, 55, 4227–4242, https://doi.org/10.1021/acs.est.0c06496, 2021.

Liu, X., Zhang, X., Dufresne, M., Wang, T., Wu, L., Lara, R., Seco, R., Monge, M., Yáñez Serrano, A. M., Gohy, M., Petit, P., Chevalier, A., Vagnot, M.-P., Fortier, Y., Baudic, A., Ghersi, V., Gille, G., Lanzi, L., Gros, V., Simon, L., Héllen, H., Reimann, S., Le Bras, Z., Müller, M. J., Beddows, D., Hou, S., Shi, Z., Harrison, R. M., Bloss, W., Dernie, J., Sauvage, S., Hopke, P. K., Duan, X., An, T., Lewis, A. C., Hopkins, J. R., Liakakou, E., Mihalopoulos, N., Zhang, X., Alastuey, A., Querol, X., and Salameh, T.: Measurement report: Exploring the variations in ambient BTEX in urban Europe and their environmental health implications, Atmospheric Chemistry and Physics, 25, 625–638, https://doi.org/10.5194/acp-25-625-2025, 2025.

Loomis, D., Guyton, K. Z., Grosse, Y., El Ghissassi, F., Bouvard, V., Benbrahim-Tallaa, L., Guha, N., Vilahur, N., Mattock, H., and Straif, K.: Carcinogenicity of benzene, The Lancet Oncology, 18, 1574–1575, https://doi.org/10.1016/S1470-2045(17)30832-X, 2017.

https://doi.org/10.5194/egusphere-2026-6854
Preprint. Discussion started: 19 November 2026
© Author(s) 2026. CC BY 4.0 License.

Ma, Q., Zhang, C., Liu, C., He, G., Zhang, P., Li, H., Chu, B., and He, H.: A review on the heterogeneous oxidation of SO_2 on solid atmospheric particles: Implications for sulfate formation in haze chemistry, Critical Reviews in Environmental Science and Technology, 53, 1888–1911, https://doi.org/10.1080/10643389.2023.2190315, 2023.

Mahura, A., Baklanov, A., Makkonen, R., Boy, M., Petäjä, T., Lappalainen, H. K., Nuterman, R., Kerminen, V.-M., Arnold, S. R., Jochum, M., Shvidenko, A., Esau, I., Sofiev, M., Stohl, A., Aalto, T., Bai, J., Chen, C., Cheng, Y., Drofa, O., Huang, M., Järvi, L., Kokkola, H., Kouznetsov, R., Li, T., Malguzzi, P., Monks, S., Poulsen, M. B., Noe, S. M., Palamarchuk, Y., Foreback, B., Clusius, P., Rasmussen, T. A. S., She, J., Sørensen, J. H., Spracklen, D., Su, H., Tonttila, J., Wang, S., Wang, J., Wolf-Grosse, T., Yu, Y., Zhang, Q., Zhang, W., Zhang, W., Zheng, X., Li, S., Li, Y., Zhou, P., and Kulmala, M.: Towards seamless environmental prediction – development of Pan-Eurasian EXperiment (PEEX) modelling platform, Big Earth Data, 8, 189–230, https://doi.org/10.1080/20964471.2024.2325019, 2024.

Mayhew, A. W., Franzon, L., Bates, K. H., Kurtén, T., Lopez-Hilfiker, F. D., Mohr, C., Rickard, A. R., Thornton, J. A., and Haskins, J. D.: The global importance of gas-phase peroxy radical accretion reactions for secondary organic aerosol loading, Atmospheric Chemistry and Physics, 25, 17 027–17 046, https://doi.org/10.5194/acp-25-17027-2025, 2025.

Mehra, A., Wang, Y., Krechmer, J. E., Lambe, A., Majluf, F., Morris, M. A., Priestley, M., Bannan, T. J., Bryant, D. J., Pereira, K. L., Hamilton, J. F., Rickard, A. R., Newland, M. J., Stark, H., Croteau, P., Jayne, J. T., Worsnop, D. R., Canagaratna, M. R., Wang, L., and Coe, H.: Evaluation of the chemical composition of gas- and particle-phase products of aromatic oxidation, Atmospheric Chemistry and Physics, 20, 9783–9803, https://doi.org/10.5194/acp-20-9783-2020, 2020.

Meng, X., Zhou, Y., Shi, S., Wang, S., Zaid, M., Zhang, H., Hu, J., Li, G., Kan, H., and Zhou, M.: Mortality and long-term exposure to source-specific $PM_{2.5}$: evidence from a national cohort study in China, The Lancet Planetary Health, 10, 101 400, https://doi.org/10.1016/j.lanplh.2025.101400, 2026.

Miao, R., Xu, R., Huang, S., Xiao, S., Wang, H., Zheng, Y., Liu, S., Li, J., Geng, G., Shrivastava, M., Dao, X., Granier, C., Brasseur, G., Karydis, V. A., Tsimpidi, A. P., Jiang, J., Daellenbach, K. R., Haddad, I. E., Prévôt, A. S. H., and Chen, Q.: Global budgets of atmospheric primary and secondary organic aerosols constrained by full-volatility-range organic emissions, EGUsphere, 2026, 1–33, https://doi.org/10.5194/egusphere-2026-3160, 2026.

Mielczarek, D. C., Matrat, M., Amara, A. B., Bouyou, Y., Wund, P., and Starck, L.: Toward the Accurate Prediction of Liquid Phase Oxidation of Aromatics: A Detailed Kinetic Mechanism for Toluene Autoxidation, Energy & Fuels, 31, 12 893–12 913, https://doi.org/10.1021/acs.energyfuels.7b00416, 2017.

Ministry of Ecology and Environment of the People's Republic of China: Ambient air quality standards, https://english.mee.gov.cn/Resources/standards/Air_Environment/quality_standard1/201605/t20160511_337502.shtml, accessed: 2026-08-28, 2016.

Miri, M., Rostami Aghdam Shendi, M., Ghaffari, H. R., Ebrahimi Aval, H., Ahmadi, E., Taban, E., Gholizadeh, A., Yazdani Aval, M., Mohammadi, A., and Azari, A.: Investigation of outdoor BTEX: Concentration, variations, sources, spatial distribution, and risk assessment, Chemosphere, 163, 601–609, https://doi.org/https://doi.org/10.1016/j.chemosphere.2016.07.088, 2016.

Molteni, U., Bianchi, F., Klein, F., El Haddad, I., Frege, C., Rossi, M. J., Dommen, J., and Baltensperger, U.: Formation of highly oxygenated organic molecules from aromatic compounds, Atmospheric Chemistry and Physics, 18, 1909–1921, https://doi.org/10.5194/acp-18-1909-2018, 2018.

Montero-Montoya, R., López-Vargas, R., and Arellano-Aguilar, O.: Volatile Organic Compounds in Air: Sources, Distribution, Exposure and Associated Illnesses in Children, Annals of Global Health, https://doi.org/10.29024/aogh.910, 2018.

Mozaffar, A. and Zhang, Y.-L.: Atmospheric Volatile Organic Compounds (VOCs) in China: a Review, Current Pollution Reports, 6, 250–263, https://doi.org/10.1007/s40726-020-00149-1, 2020.

https://doi.org/10.5194/egusphere-2026-6854
Preprint. Discussion started: 19 November 2026
© Author(s) 2026. CC BY 4.0 License.

Napari, I., Noppel, M., Vehkamäki, H., and Kulmala, M.: Parametrization of ternary nucleation rates for H2SO4-NH3-H2O vapors, Journal of Geophysical Research: Atmospheres, 107, AAC 6–1–AAC 6–6, https://doi.org/https://doi.org/10.1029/2002JD002132, 2002.

NASA Global Modeling and Assimilation Office (GMAO): Modern-Era Retrospective analysis for Research and Applications, Version 2 (MERRA-2), https://gmao.gsfc.nasa.gov/gmao-products/merra-2/, accessed: 2025-12-03, 2025.

Niu, G., Qi, X., Chen, L., Xue, L., Lai, S., Huang, X., Wang, J., Chi, X., Nie, W., Kerminen, V.-M., Petäjä, T., Kulmala, M., and Ding, A.: The variation in the particle number size distribution during the rainfall: wet scavenging and air mass changing, Atmospheric Chemistry and Physics, 23, 7521–7534, https://doi.org/10.5194/acp-23-7521-2023, 2023.

Niu, G., Qi, X., Chen, L., Ma, J., Zha, Q., Wang, J., Chi, X., Liu, T., Nie, W., Paasonen, P., Kerminen, V.-M., Petäjä, T., Kulmala, M., and Ding, A.: Cloud Condensation Nuclei and the Contribution of New Particle Formation in the Yangtze River Delta of Eastern China, Journal of Geophysical Research: Atmospheres, 131, e2025JD045 881, https://doi.org/https://doi.org/10.1029/2025JD045881, e2025JD045881 2025JD045881, 2026.

Norman, O. G., Heald, C. L., Bililign, S., Campuzano-Jost, P., Coe, H., Fiddler, M. N., Green, J. R., Jimenez, J. L., Kaiser, K., Liao, J., Middlebrook, A. M., Nault, B. A., Nowak, J. B., Schneider, J., and Welti, A.: Exploring the processes controlling secondary inorganic aerosol: evaluating the global GEOS-Chem simulation using a suite of aircraft campaigns, Atmospheric Chemistry and Physics, 25, 771–795, https://doi.org/10.5194/acp-25-771-2025, 2025.

OECD (Organisation for Economic Co-operation and Development): The Economic Consequences of Outdoor Air Pollution, Tech. rep., OECD Publishing, Paris, https://doi.org/10.1787/9789264257474-en, 2016.

Ojala, A., Le Bayon, A., Kumar, A., Vinkvist, N., Savolainen, A., Kervinen, A., Sartelet, K., Rissanen, M., and Iyer, S.: Secondary organic aerosol formation from sequential oxidation of toluene and cresols, Nature Communications, https://doi.org/10.1038/s41467-026-78858-2, 2026.

Olenius, T., Pichelstorfer, L., Stolzenburg, D., Winkler, P. M., Lehtinen, K. E. J., and Riipinen, I.: Robust metric for quantifying the importance of stochastic effects on nanoparticle growth, Scientific Reports, 8, 14 160, https://doi.org/10.1038/s41598-018-32610-z, 2018.

Pai, S. J., Heald, C. L., Pierce, J. R., Farina, S. C., Marais, E. A., Jimenez, J. L., Campuzano-Jost, P., Nault, B. A., Middlebrook, A. M., Coe, H., Shilling, J. E., Bahreini, R., Dingle, J. H., and Vu, K.: An evaluation of global organic aerosol schemes using airborne observations, Atmospheric Chemistry and Physics, 20, 2637–2665, https://doi.org/10.5194/acp-20-2637-2020, 2020.

Peräkylä, O., Riva, M., Heikkinen, L., Quéléver, L., Roldin, P., and Ehn, M.: Experimental investigation into the volatilities of highly oxygenated organic molecules (HOMs), Atmospheric Chemistry and Physics, 20, 649–669, https://doi.org/10.5194/acp-20-649-2020, 2020.

Pichelstorfer, L., Roldin, P., Rissanen, M., Hyttinen, N., Garmash, O., Xavier, C., Zhou, P., Clusius, P., Foreback, B., Golin Almeida, T., Deng, C., Baykara, M., Kurten, T., and Boy, M.: Towards automated inclusion of autoxidation chemistry in models: from precursors to atmospheric implications, Environmental Science: Atmospheres, 4, 879–896, https://doi.org/10.1039/D4EA00054D, 2024.

Pichelstorfer, L., O'Meara, S. P., and McFiggans, G.: A theory-informed, experiment-based constraint on the rate of autoxidation chemistry – an analytical approach, Aerosol Research, 3, 417–428, https://doi.org/10.5194/ar-3-417-2025, 2025.

Pierce, J. R. and Adams, P. J.: Uncertainty in global CCN concentrations from uncertain aerosol nucleation and primary emission rates, Atmospheric Chemistry and Physics, 9, 1339–1356, https://doi.org/10.5194/acp-9-1339-2009, 2009.

Poulain, L., Tilgner, A., Brüggemann, M., Mettke, P., He, L., Anders, J., Böge, O., Mutzel, A., and Herrmann, H.: Particle-Phase Uptake and Chemistry of Highly Oxygenated Organic Molecules (HOMs) From α-Pinene OH Oxidation, Journal of Geophysical Research: Atmospheres, 127, e2021JD036 414, https://doi.org/https://doi.org/10.1029/2021JD036414, e2021JD036414 2021JD036414, 2022.

https://doi.org/10.5194/egusphere-2026-6854
Preprint. Discussion started: 19 November 2026
© Author(s) 2026. CC BY 4.0 License.

Pye, H. O. T. and Seinfeld, J. H.: A global perspective on aerosol from low-volatility organic compounds, Atmospheric Chemistry and Physics, 10, 4377–4401, https://doi.org/10.5194/acp-10-4377-2010, 2010.

Rissanen, M. P., Kurtén, T., Sipilä, M., Thornton, J. A., Kangasluoma, J., Sarnela, N., Junninen, H., Jørgensen, S., Schallhart, S., Kajos, M. K., Taipale, R., Springer, M., Mentel, T. F., Ruuskanen, T., Petäjä, T., Worsnop, D. R., Kjaergaard, H. G., and Ehn, M.: The Formation of Highly Oxidized Multifunctional Products in the Ozonolysis of Cyclohexene, Journal of the American Chemical Society, 136, 15 596–15 606, https://doi.org/10.1021/ja507146s, 2014.

Roldin, P., Ehn, M., Kurtén, T., Olenius, T., Rissanen, M. P., Sarnela, N., Elm, J., Rantala, P., Hao, L., Hyttinen, N., Heikkinen, L., Worsnop, D. R., Pichelstorfer, L., Xavier, C., Clusius, P., Öström, E., Petäjä, T., Kulmala, M., Vehkamäki, H., Virtanen, A., Riipinen, I., and Boy, M.: The role of highly oxygenated organic molecules in the Boreal aerosol-cloud-climate system, Nature Communications, 10, 4370, https://doi.org/10.1038/s41467-019-12338-8, 2019.

Saide, P. E., Gao, M., Lu, Z., Goldberg, D. L., Streets, D. G., Woo, J.-H., Beyersdorf, A., Corr, C. A., Thornhill, K. L., Anderson, B., Hair, J. W., Nehrir, A. R., Diskin, G. S., Jimenez, J. L., Nault, B. A., Campuzano-Jost, P., Dibb, J., Heim, E., Lamb, K. D., Schwarz, J. P., Perring, A. E., Kim, J., Choi, M., Holben, B., Pfister, G., Hodzic, A., Carmichael, G. R., Emmons, L., and Crawford, J. H.: Understanding and improving model representation of aerosol optical properties for a Chinese haze event measured during KORUS-AQ, Atmospheric Chemistry and Physics, 20, 6455–6478, https://doi.org/10.5194/acp-20-6455-2020, 2020.

Sander, R.: Compilation of Henry's law constants (version 5.0.0) for water as solvent, Atmospheric Chemistry and Physics, 23, 10 901–12 440, https://doi.org/10.5194/acp-23-10901-2023, 2023.

Saunders, S. M., Jenkin, M. E., Derwent, R. G., and Pilling, M. J.: Protocol for the development of the Master Chemical Mechanism, MCM v3 (Part A): tropospheric degradation of non-aromatic volatile organic compounds, Atmospheric Chemistry and Physics, 3, 161–180, https://doi.org/10.5194/acp-3-161-2003, 2003.

Seidel, D. J. and Birnbaum, A. N.: Effects of Independence Day fireworks on atmospheric concentrations of fine particulate matter in the United States, Atmospheric Environment, 115, 192–198, https://doi.org/https://doi.org/10.1016/j.atmosenv.2015.05.065, 2015.

Shao, X., Wang, M., Dong, X., Liu, Y., Shen, W., Arnold, S. R., Regayre, L. A., Andreae, M. O., Pöhlker, M. L., Jo, D. S., Yue, M., and Carslaw, K. S.: Global modeling of aerosol nucleation with a semi-explicit chemical mechanism for highly oxygenated organic molecules (HOMs), Atmospheric Chemistry and Physics, 24, 11 365–11 389, https://doi.org/10.5194/acp-24-11365-2024, 2024.

Shao, X., Liu, Y., Dong, X., Wang, M., Xu, R., Thornton, J. A., Jo, D. S., Yue, M., Shen, W., Shrivastava, M., Arnold, S. R., and Carslaw, K. S.: A modeling study of global distribution and formation pathways of highly oxygenated organic molecules (HOMs) from monoterpenes, Atmospheric Chemistry and Physics, 26, 6427–6448, https://doi.org/10.5194/acp-26-6427-2026, 2026.

Shen, J., Liu, X., Zhang, Y., Fangmeier, A., Goulding, K., and Zhang, F.: Atmospheric ammonia and particulate ammonium from agricultural sources in the North China Plain, Atmospheric Environment, 45, 5033–5041, https://doi.org/https://doi.org/10.1016/j.atmosenv.2011.02.031, 2011.

Shen, L., Wang, H., Gao, W., Yang, Y., Huang, W., Wang, L., Zhang, R., Zou, J., Ji, D., and Wang, Y.: Real-time physiochemistry of urban aerosols during a regional haze episode by a single-particle aerosol mass spectrometer: Mixing state, size distribution and source apportionment, Atmospheric Pollution Research, 11, 1329–1338, https://doi.org/https://doi.org/10.1016/j.apr.2020.05.010, 2020.

Shen, Y., Virkkula, A., Ding, A., Wang, J., Chi, X., Nie, W., Qi, X., Huang, X., Liu, Q., Zheng, L., Xu, Z., Petäjä, T., Aalto, P. P., Fu, C., and Kulmala, M.: Aerosol optical properties at SORPES in Nanjing, east China, Atmospheric Chemistry and Physics, 18, 5265–5292, https://doi.org/10.5194/acp-18-5265-2018, 2018.

https://doi.org/10.5194/egusphere-2026-6854
Preprint. Discussion started: 19 November 2026
© Author(s) 2026. CC BY 4.0 License.

Shi, Y., Couvidat, F., Lannuque, V., and Sartelet, K.: Modeling secondary organic aerosols from β-caryophyllene: role of extremely low-volatile organic compounds on new particle formation and evaluation of the SOA composition, Environmental Science: Atmospheres, https://doi.org/10.1039/D5EA00133A, 2026.

Sokhi, R. S., Moussiopoulos, N., Baklanov, A., Bartzis, J., Coll, I., Finardi, S., Friedrich, R., Geels, C., Grönholm, T., Halenka, T., Ketzel, M., Maragkidou, A., Matthias, V., Moldanova, J., Ntziachristos, L., Schäfer, K., Suppan, P., Tsegas, G., Carmichael, G., Franco, V., Hanna, S., Jalkanen, J.-P., Velders, G. J. M., and Kukkonen, J.: Advances in air quality research – current and emerging challenges, Atmospheric Chemistry and Physics, 22, 4615–4703, https://doi.org/10.5194/acp-22-4615-2022, 2022.

Stolzenburg, D., Fischer, L., Vogel, A. L., Heinritzi, M., Schervish, M., Simon, M., Wagner, A. C., Dada, L., Ahonen, L. R., Amorim, A., Baccarini, A., Bauer, P. S., Baumgartner, B., Bergen, A., Bianchi, F., Breitenlechner, M., Brilke, S., Mazon, S. B., Chen, D., Dias, A., Draper, D. C., Duplissy, J., Haddad, I. E., Finkenzeller, H., Frege, C., Fuchs, C., Garmash, O., Gordon, H., He, X., Helm, J., Hofbauer, V., Hoyle, C. R., Kim, C., Kirkby, J., Kontkanen, J., Kürten, A., Lampilahti, J., Lawler, M., Lehtipalo, K., Leiminger, M., Mai, H., Mathot, S., Mentler, B., Molteni, U., Nie, W., Nieminen, T., Nowak, J. B., Ojdanic, A., Onnela, A., Passananti, M., Petäjä, T., Quéléver, L. L. J., Rissanen, M. P., Sarnela, N., Schallhart, S., Tauber, C., Tomé, A., Wagner, R., Wang, M., Weitz, L., Wimmer, D., Xiao, M., Yan, C., Ye, P., Zha, Q., Baltensperger, U., Curtius, J., Dommen, J., Flagan, R. C., Kulmala, M., Smith, J. N., Worsnop, D. R., Hansel, A., Donahue, N. M., and Winkler, P. M.: Rapid growth of organic aerosol nanoparticles over a wide tropospheric temperature range, Proceedings of the National Academy of Sciences, 115, 9122–9127, https://doi.org/10.1073/pnas.1807604115, 2018.

Stolzenburg, D., Wang, M., Schervish, M., and Donahue, N. M.: Tutorial: Dynamic organic growth modeling with a volatility basis set, Journal of Aerosol Science, 166, 106 063, https://doi.org/https://doi.org/10.1016/j.jaerosci.2022.106063, 2022.

Sun, P., Nie, W., Wang, T., Chi, X., Huang, X., Xu, Z., Zhu, C., Wang, L., Qi, X., Zhang, Q., and Ding, A.: Impact of air transport and secondary formation on haze pollution in the Yangtze River Delta: In situ online observations in Shanghai and Nanjing, Atmospheric Environment, 225, 117 350, https://doi.org/https://doi.org/10.1016/j.atmosenv.2020.117350, 2020.

Słomińska, M., Konieczka, P., and Namieśnik, J.: The Fate of BTEX Compounds in Ambient Air, Critical Reviews in Environmental Science and Technology, 44, 455–472, https://doi.org/10.1080/10643389.2012.728808, 2014.

Tang, R., Zhao, J., Liu, Y., Huang, X., Zhang, Y., Zhou, D., Ding, A., Nielsen, C. P., and Wang, H.: Air quality and health co-benefits of China's carbon dioxide emissions peaking before 2030, Nature Communications, 13, 1008, https://doi.org/10.1038/s41467-022-28672-3, 2022.

The International GEOS-Chem Community: New GEOS-Chem Developments, https://geoschem.github.io/new-developments.html, accessed: 2026-10-26, 2026.

The International GEOS-Chem User Community: geoschem/geos-chem: GEOS-Chem 14.6.3, https://doi.org/10.5281/zenodo.16538682, 2025.

Travis, K. R., Nault, B. A., Crawford, J. H., Kim, H., Chen, Q., Zheng, Y., Liu, T., Jimenez, J. L., Campuzano-Jost, P., Wennberg, P. O., Crounse, J. D., and Huey, L. G.: Year-Round Analysis of Multiphase Sulfate Production in Aerosol Particles in East Asia, ACS ES&T Air, 2, 1758–1769, https://doi.org/10.1021/acsestair.5c00136, 2025.

Trivitayanurak, W., Adams, P. J., Spracklen, D. V., and Carslaw, K. S.: Tropospheric aerosol microphysics simulation with assimilated meteorology: model description and intermodel comparison, Atmospheric Chemistry and Physics, 8, 3149–3168, https://doi.org/10.5194/acp-8-3149-2008, 2008.

https://doi.org/10.5194/egusphere-2026-6854
Preprint. Discussion started: 19 November 2026
© Author(s) 2026. CC BY 4.0 License.

Tsiligiannis, E., Hammes, J., Salvador, C. M., Mentel, T. F., and Hallquist, M.: Effect of NO_x on 1,3,5-trimethylbenzene (TMB) oxidation product distribution and particle formation, Atmospheric Chemistry and Physics, 19, 15 073–15 086, https://doi.org/10.5194/acp-19-15073-2019, 2019.

Tuovinen, S., Kontkanen, J., Cai, R., and Kulmala, M.: Condensation sink of atmospheric vapors: the effect of vapor properties and the resulting uncertainties, Environmental Science: Atmospheres, 1, 543–557, https://doi.org/10.1039/D1EA00032B, 2021.

Vehkamäki, H., Kulmala, M., Napari, I., Lehtinen, K. E. J., Timmreck, C., Noppel, M., and Laaksonen, A.: An improved parameterization for sulfuric acid–water nucleation rates for tropospheric and stratospheric conditions, Journal of Geophysical Research: Atmospheres, 107, AAC 3–1–AAC 3–10, https://doi.org/https://doi.org/10.1029/2002JD002184, 2002.

Wang, J., de Leeuw, G., Niu, S., and Kang, H.: Contrasting Aerosol Optical Characteristics and Source Regions During Summer and Winter Pollution Episodes in Nanjing, China, Remote Sensing, 11, https://doi.org/10.3390/rs11141696, 2019.

Wang, K., Ma, X., Tian, R., and Yu, F.: Analysis of new particle formation events and comparisons to simulations of particle number concentrations based on GEOS-Chem–advanced particle microphysics in Beijing, China, Atmospheric Chemistry and Physics, 23, 4091–4104, https://doi.org/10.5194/acp-23-4091-2023, 2023a.

Wang, M., Kong, W., Marten, R., He, X.-C., Chen, D., Pfeifer, J., Heitto, A., Kontkanen, J., Dada, L., Kürten, A., Yli-Juuti, T., Manninen, H. E., Amanatidis, S., Amorim, A., Baalbaki, R., Baccarini, A., Bell, D. M., Bertozzi, B., Bräkling, S., Brilke, S., Murillo, L. C., Chiu, R., Chu, B., De Menezes, L.-P., Duplissy, J., Finkenzeller, H., Carracedo, L. G., Granzin, M., Guida, R., Hansel, A., Hofbauer, V., Krechmer, J., Lehtipalo, K., Lamkaddam, H., Lampimäki, M., Lee, C. P., Makhmutov, V., Marie, G., Mathot, S., Mauldin, R. L., Mentler, B., Müller, T., Onnela, A., Partoll, E., Petäjä, T., Philippov, M., Pospisilova, V., Ranjithkumar, A., Rissanen, M., Rörup, B., Scholz, W., Shen, J., Simon, M., Sipilä, M., Steiner, G., Stolzenburg, D., Tham, Y. J., Tomé, A., Wagner, A. C., Wang, D. S., Wang, Y., Weber, S. K., Winkler, P. M., Wlasits, P. J., Wu, Y., Xiao, M., Ye, Q., Zauner-Wieczorek, M., Zhou, X., Volkamer, R., Riipinen, I., Dommen, J., Curtius, J., Baltensperger, U., Kulmala, M., Worsnop, D. R., Kirkby, J., Seinfeld, J. H., El-Haddad, I., Flagan, R. C., and Donahue, N. M.: Rapid growth of new atmospheric particles by nitric acid and ammonia condensation, Nature, 581, 184–189, https://doi.org/10.1038/s41586-020-2270-4, 2020a.

Wang, S., Wu, R., Berndt, T., Ehn, M., and Wang, L.: Formation of Highly Oxidized Radicals and Multifunctional Products from the Atmospheric Oxidation of Alkylbenzenes, Environmental Science & Technology, 51, 8442–8449, https://doi.org/10.1021/acs.est.7b02374, 2017.

Wang, Y., Mehra, A., Krechmer, J. E., Yang, G., Hu, X., Lu, Y., Lambe, A., Canagaratna, M., Chen, J., Worsnop, D., Coe, H., and Wang, L.: Oxygenated products formed from OH-initiated reactions of trimethylbenzene: autoxidation and accretion, Atmospheric Chemistry and Physics, 20, 9563–9579, https://doi.org/10.5194/acp-20-9563-2020, 2020b.

Wang, Y. X., McElroy, M. B., Jacob, D. J., and Yantosca, R. M.: A nested grid formulation for chemical transport over Asia: Applications to CO, Journal of Geophysical Research: Atmospheres, 109, https://doi.org/https://doi.org/10.1029/2004JD005237, 2004.

Wang, Z., Ehn, M., Rissanen, M. P., Garmash, O., Quéléver, L., Xing, L., Monge-Palacios, M., Rantala, P., Donahue, N. M., Berndt, T., and Sarathy, S. M.: Efficient alkane oxidation under combustion engine and atmospheric conditions, Communications Chemistry, 4, 18, https://doi.org/10.1038/s42004-020-00445-3, 2021.

Wang, Z., Tan, Y., Guo, M., Cheng, M., Gu, Y., Chen, S., Wu, X., and Chai, F.: Prospect of China's ambient air quality standards, Journal of Environmental Sciences, 123, 255–269, https://doi.org/https://doi.org/10.1016/j.jes.2022.03.036, 2023b.

Wei, K., Tang, X., Tang, G., Wang, J., Xu, L., Li, J., Ni, C., Zhou, Y., Ding, Y., and Liu, W.: Distinction of two kinds of haze, Atmospheric Environment, 223, 117 228, https://doi.org/https://doi.org/10.1016/j.atmosenv.2019.117228, 2020.

https://doi.org/10.5194/egusphere-2026-6854
Preprint. Discussion started: 19 November 2026
© Author(s) 2026. CC BY 4.0 License.

Westervelt, D. M., Pierce, J. R., Riipinen, I., Trivitayanurak, W., Hamed, A., Kulmala, M., Laaksonen, A., Decesari, S., and Adams, P. J.: Formation and growth of nucleated particles into cloud condensation nuclei: model–measurement comparison, Atmospheric Chemistry and Physics, 13, 7645–7663, https://doi.org/10.5194/acp-13-7645-2013, 2013.

WHO (World Health Organization): Air quality, energy and health: Health impacts., https://www.who.int/teams/environment-climate-change-and-health/air-quality-energy-and-health/health-impacts, accessed: 2025-01-27, 2024.

WHO (World Health Organization): Air Pollution, https://www.who.int/health-topics/air-pollution, accessed: 2025-01-27, 2025.

Wu, Y., Tillmann, R., Pfannerstill, E. Y., Khare, P., Marcillo Lara, A. C., Grasse, A., Rohrer, F., Roska, M., Depp, C., Adam, M. G., Albertin, S., Asgher, R., Bannan, T. J., Barua, S., Bates, K. H., Bell, D. M., Bohn, B., Brown, S., Buchholz, A., Chen, Y., Cho, C., Coe, H., Coggon, M. M., Fa¨rber, M., Farhoudian, S., Fry, J. L., Fuchs, H., Graus, M., El Haddad, I., He, Q., Hohaus, T., Iyer, S., Karydis, V. A., Kumar, A., Leiminger, M., Liu, L., Matthews, E., McFiggans, G., Middlebrook, A. M., Mu¨ller, M., Nissinen, A., No¨lscher, A. C., Novelli, A., Nursanto, F. R., Perrier, S., Pre´voˆt, A. S. H., Pullinen, I., Pusfitasari, E. D., Reinecke, T., Rissanen, M., Riva, M., Robinson, M. A., Schobesberger, S., Stockwell, C. E., Top, J., Tsimpidi, A. P., Vinkvist, N., Voliotis, A., Wahner, A., Wang, Y., Wang, Y., Warneke, C., Wegener, R., Yang, B., and Gkatzelis, G. I.: Toward Recreating the Breath of Cities in the Atmospheric Simulation Chamber SAPHIR, Environmental Science & Technology, https://doi.org/10.1021/acs.est.6c05767, 2026.

Xia, J., Xia, K., Huang, Z., Chen, R., Wang, Y., Qu, J. J., Singh, A., Huang, Y., Fang, Q., Li, Q., and Xu, C.: Global clean air improvements mask socioeconomic inequalities in fine particulate matter health burden, Communications Earth & Environment, https://doi.org/10.1038/s43247-026-03722-6, 2026.

Xie, Y., Dai, H., Zhang, Y., Wu, Y., Hanaoka, T., and Masui, T.: Comparison of health and economic impacts of PM2.5 and ozone pollution in China, Environment International, 130, 104 881, https://doi.org/https://doi.org/10.1016/j.envint.2019.05.075, 2019.

Xu, R., Thornton, J. A., Lee, B. H., Zhang, Y., Jaeglé, L., Lopez-Hilfiker, F. D., Rantala, P., and Petäjä, T.: Global simulations of monoterpene-derived peroxy radical fates and the distributions of highly oxygenated organic molecules (HOMs) and accretion products, Atmospheric Chemistry and Physics, 22, 5477–5494, https://doi.org/10.5194/acp-22-5477-2022, 2022.

Xue, J., Yuan, Z., Lau, A. K. H., and Yu, J. Z.: Insights into factors affecting nitrate in PM2.5 in a polluted high NOx environment through hourly observations and size distribution measurements, Journal of Geophysical Research: Atmospheres, 119, 4888–4902, https://doi.org/https://doi.org/10.1002/2013JD021108, 2014.

Yang, B., Wiser, F. C., McNeill, V. F., Fiore, A. M., Tao, M., Henze, D. K., Sen, S., and Westervelt, D. M.: Implementation and evaluation of the automated model reduction (AMORE) version 1.1 isoprene oxidation mechanism in GEOS-Chem, Environmental Science: Atmospheres, 3, 1820–1833, https://doi.org/10.1039/D3EA00121K, 2023.

Yang, C., Brean, J., Xu, W., Xu, L., Huang, W., Fan, X., Bianchi, F., Du, W., Lin, Z., Li, L., Chen, G., Zhang, Y., Cai, R., Chen, Y., Li, M., and Chen, J.: Anthropogenic Oxygenated Organic Molecules Dominate New Particle Growth in Moderate-Pollution Urban China, Environmental Science & Technology, 60, 6364–6377, https://doi.org/10.1021/acs.est.5c11555, 2026.

Yang, L., Liu, D., Yang, H., Fang, J., Meng, Q., Zhang, Y., and Ge, X.: Machine Learning-Assisted Diagnosis of Abrupt Air Pollution Emissions: Insights From Firework Emissions in China, Aerosol Science and Engineering, https://doi.org/10.1007/s41810-025-00349-6, 2025.

Yang, X., Guo, L., Zheng, Z., Riemer, N., and Tessum, C. W.: Atmospheric Chemistry Surrogate Modeling With Sparse Identification of Nonlinear Dynamics, Journal of Geophysical Research: Machine Learning and Computation, 1, e2024JH000 132, https://doi.org/https://doi.org/10.1029/2024JH000132, e2024JH000132 2024JH000132, 2024.

https://doi.org/10.5194/egusphere-2026-6854
Preprint. Discussion started: 19 November 2026
© Author(s) 2026. CC BY 4.0 License.

Yang, Y., Liao, H., and Lou, S.: Increase in winter haze over eastern China in recent decades: Roles of variations in meteorological parameters and anthropogenic emissions, Journal of Geophysical Research: Atmospheres, 121, 13,050–13,065, https://doi.org/https://doi.org/10.1002/2016JD025136, 2016.

Yin, J., Gao, C. Y., Hong, J., Gao, Z., Li, Y., Li, X., Fan, S., and Zhu, B.: Surface Meteorological Conditions and Boundary Layer Height Variations During an Air Pollution Episode in Nanjing, China, Journal of Geophysical Research: Atmospheres, 124, 3350–3364, https://doi.org/https://doi.org/10.1029/2018JD029848, 2019.

Yu, B., Yuan, Z., Yu, Z., and Xue-song, F.: BTEX in the environment: An update on sources, fate, distribution, pretreatment, analysis, and removal techniques, Chemical Engineering Journal, 435, 134 825, https://doi.org/https://doi.org/10.1016/j.cej.2022.134825, 2022a.

Yu, S., Jia, L., Xu, Y., and Pan, Y.: Molecular composition of secondary organic aerosol from styrene under different NOx and humidity conditions, Atmospheric Research, 266, 105 950, https://doi.org/https://doi.org/10.1016/j.atmosres.2021.105950, 2022b.

Zhang, H., Xing, Y., Cheng, S., Wang, X., and Guan, P.: Characterization of multiple atmospheric pollutants during haze and non-haze episodes in Beijing, China: Concentration, chemical components and transport flux variations, Atmospheric Environment, 246, 118 129, https://doi.org/https://doi.org/10.1016/j.atmosenv.2020.118129, 2021.

Zhang, H., Li, H., Zhang, Y., Wang, X., Bi, F., Meng, L., Li, Y., Zhao, L., Zhang, X., Peng, Z., Mu, Y., Mellouki, W., and Chai, F.: Synergistic generation mechanisms of SOA and ozone from the photochemical oxidation of 1,3,5-trimethylbenzene: Influence of precursors ratio, temperature and radiation intensity, Atmospheric Research, 293, 106 924, https://doi.org/https://doi.org/10.1016/j.atmosres.2023.106924, 2023.

Zhang, J., Zhao, J., Luo, Y., Mickwitz, V., Worsnop, D., and Ehn, M.: On the potential use of highly oxygenated organic molecules (HOMs) as indicators for ozone formation sensitivity, Atmospheric Chemistry and Physics, 24, 2885–2911, https://doi.org/10.5194/acp-24-2885-2024, 2024a.

Zhang, T., Qi, X., Lampilahti, J., Chen, L., Chi, X., Nie, W., Huang, X., Zou, Z., Du, W., Kokkonen, T., Petäjä, T., Lehtipalo, K., Kerminen, V.-M., Ding, A., and Kulmala, M.: Differential characterization of air ions in boreal forest of Finland and a megacity of eastern China, Atmospheric Chemistry and Physics, 25, 10 027–10 048, https://doi.org/10.5194/acp-25-10027-2025, 2025.

Zhang, X., Xue, Z., Li, H., Yan, L., Yang, Y., Wang, Y., Duan, J., Li, L., Chai, F., Cheng, M., and Zhang, W.: Ambient volatile organic compounds pollution in China, Journal of Environmental Sciences, 55, 69–75, https://doi.org/https://doi.org/10.1016/j.jes.2016.05.036, 2017.

Zhang, Y., Li, D., He, X.-C., Nie, W., Deng, C., Cai, R., Liu, Y., Guo, Y., Liu, C., Li, Y., Chen, L., Li, Y., Hua, C., Liu, T., Wang, Z., Xie, J., Wang, L., Petäjä, T., Bianchi, F., Qi, X., Chi, X., Paasonen, P., Liu, Y., Yan, C., Jiang, J., Ding, A., and Kulmala, M.: Iodine oxoacids and their roles in sub-3 nm particle growth in polluted urban environments, Atmospheric Chemistry and Physics, 24, 1873–1893, https://doi.org/10.5194/acp-24-1873-2024, 2024b.

Zhao, Q., Bi, J., Liu, Q., Ling, Z., Shen, G., Chen, F., Qiao, Y., Li, C., and Ma, Z.: Sources of volatile organic compounds and policy implications for regional ozone pollution control in an urban location of Nanjing, East China, Atmospheric Chemistry and Physics, 20, 3905–3919, https://doi.org/10.5194/acp-20-3905-2020, 2020.

Zheng, G., Duan, F., Ma, Y., Zhang, Q., Huang, T., Kimoto, T., Cheng, Y., Su, H., and He, K.: Episode-Based Evolution Pattern Analysis of Haze Pollution: Method Development and Results from Beijing, China, Environmental Science & Technology, 50, 4632–4641, https://doi.org/10.1021/acs.est.5b05593, 2016.

Zheng, X. Y., Fu, Y. F., Yang, Y. J., and Liu, G. S.: Impact of atmospheric circulations on aerosol distributions in autumn over eastern China: observational evidence, Atmospheric Chemistry and Physics, 15, 12 115–12 138, https://doi.org/10.5194/acp-15-12115-2015, 2015.

https://doi.org/10.5194/egusphere-2026-6854
Preprint. Discussion started: 19 November 2026
© Author(s) 2026. CC BY 4.0 License.



Zhong, C., Xie, Q., Ju, W., Huang, X., Zhao, J., Ding, Y., Liang, Y., and Luo, M.: Emission Characterizations of Volatile Organic Compounds (VOCs) from Light-Duty Gasoline Vehicles in China, Atmosphere, 17, https://doi.org/10.3390/atmos17010074, 2026.